POLITECNICO
MILANO 1863

SCUOLA DI INGEGNERIA INDUSTRIALE
E DELL'INFORMAZIONE

Executive Summary of the Thesis

Asteroid Gravity Field Determination using Swarms of satellites

Laurea Magistrale in Space Engineering - Ingegneria Spaziale

Author: Andrea Pietrodangelo

Advisor: Prof. Camilla Colombo

Co-advisor: Prof. Hodei Urrutxua

Academic year: 2020-2021

1. Introduction

The dynamical environment around asteroids is complex and highly nonlinear, so spacecraft operations around these bodies requires, among other things, extremely accurate information of their gravitational field. Different techniques are available for determining the gravity field of a celestial body; these techniques, however, are only as accurate as the orbit determination data is, and also depend strongly on the orbital altitude, the number of available measurements and their ground coverage, or rather, the asteroid locations that the spacecraft flies over (and thus, the spherical harmonics to which the spacecraft is exposed to).

In order to overcome the aforementioned limitations, using a *swarm* of small satellites deployed from a main satellite (i.e. a mothership) could potentially contribute to obtaining a higher number of measurements (thus providing higher redundancy and robustness of the solution), and of more diverse characteristics (i.e. measurements at different altitudes and flying over different locations on the surface), than only a single spacecraft could provide. The use of satellite swarms in the context of this research presents a novel approach to the problem of gravity field determination of an asteroids. In particular, the main interrogative is whether the determination of an asteroid gravity field from orbital data can be enhanced via the deployment of multiple small-sized spacecraft that provide inter-satellite relative position measurements. To this end, this study focuses on: 1) understanding if, and how, the proposed *swarm* approach can improve the accuracy of the gravity field solutions; and 2) assessing the performances of these newly developed methods when different kinds of observations and swarm deployment configurations are considered. In brief, the main objective was to create the basis for a feasibility study of a real mission scenario based on the aforementioned ideas.

To obtain these results, the gravitational field was modeled with a spherical harmonics expansion, which is uniquely characterised by a set of gravitational coefficients. With this model, a non-linear optimization algorithm was proposed and implemented to compute estimates of the gravity field based on orbital data. Moreover an outlier rejection algorithm was implemented to discard bad satellites from the data batch. Two more novel approaches were also treated, one focused on retrieving in a direct way a mascon model of the asteroid, where lumped masses were located in fixed positions on the asteroid's approximating ellipsoid, while the other in-

tended to formulate an augmentation of the Orbit determination algorithm proposed by Nayfeh [8]. Additionally, different swarm deployment strategies were proposed and analyzed based on the their performances in the different configurations and observables available, such as relative position in Cartesian coordinates, range and range-rate. The robustness of the proposed approach was evaluated introducing uncertainties, noise, and neglected dynamics, while assessing its sensitivity to some of the model parameters.

2. Novel contents and past works

The main focus of this research was to evaluate the performances of the swarm approach to the gravity determination problem. As a direct continuation of the research proposed by Guardalà [5], who studied the problem of single-spacecraft gravity field determination in planetary and asteroidal environment, this work is aimed to expand the methods previously used, and to introduce new ones, to build a simulation framework to test the performances of multi-spacecraft gravity field determination based on relative measurements. In particular, the batch estimation methods were augmented, in order to take into account relative position measurements. Moreover an outlier rejection algorithm was implemented to discard bad satellites from the data batch. Finally, goal was to verify which kind of measurement strategy would be the most feasible in case of a real mission scenario.
In previous works like in Bassani [1] and D'Amico [2], the problem of multi-spacecraft estimation was addressed using sequential estimation methods, namely Extended Kalman Filters, and where semi-analytical formulations are used to formulate the problem, i.e. the conversion between the osculating elements and the relative orbital elements are employed to describe the relative dynamics. These methods proved to be capable to estimate a subset of zonal harmonic coefficients. This research is on the other hand focused onto a numerical approach capable of identifying a whole subset of gravitational parameters of the spherical harmonics expansion. Moreover the sequential estimation approach was discarded for the batch estimation one since it is assumed that no real-time estimation is needed. The same estimation method was also studied to directly identify mascon models starting from measurement data. A semi-analytical approach for relative position orbit propagation was introduced, namely the Encke's method, and tested in non-Keplerian gravitational environments. Moreover a novel gravity field determination algorithm was proposed, derived from the orbit determination algorithm of Nayfeh [8].

3. Simulation framework

The problem of estimating the gravitational field is addressed in this research using the batch estimation approach solved by the means of the Least Squares Method. In particular, the problem is formulated as an augmentation of the Orbit determination problem, following the steps and ideas developed by Guardalà [5] and Kaula [7].

3.1. Gravity field model

The gravity field model used for most of the simulation of this research is the spherical harmonics expansion of the gravitational field. As shown in Montenbruck and Gill [6], the expression for the potential field U can be manipulated to show the contributions of the single spherical harmonics:

$$U = \frac{\mu}{R} \sum_{n=0}^{\bar{n}} \sum_{m=0}^{n} (C_{nm} V_{nm} + S_{nm} W_{nm}) \quad (1)$$

$$\ddot{\mathbf{R}} = \nabla U \quad (2)$$

The terms V_{nm} and W_{nm} depends on the cartesian coordinates of the s/c and can be computed as a function of the cartesian coordinates. C_{nm} and S_{nm} are the gravitational -or Stokes- coefficients, that are computed as reported in [6] and are tabulated for readily availible gravitational models of known bodies. The evaluation of the accelerations with this model is done with the Cunningham algorithm [3].

3.2. Gravity field determination

the gravity field determination problem is here formulated as minimization one in which both

the initial conditions of the spacecraft and the parameters that characterize the gravity field are part of the optimization vector for the trajectory fitting. More in detail, an optimization problem is set up where the cost function is defined as:

$$J\left(\mathbf{X}_0^*\right) = \frac{1}{2}\sum_{i=1}^{\ell}\left(\mathbf{O}_i - \mathbf{C}_i\left(\mathbf{X}_0^*\right)\right)^\top\left(\mathbf{O}_i - \mathbf{C}_i\left(\mathbf{X}_0^*\right)\right) \tag{3}$$

where observations $\mathbf{C}_i$ and $\mathbf{C}_i$ are both p-dimensional vectors of parameters evaluated at ℓ discrete time instances. The observations are here computed through numerical integration and starting from a reference state vector $\mathbf{X}_0^*$. For convenience, both the observations and the computed observations are collected in the observations $\mathbf{O}$ and computed observations $\mathbf{C}$, both $\ell \times p$ matrices.
Variables to identify are normalized and collected into the state vector $\mathbf{X}_0$:

$$\mathbf{X}_0 = \begin{bmatrix} \begin{bmatrix} \overline{\mathbf{R}}_0 \\ \overline{\mathbf{V}}_0 \end{bmatrix}_{sc_1} \\ \begin{bmatrix} \overline{\mathbf{R}}_0 \\ \overline{\mathbf{V}}_0 \end{bmatrix}_{sc_2} \\ \vdots \\ \begin{bmatrix} \overline{\mathbf{R}}_0 \\ \overline{\mathbf{V}}_0 \end{bmatrix}_{sc_N} \\ \overline{\mu} \\ \overline{\mathbf{c}} \\ \overline{\mathbf{s}} \end{bmatrix} \tag{4}$$

where N is the number of spacecrafts of the swarm, $\overline{\mathbf{R}}_0$ and $\overline{\mathbf{V}}_0$ are the initial coordinates of each satellite, that have to be estimated. We will consider the satellite number 1 the mothership, while the others will be the child-ships. $\overline{\mu}$ is the normalized gravitational constant, $\overline{\mathbf{c}}$ and $\overline{\mathbf{s}}$ are vectors collecting the normalized Stokes coefficients. Since the objective is to analyze different kind of relative measurements, the generic $\mathbf{O}^{sc_n}$ and $\mathbf{C}^{sc_n}$ will contain different kind of data depending on the case at study, namely relative positions and velocities in cartesian coordinates ($\mathbf{\Delta R_n}$ and $\mathbf{\Delta V_n}$), or range and range-rate (r_n and v_n). Noise is also included in the observations. Measurement uncertainty is simulated adding a relative random offset. The scheme of the algorithm is then summarized:

- The state vector (4) is updated by the Levemberg-Marquadt solver;
- The swarm trajectories are propagated utilizing the initial conditions and gravitational parameters contained in the state vector;
- The absolute coordinates of the secondaries are converted into relative coordinates w.r.t. the primary and collected into the C^{Nk}
- Compute J cost function;
- Check the convergence criteria;

The quality of the solution was evaluated using the Hilbert distance [9] between the real and estimated field, chosen ad a Figure of Merit (FM).

4. Swarms configurations

The swarms will be characterized by the mothership satellite osculating orbital elements, that will deploy, in one or more points of its trajectory, a certain number of secondary satellites, according to the configuration of choice. The objective was to come up with simple yet effective deployment schemes, that would allow for a systematic study of their performances. Hence the focus was put on circular orbits.
As a remark, the terms *polar* and *equatorial* orbits utilised in the following refer to orbits whose orbital plane is parallel to the spinning axis for the former, perpendicular to it for the latter. The trajectories are computed through independent integration of the dynamics equations of each satellite.

- Equatorial Scanner: the mothership is placed on equatorial orbit, and at fixed time-steps it'll release a child-ship, injecting each of them on orbits with a certain inclination i, and equally spaced RAANs, along the 360° span. From this concept an infinity of different configurations can be generated, depending on the selected inclination.
- Polar Scanner: the mothership is placed on a polar orbit and when in azimutal position, it releases radially the childships, that will still be on polar orbits but with equally spaced RAANs, along the 360° span.

- Inclination Fan: the child-ships are placed on orbits with different inclinations, spanning from -90 to 90, by the mother-ship that will have the same osculating elements, but with a certain inclination i. From this concept an infinity of different configurations can be generated, depending on the selected inclination.

5. Pair of satellites

The first results were obtained considering only couples of satellites belonging to a swarm, being one of them the mother-ship. As many optimization problems are solved as the number of secondaries in the swarm. That is, if the swarm is composed of n satellites, $n-1$ solutions are found, each one extracted using the measurements of the mother-ship and one of the child-ships. The goal is to understand how the solution how the solution behaves when adding a secondary spacecraft relative coordinates depending on its orbit with respect to the primary. Simulations are done with circular orbits of semi-major axis $a = 40km$, whereas the noise level $\delta = 1 \cdot 10^{-10}$. As a further remark, since the method proves to effectively estimate the initial conditions of the spacecrafts, with relative errors of -at least- 2 orders of magnitude lower than the other optimimsation variables.

In Fig. 1 the Figures of Merit relative to each optimisation are reported, against the relative inclination -with respect to the primary- of each secondary analysed. A swarm of 40 satellites was considered. The analysis of the FM shows a clear profile, values ranging in the order of 10^{-12}, where the highest -worse- values are concentrated around $\Delta i = 0$, indicating that when the secondary is orbiting *close* to the primary, a small improvement in the solution is achieved. An explanation to this behaviour could rely in the redundancy of the information contained in the measurements. In fact, since the gravitational force sensed by a satellite is only function of its ACAF position, the two closely orbiting spacecrafts will *sense* a similar force, providing the solver with redundant data.

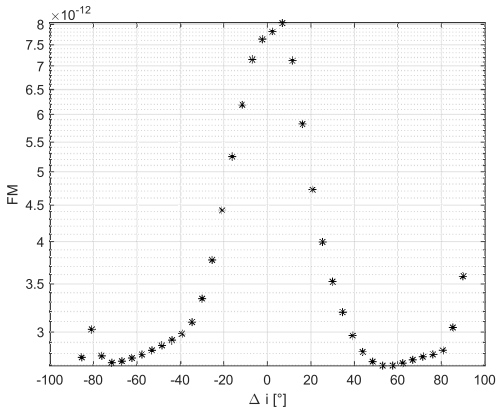

Figure 1: Inclination fan simulation results with relative position Cartesian coordinates - $i_{primary} = 90°$

6. Swarm optimization

It will be now discussed how the solution improves when increasing the size of the swarm, addressing more fundamental aspects regarding the sensitivity of the model to certain parameters, like: noise, size of the semi-major axis, observation time and un-modeled dynamics neglected in the model like the SRP perturbation.

6.1. Size of the swarm

One of the main interrogatives posed for this research was to understand whether increasing the number of satellites in the swarm more precise solution could be achieved. Results for a polar scanner swarm, with semi-major axis $a = 40km$ are reported in 2 for an increasing number of satellites belonging to the swarm (from 2 to 50). The figure of merit is sparsely improving when considering more secondaries, thus more data to feed the solver. Although kind of irregularly, the cloud of points is descending, and flattening out when passed the 30 spacecrafts. In this region the best solutions are found, with a FM more than 20 times smaller than when considering 2 satellites only.

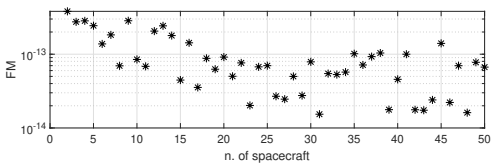

Figure 2: Polar scanner results swarms with increasing satellites

6.2. Noise level

Being the noise level on measurements δ, on the Cartesian coordinate R_I at a given time t:

$$R_x^{\text{noise}}(\bar{t}) = R_x + \delta \cdot R_x \tag{5}$$

The same kind of optimization was run including in the model an increasing amount of noise in the measurements, starting from 0. The results shown in 3 for a polar inclination fan swarm, that the sensitivity of the method to noise is very high, thus high-accuracy results are guaranteed just with very precise measurements.

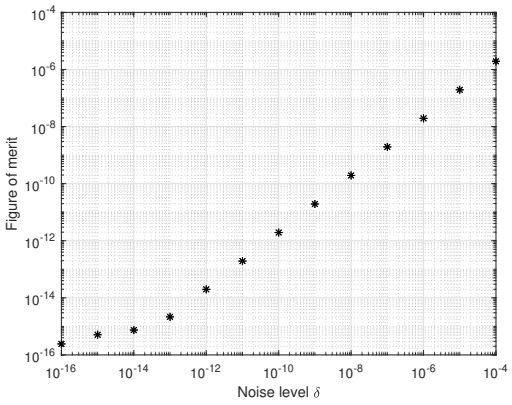

Figure 3: Effect of the noise level on the solution

The evolution of the FM with respect to the noise is linear in a log-log plot. In particular, except the points with lower noise, that show no clear relation with it, the evolution of the FM roughly follows $\log_{10}(d_H) \approx \log_{10}(\delta) - 2$
Thus, if the observation noise is small enough, the solution is dominated by numerical noise, otherwise, the solution is ruled by the effect of the observation noise.

6.3. Size of the orbit

In the following figures, results for polar scanner swarms satellites, optimised in pairs, are reported for different orbit sizes, namely: $a = 40km$, $a = 25km$. Simulations were repeated considering range and range-rate measurements to compare any possible difference. Figures clearly show that, as expected, with low altitude orbits an improvement in the accuracy of the solution is achieved.

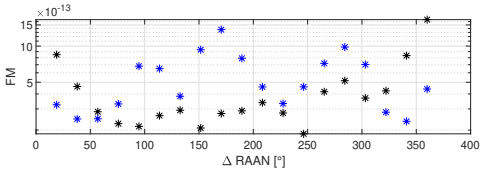

Figure 4: Polar scanner results for $a = 40$. Black: relative position coordinates; Blue:range and range-rate

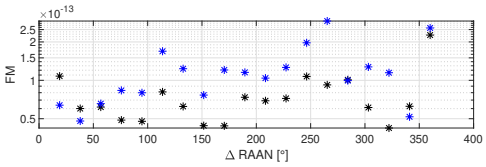

Figure 5: Polar scanner results for $a = 25$. Black: relative position coordinates; Blue:range and range-rate

6.4. Observation time

Keeping the same sampling time, polar inclination fan swarms were propagated for 1, 2 and 5 orbital periods, with increasing swarm size. Chart in 6 suggest that projecting the trajectories for longer time-span doesn't seem to have a big influence on the solution, while the effect of the increasing swarm size is more evident. The reason for this behaviour could be attributed to the performances of the integration scheme.

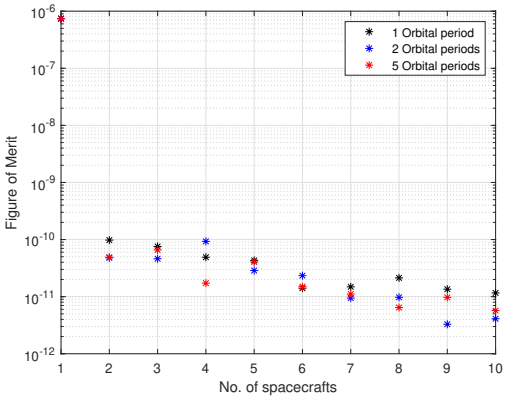

Figure 6: Solution for increasing observation time and spacecrafts

7. Solar radiation pressure

In 6 the equation for the SRP force acting on the satellite is reported:

$$\mathbf{F_{SRP}} = -v \cdot \frac{S}{c} \cdot C_R \cdot A_s \hat{\mathbf{S}} \qquad (6)$$

where v is the shadow boolean function, S is the solar constant, c is the speed of light, C_R the reflectivity coefficient, A_s is the *wet* area of the satellite and $\hat{\mathbf{S}}$ is the Sun direction unit vector. In 7 a comparison of the accelerations proportioned by the single J terms of the spherical harmonics expansion of Eros 433 gravity field, and the SRP acting on a spacecraft orbiting Eros, as a function of the distance from the body. This rough computation was made to have an understanding of the limitations of the model, i.e. when the effect of the unmodeled SRP becomes comparable with the considered dynamics. The satellites mass was chosen as $m = 0.01kg$, $v = 1$ and their wet area $A_s = 10^{-5}m^2$. The results reflect that the SRP acceleration should not be neglected, especially when dealing with altitudes higher than 50km, since its value becomes comparable with the one proportioned by the gravitational harmonics.

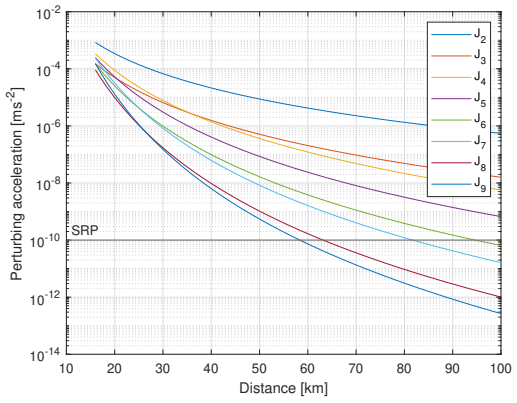

Figure 7: SRP and J_n acceleration comparison

8. Type of measurements

A quantitative analysis was sought in order to retrieve the best performing measurement strategy for this problem. To do this, a statistical approach was utilized. In particular, a database of simulations was built, containing the solutions for 120 simulations, generated with different kinds of swarm configurations and number of satellites. Care was taken in selecting fixed noise level and orbit sizes for all iteration.

Each scenario was repeated 3 times, and optimized each time with one of the different measurements approach discussed. After collecting all the solutions, each FM obtained from range and range-rate measurements, and from range measurements only, was subtracted to the ones obtained with relative position Cartesian measurements.
These two sets of data, were used to generate histograms where the bar height reflects the number of simulations in which the values of $FM_{cart} - FM_{range-rr}$ and $FM_{cart} - FM_{range}$ fall within that fixed interval.

Histograms are shown in Fig. 8 and 9, while statistical facts are reported in 1 and 2.
On average, the relative position in Cartesian coordinates approach gives the best solutions. Based on the same data, it can be said that the range only measurement approach result in the worst solutions. However the type of measurement selected strongly affects the technological requirements of a real-life mission. In particular, range and range-rate data can be obtained very easily. This means that the child-ship could be small and *stupid*. For this reason, the selection of only range measurements would be justified, accepting an average reduction of $2.11 \cdot 10^{-12}$ in the Figure of Merit in exchange of a lightweight and compact instrumentation.

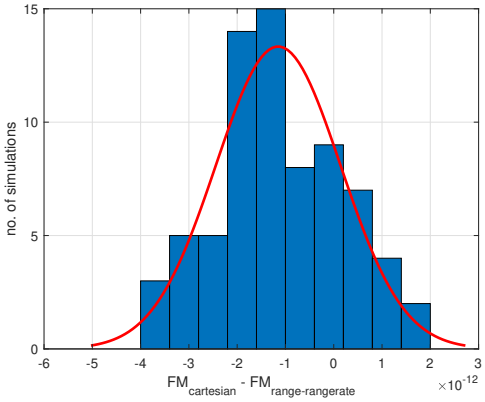

Figure 8: FM comparison between relative Cartesian coordinates and range+range-rate measurements

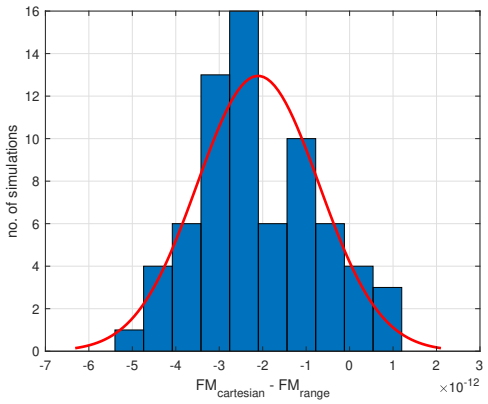

Figure 9: FM comparison between relative Cartesian coordinates and range measurements

Table 1: Measurements comparison against the FM obtained with Cartesian relative positions

VS Cart.rel.pos.	Range and range-rate
μ	$-1.15 \cdot 10^{-12}$
μ C.I.	$[-1.45 \cdot 10^{-12}, -8.47 \cdot 10^{-13}]$
σ	$1.29 \cdot 10^{-12}$
σ C.I.	$[1.11 \cdot 10^{-12}, 1.55 \cdot 10^{-13}]$

Table 2: Measurements comparison against the FM obtained with Cartesian relative positions

VS Cart.rel.pos.	Range only
μ	$-2.11 \cdot 10^{-12}$
μ C.I.	$[-2.44 \cdot 10^{-12}, -1.77 \cdot 10^{-12}]$
σ	$1.40 \cdot 10^{-12}$
σ C.I.	$[1.20 \cdot 10^{-12}, 1.69 \cdot 10^{-12}]$

8.1. Outlier rejection

We want now to analyse if and how the solution could improve if an effective method of *filtering* the data for the estimation problem could be found. The problem of identifying outliers in this application is non-trivial, since there's no *a priori* way to determinate which solutions are the better, since no information on the actual field is known. A method based on the solution of the state vector was implemented to this scope. Consider a swarm of N particles and that n is the dimension of the state vector. The elements of $\hat{\mathbf{X}}_\mathbf{0}$ can be seen as the spatial coordinates of the N solution. If it is assumed that a sufficient number of solutions has succeeded in converging, those $\hat{N}$ points create a cluster around the global minimum (namely, the inliers), and the remaining $N - \hat{N}$ out-of-cluster rejected points are referred to as outliers. The clustering technique implemented for the research of the outliers is the Density-Based Spatial Clustering of Applications with Noise (DBSCAN). [4] The general scheme of the algorithm implemented is reported in Fig. 10 and here summarised. Given N orbiting spacecrafts, where the spacecraft 1 is the mother-ship

- $N-1$ different solutions for the gravity field assessment ($\hat{X}_0$), one for each pair primary-secondary, are obtained;
- Selected a suitable ϵ and N_{min}, DBSCAN identifies the outlier solutions;
- The filtered best estimate solution $\hat{\mathbf{X}}_\mathbf{0}$, is computed discarding data from the outliers.

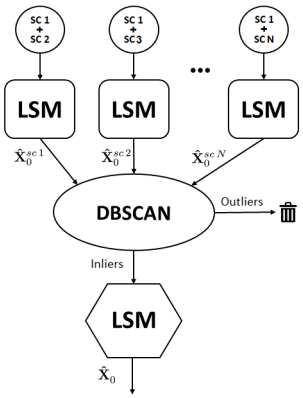

Figure 10: Outlier rejection algorithm

Let's consider for example the solutions relative to a swarm of 40 spacecrafts in polar inclination fan. If for example we include in our model the presence of high noise (5 increase in the noise level) on some randomly extracted spacecrafts from the swarm, the solution profile of the FM looks as in 11. It's clear that some points are offset because of the high noise content. The DBSCAN algorithm applied to this situation is able to distinguish them from the other clustered solutions. The parameters were set as $\epsilon = 1 \cdot 10^{-8}$ and $N_{min} = 5$. Optimizing the satellites data in batches, belonging to the full swarm or the filtered swarm, it is found that the filtered solution is indeed better than the complete swarm one, containing high noise data from the outliers. This proves that the algorithm can be valuable for data filtering in this scope.

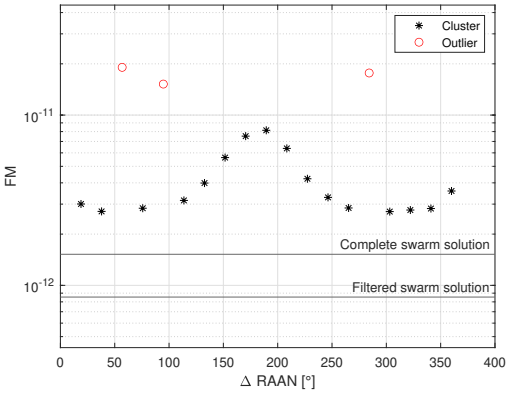

Figure 11: Outlier rejection results

9. Alternative approaches

9.1. Mascon model

When dealing with the gravity field determination problem, some novel and alternative pathways have been implemented and tested. One of them relies in the evaluation of the problem modeling the gravity field with a mascon model. The set up of the problem remains unchanged, while the modification relies in the newly defined parameters to estimate.

For this analysis, the mascon model was defined as a list of lumped masses each of them with a fixed position, uniformly placed on the surface of the ellipsoid that approximate the asteroid to analyze. Since the position of the mascons is fixed, the parameters to estimate in this approach are the mascon masses, collected in the $k \times 1$ vector $\overline{\mathbf{m}}$, where k is the number of mascons. mascon models need a high number of mascons to generate a good estimated gravity field. For this reason, the optimization problem can become very lengthy, in terms of computational time.

As a proof-of-concept, this method was tested first using only measurement data coming from the mother-ship (i.e. its absolute coordinates Cartesian position).

In Fig. 12 the solution for this kind of problem is shown. 6400 mascons were uniformly placed onto the surface of the ellipsoid approximating Eros 433. Remarkably, the method converges and the total mass of the mascon model (i.e. the sum of all the lumped masses) is equal to the mass of the asteroid, with a relative error of 10^{-8}. It's worth to underline the insurgence of some negative masses. This happened since no constraint was put to the optimization: negative masses are in fact acceptable since we're merely looking for a mathematical representation of the gravity field.

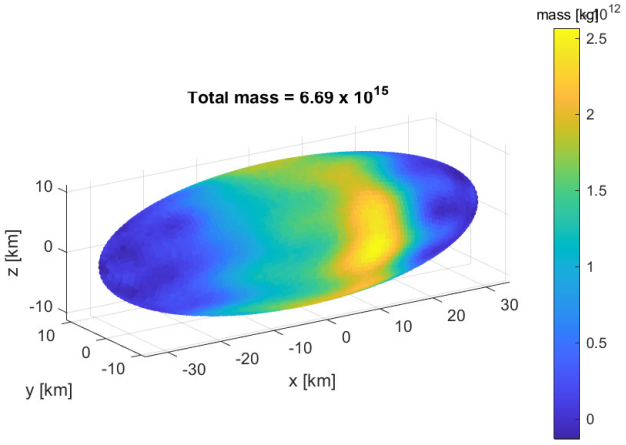

Figure 12: Mascon model solution

9.2. Nayfeh's augmented algorithm

The non-linear orbit determination method proposed by Nayfeh [8], is based upon the idea that if the exact orbit could be determined, the residuals (defined as measured minus computed values) would represent the noise. In case of random noise, then the coefficients of any polynomial that fits through the residuals in the least-squares sense must vanish.Being it extremely effective for orbit determination, a generalization of this method was also used to estimate perturbative parameters like the ballistic coefficient in the case of drag estimation. Taking inspiration from it, a method to estimate gravitational parameter was derived.

Assuming that a 2-nd order spherical expansion is considered, and that the perturbation is provided by the C terms only, the method is described in this way:

- We fit the first, say, ten data points to a straight line time-dependent vector $\mathbf{a}_0 + \mathbf{b}_0 t$ in least-squares sense. We choose $\mathbf{a}_0$ and $\mathbf{b}_0$ to be the initial position and velocity of the trajectory and guess values for $C_{20}/\mu, C_{21}/\mu$, and C_{22}/μ. Using these values for the aerodynamic parameters and the initial position and velocity, we calculate a reference trajectory by integrating the equations of motion, and calculate the

initial acceleration $\mathbf{c}_0$.

- We form the residual differences between the measured discrete data points and the values obtained from the computed reference trajectory at the corresponding times. We fit these residuals in a least-squares sense to a parabolic time-dependent vector $\Delta\mathbf{a_0} + \Delta\mathbf{b_0}t + \frac{1}{2}\Delta\mathbf{c_0}t^2$
- We update the initial position, velocity, and acceleration. Thus,

$$\mathbf{a_1} = \mathbf{a_0} + \frac{1}{2}\Delta\mathbf{a_0}$$
$$\mathbf{b_1} = \mathbf{b_0} + \frac{1}{2}\Delta\mathbf{b_0}$$
$$\mathbf{c_1} = \mathbf{c_0} + \frac{1}{2}\Delta\mathbf{c_0}$$

  The new initial position, velocity, and acceleration obtained are substituted in the eqs of motion. New values for $C_{20}/\mu, C_{21}/\mu$, and C_{22}/μ are obtained inverting the system. Using the new initial position $\mathbf{a}_1$, velocity $\mathbf{b}_1$, and gravitational coefficients, we calculate a new reference orbit and continue iterating until the change in initial position, velocity, and acceleration is smaller than some assigned convergence numbers.

It is worth to underline that the method only allows for the estimation of 3 parameters, being them estimated inverting the dynamics equations. In this sense, it could be possible to estimate more than three parameters if more than one spacecraft is considered. After extensive iterations and simulations, this method proved ineffective when estimating gravitational parameters. While the convergence is achieved for the initial conditions of the satellite, no improvement is made on the relative error of the gravitational coefficients. This is due to the failure of exactly estimating the initial acceleration with this method.

10. Conclusions

Started as a continuation of the research proposed by Guardalà [5], where gravity field determination was addressed in detail using a single or a multi-spacecraft approach mostly in Earth environment and using absolute coordinates measurements only, the problem was reformulated, and this thesis analysed the problem of gravity field determination of asteroids through a novel concept, namely the recovery of it using relative coordinates measurements of a swarm of small satellites. The objectives identified at the beginning of this work were fully achieved, and most of the questions posed were answered thanks to the results obtained. In particular, the research demonstrated not only that it is possible to estimate the gravity field of a small body using relative position measurements obtained from a swarm of formation flying satellites with respect to a primary one, but also that a refinement of the solution can be obtained with that.

References

[1] Alessandra Bassani. Recovery of the gravity field of a small body through autonomous and relative navigation between two spacecraft. 2020.

[2] Simone D'Amico Corinne Lippe. Spacecraft swarm dynamics and control about asteroids. 67.

[3] Leland E. Cunningham. On the computation of the spherical harmonic terms needed during the numerical integration of the orbital motion of an artificial satellite. *Celestial Mechanics 2.2*, pages 207–216, 1970.

[4] Martin Ester et al. A density-based algorithm for discovering clusters in large spatial databases with noise. page 226–231, 1996.

[5] G. Guardalà. Single and multi-spacecraft solutions for the gravity field determination of irregular bodies.

[6] Connie J. Weeks James K. Miller and Lincoln J. Wood. Orbit determination strategy and accuracy for a comet rendezvous mission. *Satellite Orbits*, pages 53–68, 244–247, 2000.

[7] William Mason Kaula. Theory of satellite geodesy. *Dover Publications Inc.*, pages 1–11, 100–107, 1966.

[8] Ali Hasan Nayfeh. Non-linear orbit determination methods. *Satellite Orbits*, pages 1–12, 1968.

[9] Carlson Stephan C. Metric Space. European involvement in juno.

POLITECNICO
MILANO 1863

SCUOLA DI INGEGNERIA INDUSTRIALE
E DELL'INFORMAZIONE

Asteroid gravity field determination using swarms of satellites

Supervisor
Prof. Camilla Colombo

Co-Supervisor
Prof. Hodei Urrutxua

Candidate
Andrea Pietrodangelo – 919612

Academic Year 2020 – 2021

Acknowledgements

I would like to acknowledge and thanks my thesis supervisor, Dr. Camilla Colombo, of the Aerospace Science and Technology Department at Politecnico di Milano, for giving me the opportunity to work on this topic and for all the precious advices I received from during this *journey*.
I would also thank Politecnico di Milano for awarding me with the scholarship "Borsa di studio tesi all'estero" that allowed me to spend a wonderful time in Madrid while working on this thesis.
Last but not the least, thanks to my co-supervisor Hodei Urrutxua, of the Aerospace Department at Universidad Rey Juan Carlos, for accepting me as his student and for the patient support and caring advices; many of the concept developed in this research come from his ideas, and the realisation of them could only be achieved thanks to his tutoring. I'm really grateful for meeting a person of rare kindness like you.

Grazie ai miei genitori per essere sempre al mio fianco, e per supportarmi in ogni mia decisione. Questo lavoro è dedicato a voi.

Abstract

Missions to explore near-Earth asteroids are gaining popularity thanks to their enormous scientific and technological fallouts. As a matter of fact, missions to asteroids are not only being conceived for their obvious scientific implications and contributions to our understanding of the evolution processes of the Solar System formation, but there is also a growing interest asteroid missions both, as potential assets for mining and resource exploitation, and for planetary defense purposes, so asteroid deflection technologies can be demonstrated, in case they were needed one day.

The dynamical environment around asteroids is complex and highly nonlinear, so spacecraft operations around these bodies requires, among other things, extremely accurate information of their gravitational field. This information is not only vital for the safe operations of the spacecraft, but can also provide valuable information from which scientific data can be derived, such as the asteroid's composition, internal structure and physical properties. Different techniques are available for determining the gravity field of a celestial body; however, for the case of asteroids and due to a lack of on-ground infrastructure, the only methods available are those based on inference from the perturbed orbital motion of a spacecraft orbiting the asteroid. These techniques, however, are only as accurate as the orbit determination data is, and also depend strongly on the orbital altitude, the number of available measurements and their ground coverage, or rather, the asteroid locations that the spacecraft flies over (and thus, the spherical harmonics to which the spacecraft is exposed to).

In order to overcome some of the aforementioned limitations, using a *swarm* of small satellites deployed from a main satellite (i.e. a mothership) could potentially contribute to obtaining a higher number of measurements (thus providing higher redundancy and robustness of the solution), and of more diverse characteristics (i.e. measurements at different altitudes and flying over different locations on the surface), than only a single spacecraft could provide; therefore, a swarm could potentially improve the number and quality of the data, and thus yield a better fidelity of the gravity field determination solution. Hence, the use of satellite swarms presents a novel approach to the problem of gravity field determination of an asteroids, which is investigated in this thesis in an attempt to develop new, innovative methods for asteroid gravimetry. In particular, the main interrogative is whether the determination of an asteroid gravity field from orbital data can be enhanced via the deployment of multiple small-sized spacecraft that provide inter-satellite relative position measurements. To this end, this study focuses on: 1) understanding if, and how, the proposed *swarm* approach can improve the accuracy of the gravity field solutions; and 2) assessing the performances of these newly developed method when different kinds of observables

and swarm deployment configurations are considered. In brief, the main objective was to create the basis for a feasibility study of a real mission scenario based on the aforementioned ideas.

To obtain these results, the gravitational field was modeled with a spherical harmonics expansion, which is uniquely characterised by a set of gravitational coefficients. With this model, a non-linear optimisation algorithm was proposed and implemented to compute estimates of the gravity field based on orbital data. Two more novel approaches were also treated, one focused on retrieving in a direct way a mascon model of the asteroid, where lumped masses were located in fixed positions on the asteroid's approximating ellipsoid, while the other intended to formulate an augmentation of the Orbit determination algorithm proposed by Nayfeh [1]. The aforementioned framework was then used to analyze different approaches to the problem of estimation of the gravitational parameters using a swarm of satellites. The advantage of a swarm is that it allows for inter-satellite relative measurements, and for this reason techniques of relative motion propagation were investigated an implemented. Additionally, different swarm deployment strategies were proposed and analyzed based on the their performances in the different configurations and observables available, such as relative position in Cartesian coordinates, range and range-rate. Based on these analyses, it was possible to make a preliminary assessment of the technological complexity of such a distributed gravity sensing system, and the number of spacecraft that the swarm would be comprised of to provide reliable estimates. The robustness of the proposed approach was evaluated introducing uncertainties, noise, and neglected dynamics, while assessing its sensitivity to some of the model parameters.

Sommario

Le missioni per esplorare asteroidi vicini alla Terra stanno diventando sempre più popolari a causa della ricaduta scientifico-tecnologica che possono generare. Infatti, oltre ad avere implicazioni sugli attuali modelli di formazione del nostro Sistema Solare, l'interesse è crescente verso lo studio della deflessione di asteroidi, la difesa planetaria e verso tecnologie di mining per lo sfruttamento delle risorse in-situ. Sfortunatamente queste operazioni necessitano di informazioni estremamente precise sul campo gravitazionale del corpo di interesse. E' inoltre necessario caratterizzare l'ambiente asteroidale per selezionare i candidati per missioni esplorative e stabilirne composizione e proprietà fisiche. La gravità di un corpo si osserva tipicamente misurandone l'effetto sulla traiettoria di un satellite che orbita presso lo stesso. Riuscendo a misurare il movimento di un satellite è possibile stimare le proprietà gravitazionali del corpo centrale, ma l'accuratezza della stessa stima dipende dal numero, dalla precisione e dalla diversità geometrica delle misurazioni. L'uso di uno "sciame" di piccoli satelliti tutti uguali tra loro (autonomi o no) dispiegati da un satellite principale, potrebbe porre una soluzione al problema, nonché diminuire il rischio associato alla missione a causa della ridondanza dei satelliti stessi. Sulla necessità di investigare metodi e soluzioni innovativi per la gravimetria asteroidale getta le basi questo studio, il cui obiettivo è quindi di sviluppare nuovi approcci al problema e di ottenere una strategia efficace per la determinazione della gravimetria degli asteroidi. In particolare, il principale interrogativo proposto riguarda il miglioramento della stima di campo gravitazionale in caso di un approccio multi-satellite con misure relative. A differenza di altri studi, ci si soffermerà a capire se e come un approccio del genere possa dare luogo a stime più accurate, e successivamente a studiarne le performances utilizzando diversi tipi di misura delle coordinate relative. Lo scopo è principalmente quello di creare le fondamenta per uno studio di fattibilità per una missione reale basato sulle idee precedentemente menzionate.
Per ottenere questi risultati, in primo luogo il campo gravitazionale è stato modellato tramite uno sviluppo in armoniche sferiche, il quale è unicamente caratterizzato dai valori dei coefficienti gravitazionali. Con questo modello sono stati proposti ed implementati algoritmi di ottimizzazione non-lineare utilizzati per la stima del campo gravitazionale basata su dati orbitali. In più, sono stati trattati altri approcci innovativi: uno basato sulla stima diretta del campo gravitazionale modellato con mascon models, dove le masse concentrate sono state posizionate in dei punti equispaziati sull'ellissoide che approssima l'asteroide; l'altro invece propone un nuovo algoritmo di stima del campo gravitazionale basato sull'algoritmo di determinazione orbitale di Nayfeh.

Successivamente si sfrutterà questo framework per analizzare vari approcci di determinazione dei parametri gravitazionali mediante sciami ("swarm") di satelliti. Il vantaggio dello sciame è che permette di ottenere misurazioni relative infra-satellite, ragion per cui sono state inoltre implementate tecniche di propagazione basate sul moto relativo. A questo proposito sono state proposte una serie di strategie di dispiegamento ed in base ad esse analizzate le performances del sistema nelle varie configurazioni e tipi di misurazioni disponibili, dalla semplice distanza relativa infra-satellite e arrivando alla completa disponibilità di posizioni relative in riferimento Cartesiano. In base a queste analisi si è stabilita la complessità tecnologica delle misure necessaria per gli individui dello sciame, e il numero di particelle necessarie per una stima affidabile. Verrà inoltre valutata la robustezza del metodo infine adottato introducendo incertezze, rumori di misura e dinamiche trascurate, mentre infine è stata studiata la sensitività del modello ai diversi parametri dello stesso.

Contents

List of Figures

List of Tables

Chapter 1

Introduction

Missions to explore near-Earth asteroids are gaining popularity thanks to their possible scientific and technological fallouts. Indeed, as McMahon member of the NASA OSIRIS-REx mission team said, "you need to know the gravitational field for spacecraft operations, really to enable all the other sciences" [9]. In fact, other than enabling accurate trajectory simulations in order to analyse, for example, asteroid landing missions, the highly precise gravity field determination can allow the study of a body structure and interior. Covering several aspects, the possible motivations of the study small solar system structure and gravity field can be resumed as:

- Planetary defense: accurate knowledge of a potential colliding asteroid characteristics such as mass, density and shape can enable deflection strategies like the ones that have been proposed in the literature; that include kinetics impactors [10] [11], gravity tugs [12] detonation nuclear devices [13], and others.
- In-situ resources exploitation: precise gravimetry is required to land on an asteroid and the knowledge of their structure is needed to select targets for in-situ resources exploitation like water resupply for propellant production [14], or asteroid mining for precious metals collection.
- Solar System formation: being asteroids left-overs of the formation process of the Solar System, gaining knowledge about their structure and porosity can help to gain knowledge about the early stages of the Solar System existence, and its accretional and collisional environment [15] [16]

The target of this study is then to come up with a framework that allows for the enhancement of the estimation of the gravity field of asteroids, using a multi-spacecraft approach with relative measurements. Differently from other studies, this is focused on understanding if and how this kind of approach can improve the accuracy of the solutions, and after that assessing the performances of this method when different kind of measurement strategies are taken into account. Furthermore the framework built serve as a proof of concept posing the basis for a feasibility analysis based on a real mission scenario.

1.1 Technological outline

A number of technologies employed to obtain measurements required for the gravity determination are now briefly presented. Different techniques have been designed for specific purposes and can be subdivided in categories which define their methods such as [17]:

- Earth to Space methods, where satellite measurements are taken from ground;
- Space to Earth methods, where the satellite takes measurements looking at the Earth;
- Space to Space methods, where satellite measurements are taken from another spacecraft;

In these categories belong a number of technologies apt to retrieve the measurements needed, based on the specific application. Some of these, relevant to the scope of this dissertation will now be briefly explained,

1.1.1 Charge-Coupled Device camera observations

This technology is used to compute the direction of a satellite during his passage above the station. The process is the following Figure (1.1): by taking 2 pictures of the satellite at the same time from separate positions it's possible to determine the plane containing the 3 aformentioned points (ground stations and satellite). Using the information coming from another ground station, it's possible to intersecate the planes to obtain the direction vector.

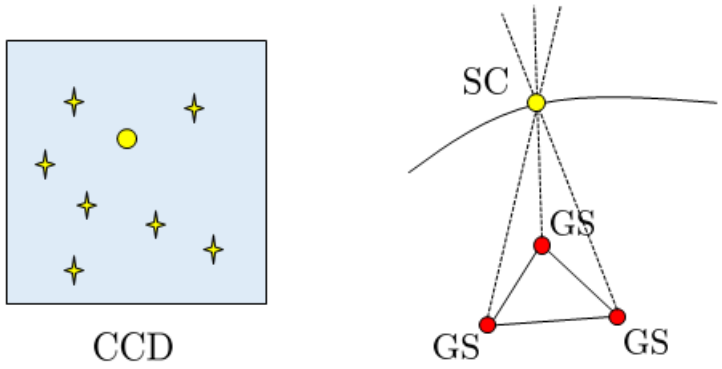

Figure 1.1. CCD camera observations

Being mainly a Earth to Space technology, optical tracking is also used in reverse mode exploiting computer vision methods to identify potential landmarks on the surface for Orbit Determination and navigation [18]. A peculiar example of this technique is the Japanese mission Experimental Geodetic Satellite (EGS), launched in 1986 [19]. Essentially, the spacecraft was a sphere all covered with mirrors which permitted the reflection of laser pulses from the ground (Fig. 1.2).

Figure 1.2. EGS Spacecraft [2]

1.1.2 Radars and lasers

Radar and lasers are already widely used for positioning and represent a useful tool for geodetic studies. An example of Satellite Laser Ranging implementation are the missions Starlette and Stella (1975 and 1993) [20], two identical spacecrafts whose precise tracking lead to accurate detection of ocean tides higher wavelengths. CNES specifically designed them in order to be weakly affected by other perturbations like Solar Radiation Pressure (SRP) and atmosperic drag. Radars are widely used in satellite altimetry and for Doppler ranging. A fitting example of the latter is the DORIS technology, which is an up-link device Doppler system. The receiver is placed into the spacecraft while 50 ground beacons allow for geocentric positioning with a precision of $1 - 2$ cm. Another one is the Deep Space Network (DSN) radio technology. Thanks to its accuracy, the Gravity field of Jupiter has been finely estimated in the Juno mission, whose velocity was determined with an error of 0.001 mm s^{-1} [21]. Satellite altimetry has been mainly achieved using radars, but recent missions started to use lasers for altimetry purposes. The mean sea level was measured with 1 cm accuracy by the laser altimeter in the ICESat mission by NASA [22]. These performances make them a crucial tool for gravity field modeling and mapping.

The concept of radar or laser ranging is to measure the time inter-passed between the emission of a electromagnetic pulse and the receiving of its reflection. In this way, neglecting the relativistic effects, it is easy to infer the range of the reflecting body [3]:

$$\Delta r = \frac{1}{2} c \Delta t \tag{1.1}$$

where c is the speed of light and Δt is the time measured. Radar frequencies can be used in any weather conditions, however they will be affected but atmospheric refraction. Lasers on the other hand will minimally suffer from that and thus have way higher accuracy. This method can be used both in Earth-to-space(E2S) and Space-to-space (S2S) configurations, making it a suitable choice for inter-spacecrafts ranging tool.

Another way to exploit e.m. signals is using the Doppler method. When a signal is transmitted from the satellite to the ground station (or viceversa), the relative velocity between the two will induce a frequency shift in the reflected signal ruled by the Doppler effect equation [3]:

$$f_r(t) = f_s(1 - \frac{1}{c}\frac{ds}{dt}) \tag{1.2}$$

where f_r is the reflected signal frequency, f_s is the initial signal frequency, c is the speed of light and $\frac{ds}{dt}$ is the relative velocity between the source and the satellite. Being used to extract the range-rate, this formula is also used to compute the range. Referring to Fig. 1.3 the doppler positioning requires 2 measurements or passages for the problem to be solved. A single measurement defines a hyperbolic region of possibles location of the receiver, while the intersection of 2 non redundant hyperbolic regions define the receiver coordinates.

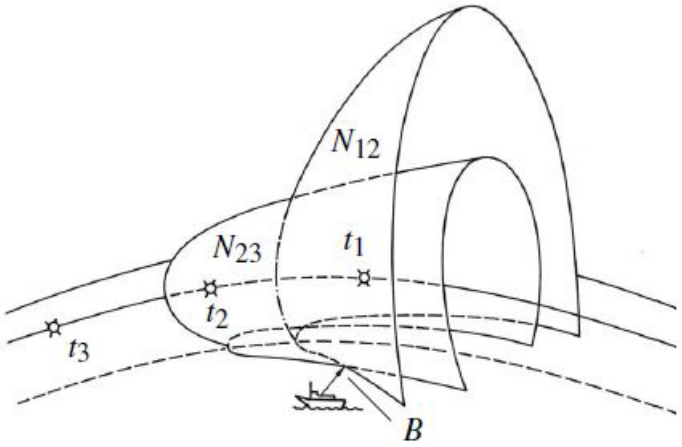

Figure 1.3. Doppler positioning measurement [3]

In satellite altimetry, the radar signal is reflected by the sea surfaces and the echo measurement allows for the determination of the satellite altitude. The measured altitude a_0 can be compared with the theoretical altitude h computed with respect to the reference ellipsoid when the orbit is known, their discrepancy is defined as the mean sea level M or geoid (i.e. the equipotential surface that accounts for both, potential and centrifugal potential).

$$M = h - a_0 \tag{1.3}$$

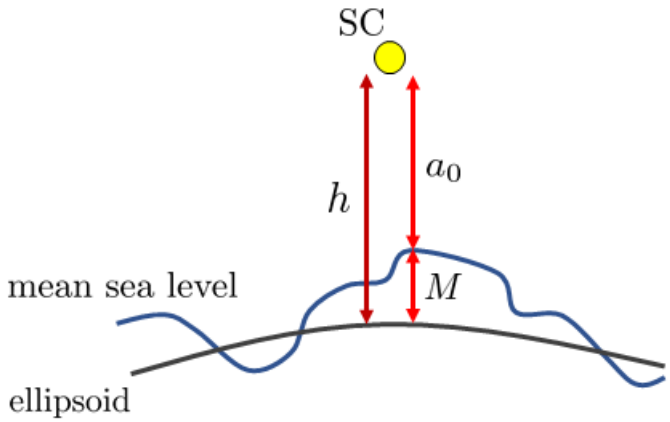

Figure 1.4. Satellite altimetry

1.2 Gravity field determination in past missions

In the last 25 years, the introduction and developement of new concepts gave the possibility of accurately map the Earth gravity field (EGF). These ideas, proposed by Rummel et al. [23], are the Satellite-to-Satellite Tracking (SST) and Satellite Gravity Gradiometry (SGG). The determination of the gravity field is achieved by tracking the relative motion of test masses (i.e. satellites). SST is also defined in two concepts, the SST-HL (high-low) and SST-LL (low-low). In the case of SST-HL, measurements are obtained by high orbiting GPS satellites, to extract the 3D acceleration measurement in the low Earth's orbiter (LEO). For SST-LL the acceleration difference over the inter-satellite distance and in the line-of-sight (LOS) of the two low Earth's orbiters is measured. In the case of SSG it is the measurement of acceleration differences in 3D over the time baseline of the gradiometer.
One example of this is the CHAMP mission, that proved the SST concept effective by improving the models available at the time. GRACE was used to test the SST-LL concept, leading to the improvement of long wavelength coefficients and to the estimation of time varying gravitational perturbations due to water and ice movements and sea level. The GOCE mission was a spacecraft designed to automatically counteract the drag forces unlike CHAMP and GRACE that used accelerometers to measure non-gravitational forces. A more refined technology lead to big improvements on the short wavelengths estimation of the gravity field. The technology of GRACE has been also used for the GRAIL mission from NASA, that enabled a fine estimation of the Moon gravity field, and the GRACE-FO mission, that employs laser ranging technology to continue the tasks of its predecessor [23] [24]

1.3 Small Solar System bodies

The Small Solar System bodies (SSSBs) are defined by the International Astronomical Union (IAU) as all other objects except satellites, orbiting the Sun - that is excluding

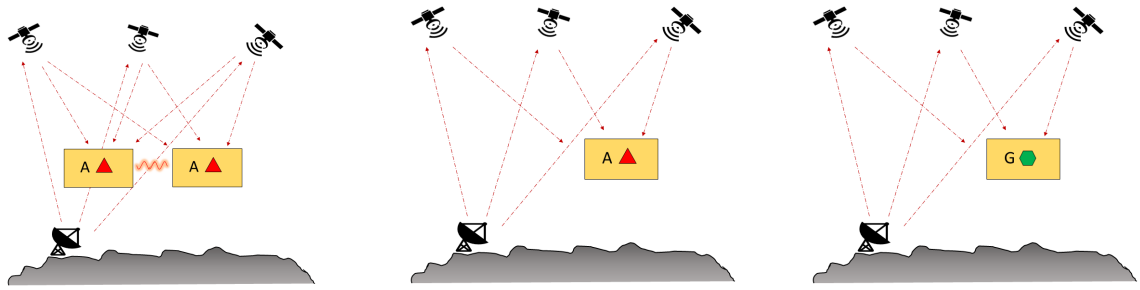

(a) SST-LL (b) SST-HL (c) SGG

Figure 1.5. Satellite tracking and gradiometry

planets, small planets [25]. In practice, the SSSBs are the asteroids and the comets that are focus of this research. Our Solar System originated from a disk of space dust that was rotating around the Sun. Those leftovers became planets, asteroids and comets. Most of the known asteroids are located in the Kuiper belt and while many of them are formed by loose pieces of rubble, others like Vesta and Ceres – the largest bodies in the Main Belt – have a layered interior, with denser material in their cores that proves they would become major planets if only they had enough material [26]. Due to their common origin, the study of asteroids can give insights about the formation of the planets themselves.

Furthermore, the composition of asteroids includes a number of heavy materials like iron, nickel, gold and platinum. For this reason scientists are trying to exploit the presence of these elements for restock and resupply purposes in future exploration missions [27].

Another concern about asteroids is an planetary impact with one of them, that may cause local devastation as already happened in 2013 Chelyabinsk event or in the Tunguska event [28]. Several models tried to estimate the return time of an asteroid impact depending on its size, and it's reported that the return time of a Tunguska-like event is between 300 to 3000 years [27]. Luckily, the impact probability gets lower as the size of the asteroid increases. For the aforementioned reasons, several missions were and are being conceived with the objective of the study of asteroids.

Asteroids are characterized by irregular shape as their mass is too small to generate a gravitational pull strong enough to reach spherical form, and their surface is often modified by impacts. They can have a solid internal structure, indicating that the core somehow melted in the past; while others are just rubble piles held together by their own gravity [26]. Their orbits can be hyperbolic or elliptical and mostly move in the same direction as the planets [29].

1.3.1 Missions to SSSBs

Several methods and missions, like the aformentioned ones, made the Earth's gravity models significantly improve. On the other hand, these methods require very precise measurements that can mostly be achieved in Earth environment, makes them not

adapt for small body applications. After a brief introduction about small bodies, this paragraph will cover past small bodies missions that served the scope of their gravity field modeling.

The NASA mission NEAR was a milestone in this context, as was the first one to orbit and study a minor body (Eros 433 [30]). This mission used laser ranging and optical landmark tracking to estimate a constant density shape model of the asteroid. After that, this model was employed for OD and allowed the estimation of the gravity field up to order and degree 15 and of the internal structure of the body.

Hayabusa was a mission from JAXA, directed to asteroid Itokawa, its objective was to test technologies to obtain and return samples from the surface of an asteroid. In this mission the spacecraft did not orbit the body, but hovered above it being it's trajectory on the radial line connecting the Earth with Itokawa. Thanks to imaging and features tracking the global shape of the body was determined, then combining data from laser altimetry, cameras and range-Doppler, also mass and density were estimated. Using similar technologies, NASA mission DAWN orbited Ceres and Vesta and successfully retrieved shape models and gravity fields using landmark tracking and Doppler tracking. [31]

The Rosetta mission, the first comet rendez-vous achieved, was used by the Radio Science Investigations experiment to show how the Doppler effect on the carrier wave of the Transmission Telecommunication and Control system could be exploited determine the mass, density and basic harmonics of the comet. In the study of Patzold et al [32] is also underlined the non-negligible effect of the comet out-gas in the perturbing acceleration.

OSIRIS-REx is an ongoing NASA's mission that began in 2016. The key science objectives are return and analyse a sample from Bennu's surface, map the asteroid, document the sample site, measure the orbit deviation due to the Yarkovsky effect and compare observations at the asteroid to ground-based observations [33]. From the mission plan, the window for departure from the asteroid will open in March 2021 and OSIRIS-REx will return to Earth in September 2023. McMahon et al. [34] explain how radiometric tracking data with landmark tracking and altimetry data are exploited to obtain the harmonics up to 4th degree. More recently, Scheeres et al. [35] have proposed to use the particles ejected from the asteroid, which would allow to estimate the gravity field up to degree 8 or 9.

The future NASA mission Psyche (launch scheduled in 2022), targeted to the metal asteroid 16 Psyche, will also exploit radio science technology (X-band), i.e. the DSN, for precise Orbit Determination purposes [36].

In this work, with formation flying architecture is intended two spacecraft orbiting around a target and the secondary spacecraft, called child-ship, moves in a fixed relative trajectory with respect to the main satellite, called mother-ship. The satellites play the role of a "virtual satellite" that should provide previously unobtainable science data, using relatively cheap satellites. Multiple scientific instruments often present competing and conflicting requirements on one satellite design and its operation.

Separating scientific payloads onto several simpler single-string satellites, especially with small satellites, can accomplish the same complex missions without the added design and operational overhead. Another reason to use small satellite's formation flying is the flexibility of the scientific instruments which can often be increased by expanding the effective observation baselines. [37]

Different authors are investigating solutions to study the dynamical environment of small bodies using more than one spacecraft and different type of measurements with or without the need of the DSN.
Leonard et. al [38] found that two spacecraft orbiting an asteroid can estimate at the same time the gravity field of the central body and the state of the spacecraft.
Hesar et. al [39] combines the use of satellite to satellite radiometric measurement to the on-board optical navigation.
Proposals studied by Atchinson [40] and Ledbetter et al. [41] involve the idea of deploying a swarm of probes tracked from a chief, that is radiometrically tracked by DNS, while flying-by the asteroid. The short duration of the observations enabled the estimation of the mass of the asteroid. [40].
Fujimoto et al. [42] proposed a mission architecture which consists of a swarm of optically trackable miniaturised satellites ejected by two chief spacecraft. The particles perform a close-approach hyperbolic fly-by, while the two spacecraft remain at safe distance.

1.4 Thesis outline

The thesis organisation is hereby briefly presented:

- **Chapter 1**: introductory remarks about the context of this work and generalities about the rationale of asteroids study are presented, while providing the aims and the novelties proposed in this research.
- **Chapter 2**: in this chapter previous missions about gravity field determination are treated to provide the background needed to highlight critical points to be overcome; moreover generalities about small solar system bodies and in particular asteroids are presented, while focusing on Eros 433 generalities, whose model was used to generate the simulations obtained throughout the research.
- **Chapter 3**: the available technologies to obtain the measurements treated in this work are presented and contextualised in the scope of the missions that exploited them.
- **Chapter 4**: theoretical tools for gravity field determination are explained in detail, namely the selected reference frames, the gravity field models, and the optimisation techniques that constituted the framework implemented in this research.
- **Chapter 5**: theoretical tools for orbit propagation are addressed, focusing on the problem of multi-spacecraft integration techniques. In particular, the problem of the catastrophic cancellation will be addressed to make a comparison between the relative coordinates propagation method proposed by Encke and an independent absolute coordinates propagation approach, in the context of close formation flying.
- **Chapter 6**: here the general algorithm used to produce the significant results is presented along with its hypothesis and the performance index selected to evaluate the quality of the solutions. Moreover the swarm configurations adopted are reported and explained, followed by the presentation of the first important results obtained when analysing only pairs of space-crafts belonging to the aforementioned swarming approaches.
- **Chapter 7**: this chapter contains the most important results of this research, addressing the questions posed at the beginning of it. Results for complete swarms optimisations are reported, investigating the improvement of the solutions for an increasing swarm size. Strategies to the refinement of the solutions are proposed such as an outliers rejection algorithm for pre-determination swarm data filtering. Moreover the sensitivity of the model to the noise level, the observation time and the size of the orbits is analysed. A brief discussion about the robustness to the SRP perturbation, not included in the model, follows. To conclude, a statistical assessment of the solution quality is reported to determinate which of the measurements strategies generate the best outcomes.
- **Chapter 8**: a summary of all the work presented throughout the dissertation is presented along with suggestions about future developments.

Novel contents and past works

The main focus of this research was to evaluate the performances of the swarm approach to the gravity determination problem. As a direct continuation of the research proposed by Guardalà [43], who studied the problem of single-spacecraft gravity field determination in planetary and asteroidal environment, this work is aimed to expand the methods previously used, and to introduce new ones, to build a simulation framework to test the performances of multi-spacecraft gravity field determination based on relative measurements. In particular, the batch estimation methods were augmented, in order to take into account relative position measurements. Moreover an outlier rejection algorithm was implemented to discard bad satellites from the data batch. Finally, goal was to verify which kind of measurement strategy would be the most feasible in case of a real mission scenario.
In previous works like in Bassani [44] and D'Amico et al. [45], the problem of multi-spacecraft estimation was addressed using sequential estimation methods, namely Extended Kalman Filters, and where semi-analytical formulations are used to formulate the problem, i.e. the conversion between the osculating elements and the relative orbital elements are employed to describe the relative dynamics. These methods proved to be capable to estimate a subset of zonal harmonic coefficients. This research is on the other hand focused onto a numerical approach capable of identifying a whole subset of gravitational parameters of the spherical harmonics expansion. Moreover the sequential estimation approach was discarded for the batch estimation one since it is assumed that no real-time estimation is needed. The same estimation method was also studied to directly identify mascon models starting from measurement data. As already done by Guardalà [43], a semi-analytical approach for relative position orbit propagation was introduced, namely the Encke's method, however it was only treated for Keplerian orbits. In this case it was implemented and tested for non-Keplerian (i.e. perturbed) gravitational environments. Moreover a novel gravity field determination algorithm was proposed, derived from the Orbit Determination algorithm of Nayfeh [1].

Chapter 2

Modeling of the gravity field

This chapter recalls the theoretical tools and the models that will be used throughout all the research work. In particular, a description of the mathematical modeling framework is presented: the reference frames selected, the types of gravitational field models.

2.1 Reference frames

Firstly, let us define the reference frames used in the building of this model. Since the spacecrafts will move about an asteroid, 2 main reference frames are employed, whose origins are fixed to the center of mass of the asteroid:

Asteroid Centred Inertial (ACI) that is analogue to the Earth Centered Inertial (ECI) for Earth. For the latter, the system has its centre in the Earth, the x axis in the direction of the vernal equinox at J2000 epoch and the z component in the direction of the axis of rotation.Accordingly, the ACI is an inertial reference frame identified by the Cartesian triplet $\hat{\mathbf{I}}, \hat{\mathbf{J}}, \hat{\mathbf{K}}$ and origin in the center of the asteroid. The $\hat{\mathbf{K}}$ axis is aligned with the spin axis of the asteroid and the plane containing $\hat{\mathbf{I}}$ and $\hat{\mathbf{J}}$ is the equatorial plane.

Asteroid Centred Asteroid Fixed (ACAF), analogue to the ECEF for Earth, has its axes fixed to the spinning body, where the first one is directed towards the largest dimension of the asteroid in the equatorial plane (considered to be the prime meridian for the asteroid). It's identified by the Cartesian triplet $\hat{\mathbf{i}}, \hat{\mathbf{j}}, \hat{\mathbf{k}}$ where $\hat{\mathbf{K}} = \hat{\mathbf{k}}$.

Assuming a constant and known angular rate of the spinning body, it's straightforward to write the transformation from one frame to the other, using the rotation matrix associated to the third axis:

$$\begin{bmatrix} \hat{\mathbf{i}} \\ \hat{\mathbf{j}} \\ \hat{\mathbf{k}} \end{bmatrix} = \begin{bmatrix} \cos(\omega_{body} t) & \sin(\omega_{body} t) & 0 \\ -\sin(\omega_{body} t) & \cos(\omega_{body} t) & 0 \\ 0 & 0 & 1 \end{bmatrix} \begin{bmatrix} \hat{\mathbf{I}} \\ \hat{\mathbf{J}} \\ \hat{\mathbf{K}} \end{bmatrix} \tag{2.1}$$

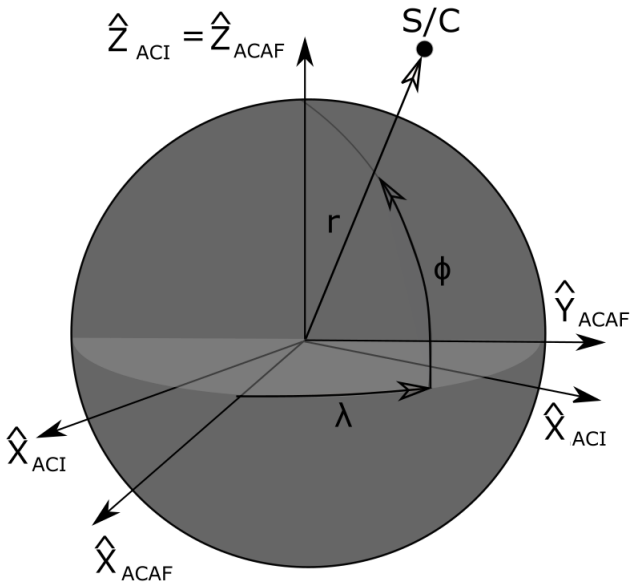

Figure 2.1. Asteroid reference frames

2.2 Gravity field models

The mathematical definition of the gravitational field is of crucial importance when modeling the dynamics of a satellite about an irregular body. It is known that as a first approximation, the motion of a satellite under the influence of a gravitational field is ruled by the simple law:

$$\ddot{\mathbf{R}} = -\frac{GM_{body}}{R^2}\hat{\mathbf{R}} = -\frac{\mu_{body}}{R^2}\hat{\mathbf{R}} \tag{2.2}$$

where M_{body} is the mass of the central body, source of the gravitational field (i.e. asteroid or planet), G is the universal gravitational contant, $\hat{\mathbf{R}}$ is the satellite position unit vector, μ_{body} is the central body gravitational parameter. The solution of this second order differential equation, which resembles an undamped harmonic oscillator, are trajectories that result from conic sections with fixed plane. This is the so called Keplerian motion. This result holds true only in case the source is perfectly uniform in density and shape, such that the gravitational field generated is a radially symmetric one. Even though this hypothesis can never hold in a real-life scenario, keplerian motion can be used to study planetary orbits as a first approximation, due to their more uniform shape. Way different situation is to study orbits around small and irregular bodies whose gravitational field is way far from a radially symmetrical one. In these cases, it can be convenient to write the dynamics of the satellite as influenced by the keplerian gravitational force plus a perturbation term A_p that models the deviation from the spherical field case:

$$\ddot{\mathbf{R}} = \hat{\mathbf{R}} = -\frac{\mu_{body}}{R^2}\hat{\mathbf{R}} + \mathbf{A_p} \tag{2.3}$$

It's worth noting that the magnitude of the perturbation term is usually small for planets, for instance it's about three orders of magnitude smaller than the keplerian acceleration in the Earth case, while the magnitudes can be comparable when the shape of the body is highly irregular like for asteroids. It's also important to point out that the perturbing term A_p can be used to model any kind of perturbation influence on the spacecraft, like Solar Radiation Pressure (SRP) and atmospherical drag if there's any. In particular, the SRP influence on the dynamics will be studied in a latter section according to this expression to highlight the relative influence of both kind of perturbations.

In the case of non-uniform gravity field, the term A_p can be modeled according to different methods. The two most important ones, that apply to the scope of this dissertation, are:

- Expansion in spherical harmonics
- Mascon Models

2.2.1 Potential field expansion in spherical harmonics

When studying Keplerian orbits, it can be shown that the gravitational acceleration $\ddot{\mathbf{R}}$ can be computed as the gradient of a scalar field U, resulting in an easy expression for U:

$$\ddot{\mathbf{R}} = \nabla U \tag{2.4}$$

$$U = \frac{\mu}{R} \tag{2.5}$$

Where R is the modulus of the position vector $\mathbf{R}$. The expression for the potential field can be generalized for a given mass distribution as the integral sum of infinitesimal contributions yield by mass elements:

$$U = G\int_V \frac{\rho(\mathbf{S})}{\|\mathbf{R}-\mathbf{S}\|}dV \tag{2.6}$$

where $\rho(\mathbf{S})$ is the function describing the density distribution inside the body V and S is the position vector of the infinitesimal mass element dm.

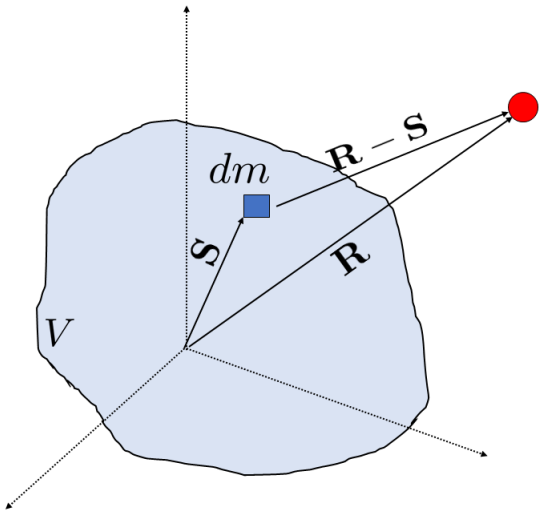

Figure 2.2. Infinitesimal contribution to gravity potential

As shown in Montenbruck and Gill [46], the integral evaluation can be done expanding the inverse of the distance using a series of Legendre Polynomials. According to this method, the expression for the potential field U can be manipulated to show the contributions of the single spherical harmonics [47]:

$$U = \frac{\mu}{R} \sum_{n=0}^{\infty} \sum_{m=0}^{n} \frac{R_{body}^{n}}{R^{n}} P_{nm}(\sin \varphi) \left(C_{nm} \cos(m\lambda) + S_{nm} \sin(m\lambda) \right) \tag{2.7}$$

where P_{nm} are the Legendre polynomials of degree n and order m, and C_{nm} and S_{nm} are the gravitational -or Stokes- coefficients defined according to the following expressions:

$$\begin{aligned} C_{nm} &= \frac{2 - \delta_{0m}}{M} \frac{(n-m)!}{(n+m)!} \int_{V} \frac{S^{n}}{R^{n}} P_{nm} \left(\sin \varphi' \right) \cos \left(m\lambda' \right) \rho(\mathbf{S}) dV \\ S_{nm} &= \frac{2 - \delta_{0m}}{M} \frac{(n-m)!}{(n+m)!} \int_{V} \frac{S^{n}}{R^{n}} P_{nm} \left(\sin \varphi' \right) \sin \left(m\lambda' \right) \rho(\mathbf{S}) dV \end{aligned} \tag{2.8}$$

where the angles ϕ and λ describe the asteroid-centric latitude and longitude associated to $\mathbf{R}$ while $\phi\prime$ and $\lambda\prime$ are associated to the point $\mathbf{S}$. The Stoke's Coefficients can also be distinguished according to their indices, and they're usually classified into:

- Zonal coefficients when $m = 0$;

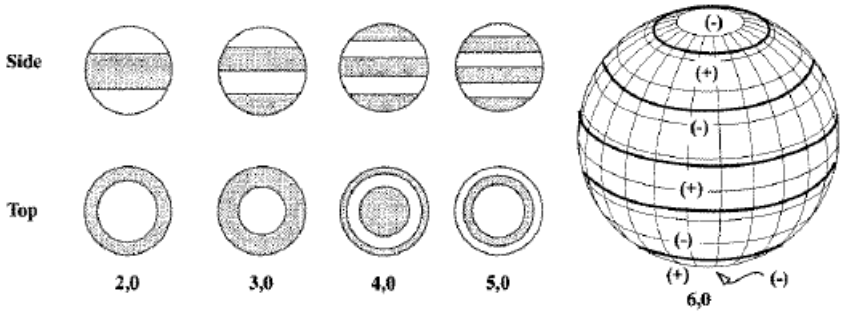

Figure 2.3. Zonal harmonics [4]

- Tesseral coefficients when $m < n$;

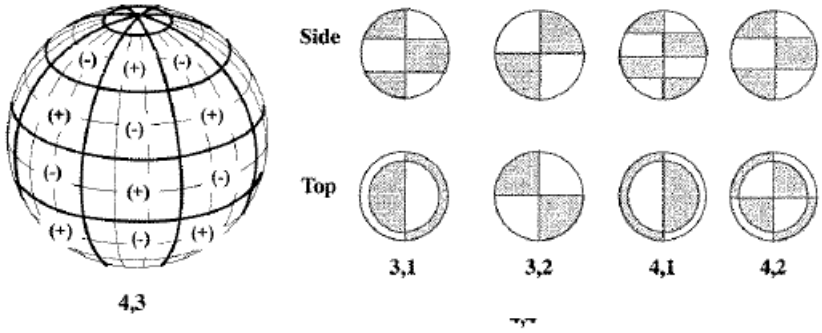

Figure 2.4. Tesseral harmonics [4]

- Sectorial coefficients when $m = n$.

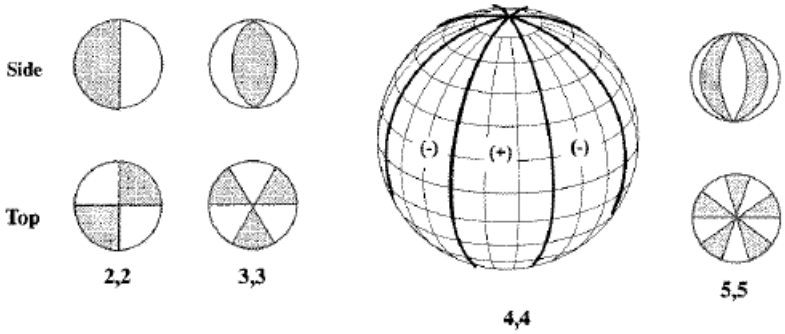

Figure 2.5. Zonal harmonics [4]

Given this, and looking at eq. 2.8, it's easy to show that all zonal $S_{n0} = 0$ since they contain the term $sin(0 \cdot \lambda)$ while the terms C_{n0} are used under the notation $J_n = -C_{n0}$ Equation 2.7 shows that the computation of the gravitational potential requires the evaluation of the spherical coordinates of the satellite and of the Legendre polynomials.

A recursion algorithm proposed by Cunningham, shows that it's possible to skip this passage and offers an efficient method to compute U as a function of cartesian coordinates. Being the ACAF coordinates of the satellite:

$$\begin{aligned} x &= R\cos\varphi\cos\lambda \\ y &= R\cos\varphi\sin\lambda \\ z &= R\sin\varphi \end{aligned} \tag{2.9}$$

Cunningham [48] shows that the potential field can be written in a compact form :

$$U = \frac{\mu}{R}\sum_{n=0}^{\infty}\sum_{m=0}^{n}\left(C_{nm}V_{nm} + S_{nm}W_{nm}\right) \tag{2.10}$$

The advantage of using spherical harmonics expansion is that it allows to truncate the series to desired degree and order that are relevant to the dynamical model that is being studied.

$$U = \frac{\mu}{R}\sum_{n=0}^{\bar{n}}\sum_{m=0}^{n}\left(C_{nm}V_{nm} + S_{nm}W_{nm}\right) \tag{2.11}$$

$$\ddot{\mathbf{R}} = \nabla U \tag{2.12}$$

The terms V_{nm} and W_{nm} depends on the cartesian coordinates of the s/c and can be computed as a function of the cartesian coordinates through a recursion algorithm proposed by Cunningham [48] as it follows:

$$\begin{aligned} V_{mm} &= (2m-1)\left\{\frac{xR}{R^2}V_{m-1,m-1} - \frac{yR}{R^2}W_{m-1,m-1}\right\} \\ W_{mm} &= (2m-1)\left\{\frac{xR}{R^2}W_{m-1,m-1} + \frac{yR}{R^2}V_{m-1,m-1}\right\} \end{aligned} \tag{2.13}$$

$$\begin{aligned} V_{nm} &= \left(\frac{2n-1}{n-m}\right)\frac{zR}{R^2}V_{n-1,m} - \left(\frac{n+m-1}{n-m}\right)\frac{R^2}{R^2}V_{n-2,m} \\ W_{nm} &= \left(\frac{2n-1}{n-m}\right)\frac{zR}{R^2}W_{n-1,m} - \left(\frac{n+m-1}{n-m}\right)\frac{R^2}{R^2}W_{n-2,m} \end{aligned} \tag{2.14}$$

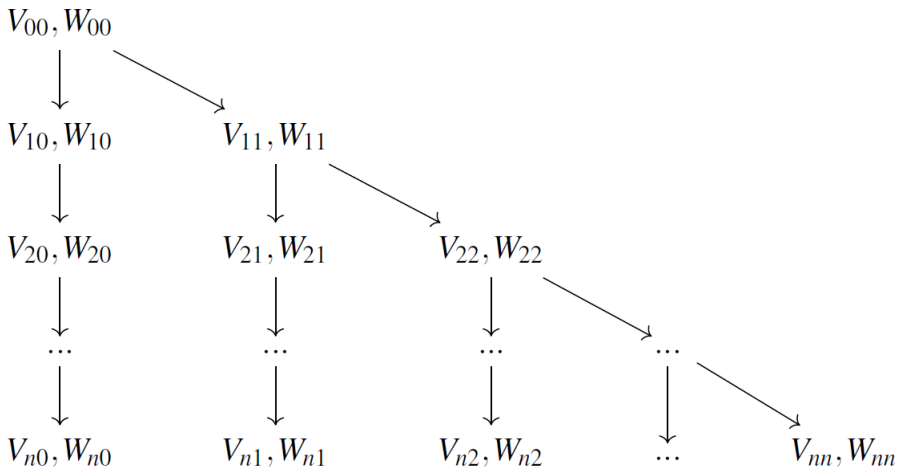

The initialization of the method is based on the computation of the first two terms:

$$\begin{aligned} V_{00} &= \frac{R}{R} \\ W_{00} &= 0 \end{aligned} \tag{2.15}$$

After that, the zonal and the sectorial terms can be recurrently computed according to equations (2.13) and (2.14) respectively. The procedure is concluded when all the terms up to the desired degree and order are computed. Finally, to compute the accelerations in the ACAF frame, the contribution of each harmonic term is computed and linearly superimposed to obtain the total gravitational acceleration:

$$\ddot{x}_p = \sum_{n=1}^{\bar{n}} \sum_{m=0}^{n} \ddot{x}_{nm} \quad , \quad \ddot{y}_p = \sum_{n=1}^{\bar{n}} \sum_{m=0}^{n} \ddot{y}_{nm} \quad , \quad \ddot{z}_p = \sum_{n=1}^{\bar{n}} \sum_{m=0}^{n} \ddot{z}_{nm} \tag{2.16}$$

Where each contribution is computed through the relations:

$$
\begin{aligned}
\ddot{x}_{nm} &\overset{m=0}{=} \frac{\mu}{R^2}\left\{-C_{n0}V_{n+1,1}\right\} \\
\ddot{x}_{nm} &\overset{m\geq 0}{=} \frac{\mu}{R^2}\frac{1}{2}\left\{\left(-C_{nm}V_{n+1,m+1} - S_{nm}W_{n+1,m+1}\right) + \right. \\
&+ \left.\frac{(n-m+2)!}{(n-m)!}\left(+C_{nm}V_{n+1,m-1} + S_{nm}W_{n+1,m-1}\right)\right. \\
\ddot{y}_{nm} &\overset{m=0}{=} \frac{\mu}{R^2}\left\{-C_{n0}W_{n+1,1}\right\} \\
\ddot{y}_{nm} &\overset{m\geq 0}{=} \frac{\mu}{R^2}\frac{1}{2}\left\{\left(-C_{nm}W_{n+1,m+1} + S_{nm}V_{n+1,m+1}\right) + \right. \\
&+ \left.\left.\frac{(n-m+2)!}{(n-m)!}\left(-C_{nm}W_{n+1,m-1} + S_{nm}V_{n+1,m-1}\right)\right\}\right. \\
z_{nm} &= \frac{\mu}{R^2}\left\{(n-m+1)\left(-C_{nm}V_{n+1,m} - S_{nm}W_{n+1,m}\right)\right\}
\end{aligned}
\tag{2.17}
$$

In conclusion, the acceleration vector must be expressed in the ACI frame in order to be taken into account when integrating the ordinary differential equations to propagate the orbital motion.

The magnitude of the gravitational coefficients C_{nm} and S_{nm} covers a wide range of values and they gets increasingly smaller when considering higher orders and degrees. For this reason a normalization of this coefficients is often considered, in order to keep low the range of magnitudes these coefficients can assume .

$$
\left\{\begin{array}{c}\bar{C}_{nm}\\ \bar{S}_{nm}\end{array}\right\} = \sqrt{\frac{(n+m)!}{(2-\delta_{0m})\,(2n+1)(n-m)!}}\left\{\begin{array}{c}C_{nm}\\ S_{nm}\end{array}\right\} \tag{2.18}
$$

2.2.2 Gravitational coefficients of planets and asteroids

To give a quantitative grasp of nowadays available spherical harmonics models, in the following tables the values of C_{nm} and S_{nm} of the Earth and Eros 433 are reported. In particular, the gravity model shown for the Earth is the Earth Geopotential Model 1996 (EGM96), an accurate model of degree and order 360 obtained collecting data from several geodetic missions [7]. While NEAR15A is the 15th degree and order gravity model used for Eros 433 obtained from radiometric tracking (Doppler and range data) and landmark tracking of the NEAR spacecraft [8].

To make a comparison, the spherical harmonics of Eros take vastly higher values with respect to the Earth ones, and that's due to the irregular shape of the asteroid that promotes the insurgence of non-Keplerian forces acting on the s/c. It's worth to note that the coefficients of degree $n = 1$ are zero when the origin of the reference frame is in the centre of mass of the body, while if $\hat{\mathbf{K}}$ is also the spinning axis of the body, i.e. the axis of maximum moment of inertia, the terms C_{21} and S_{21} vanish. In reality, as it happens with the Earth and more evidently with small bodies like Eros,

Table 2.1. EGM96 $\bar{C}_{nm}$ normalised coefficients [7]

n	0	1	2	3
0	$+1.00$			
1	0.00	0.00		
2	$-4.84 \cdot 10^{-4}$	$-1.87 \cdot 10^{-10}$	$+2.43 \cdot 10^{-6}$	
3	$+9.57 \cdot 10^{-7}$	$+2.03 \cdot 10^{-6}$	$+9.05 \cdot 10^{-7}$	$+7.21 \cdot 10^{-7}$

Table 2.2. EGM96 $\bar{S}_{nm}$ normalised coefficients [7]

n	0	1	2	3
0	0.00			
1	0.00	0.00		
2	0.00	$1.20 \cdot 10^{-9}$	$-1.40 \cdot 10^{-6}$	
3	0.00	$+2.49 \cdot 10^{-7}$	$-6.19 \cdot 10^{-7}$	$+1.41 \cdot 10^{-6}$

Table 2.3. NEAR15a $\bar{C}_{nm}$ normalised coefficients [8]

n	0	1	2	3
0	$+1.00$			
1	0.00	0.00		
2	$-4.84 \cdot 10^{-4}$	$-1.87 \cdot 10^{-10}$	$+2.43 \cdot 10^{-6}$	
3	$+9.57 \cdot 10^{-7}$	$+2.03 \cdot 10^{-6}$	$+9.05 \cdot 10^{-7}$	$+7.21 \cdot 10^{-7}$

Table 2.4. NEAR15a $\bar{S}_{nm}$ normalised coefficients [8]

n	0	1	2	3
0	0.00			
1	0.00	0.00		
2	0.00	$1.20 \cdot 10^{-9}$	$-1.40 \cdot 10^{-6}$	
3	0.00	$+2.49 \cdot 10^{-7}$	$-6.19 \cdot 10^{-7}$	$+1.41 \cdot 10^{-6}$

the spinning axis is not fixed, and thus it can't be always aligned with the $\hat{\mathbf{K}}$ axis, so the terms C_{21} and S_{21} although small are not null.

2.2.3 Mascon models

A second, commonly used approach for evaluating asteroid gravitation is to fill the body with point masses ('mascons' - mass concentrations) on an evenly spaced grid [49], or arbitrarily distributed according to different logics. The points are assigned individual masses so that the total asteroid mass is realized. The mascon approach is simple to develop but has several deficiencies, for example mascon gravitation provides no information about whether the field point is inside or outside the body. They are however suited for small bodies due to their ability to model irregular shapes and density distribution, with an arbitrary resolution dependent on the grid scheme and number of mascons employed.

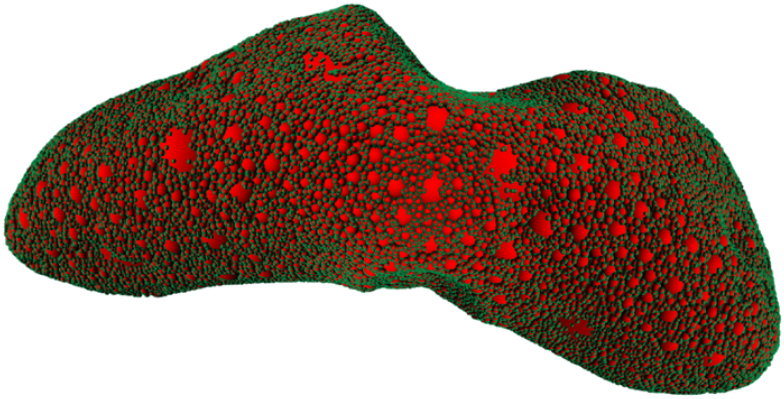

Figure 2.6. Eros 433 mascon model [5]

Mascon models are well capable of representing localized gravitational anomalies while providing a good approximation of the far-field environment. The discretized mass distribution however makes the potential evaluations degrade in proximity of an element. [50]
In the case of lumped masses mascons, he mathematical formulation of the mascon models relies in the discretization of the integral expression of the gravity potential of a distributed body, already reported in the previous section:

$$U = G \int_V \frac{\rho(\mathbf{S})}{\|\mathbf{R} - \mathbf{S}\|} \mathrm{V} \tag{2.19}$$

That is manipulated to obtain:

$$U = G \sum_{n=1}^{\tilde{n}} \frac{m_n}{\|\mathbf{R} - \mathbf{S_n}\|} V_n \tag{2.20}$$

where m_n and V_n are the mass and the volume of the n-th mass element and $\mathbf{S_n}$ its position vector in ACI frame.
Consequentially, the gravitational acceleration $\mathbf{a}$ associated to the mascon model at a certain position $\mathbf{R}$ is:

$$\mathbf{a} = -G \sum_{n=1}^{\tilde{n}} \frac{m_n}{\|\mathbf{R} - \mathbf{S_n}\|^3} (\mathbf{R} - \mathbf{S_n}) V_n \tag{2.21}$$

Even though at the beginning of this research a gravity field estimation method based on Mascon Models was proposed and implemented, this idea was set aside mainly due to computational limitations. It is in fact true that to model with fidelity a gravitational field using mascons, several tens of thousands of point masses would be required. Supposing that the estimation of the model would be based on the retrieval of each mascon mass, that would generate a high-dimensional optimisation problem requiring a very big amount of time for each simulation to be completed. For this reason, the spherical harmonics approach will be the main focus of this research, however a newly defined approach will be shown, using mascon models for gravity field estimation.

Chapter 3

Estimation of the gravity field

The gravity field determination problem can be considered as an augmentation of the orbit determination problem. It is a highly relevant aspect in space mission to rely in the knowledge of the spacecraft position and trajectory with high accuracy. The orbit determination problem and its objective is to estimate the initial state of the spacecraft, i.e. initial position and velocity, such that the propagated trajectory from that state is as close as possible to the sets of measurements available. As reported by Tapley et al. [51], since the observations will always be biased by random and systematic noise, and being the dynamical model used for the propagation a mere approximation of the real phenomena, the orbit determination problem translates into an optimisation one, in which a cost function is defined as the residual yield by the deviation of measured and computed trajectories, while the initial state represent the input to this function. Orbit determination can be achieved with different kinds of approaches, namely the preliminary orbit determination and the statistical orbit determination. The first approach is used when no a priori knowledge of the orbit is available and with limited dataset. On the other hand the latter is used to improve a priori given orbital elements. It's clear then that the preliminary orbit determination is of crucial importance when analyzing unknown objects or newly discovered asteroids or comets.

Several estimation techniques exist to solve this kind of problem, that can be categorized into two groups:

- batch estimation;
- sequential estimation;

While in the batch estimation, the complete set of measurements is readily available to carry on the optimization, so that at each iteration of the method the full dataset is processed to yield the estimation; in the sequential estimation the data is, as the names suggests, sequentially received and it's processed when it becomes available.

The most famous batch estimation technique is the least squares method, but other methods exist like the Bayesian estimation. Sequential estimation techniques mainly include Kalman Filters and Extended Kalman Filters.
According to Tapley et al. [51], both batch and sequential methods produce the same

estimates when the same data and sample times are given. However it's worth to underline the main aspects that must be considered when selecting one or the others:

- Non-linearities: batch estimation methods like LSM involve the linearization of the dynamics so that several iterations are required for convergence; sequential techniques like the EKF overcome this issue reducing the amount of iteration needed.
- Large deviations: both techniques fail when the initial reference trajectory is too far from the observed one.
- Bad measurements: batch estimation allows for the rejection of bad points beforehand.
- Application: Kalman filters are convenient for real-time applications with continous update of the determined orbit, or when memory constraints limit the possibility of storing large amount of data before transmission. Batch processors on the other hand are used for offline estimation, like in satellite geodesy.

3.1 The orbit determination framework

After discussing generally the orbit determination problem, let us introduce the mathematical framework utilized in this context.

Referring to 3.1 the true trajectory is the real track of the satellite, propagated from the true initial state $\mathbf{X}_0$. Then we have the nominal trajectory (or design trajectory), which is the trajectory of the satellite, integrated from the nominal initial state $\mathbf{X}_0$. The best estimated trajectory is the numerical propagation of the orbit starting from the best. estimate initial state $\hat{\mathbf{X}}_0$, i.e. the outcome of the orbit determination process.

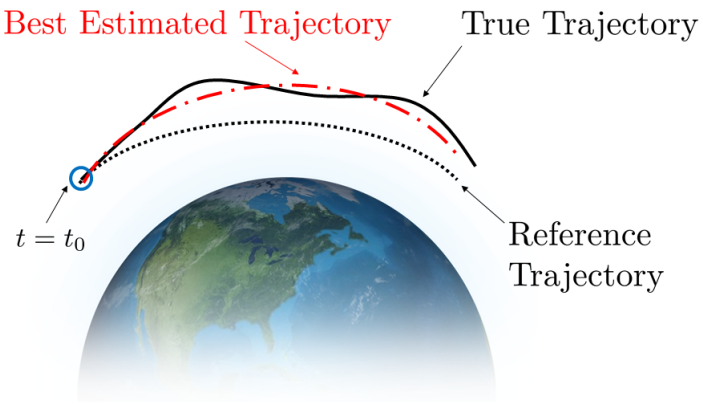

Figure 3.1. Orbit determination

Being the the non-linear dynamics and output equations:

$$\begin{array}{ll} \dot{\mathbf{X}} & = \mathbf{F}(\mathbf{X}, t), \qquad\quad \mathbf{X}(t_0) = \mathbf{X}_0 \\ \mathbf{Y}_i & = \mathbf{G}(\mathbf{X}_i, t_i) + \varepsilon_i \quad i = 1, \ldots, \ell \end{array} \tag{3.1}$$

where $\mathbf{X_0}$ is the unknown n-dimensional state vector at the time t_0, $\mathbf{Y_i}$ is a p-dimensional set of observations that are used to obtain a best estimate $\hat{X}_0$ and ϵ_i represents the errors in the observations.
To exploit readily available methods of linear estimation, the problem needs to be linearized, under the assumption that reference and true trajectory remain sufficiently close. The Taylor series expansion of the dynamical equations, truncated up to order one, is:

$$\begin{aligned} \dot{\mathbf{X}}(t) = \mathbf{F}(\mathbf{X}, t) &\approx \mathbf{F}(\mathbf{X}^*, t) + \left[\frac{\partial \mathbf{F}(t)}{\partial \mathbf{X}(t)}\right]^* [\mathbf{X}(t) - \mathbf{X}^*(t)] \\ \mathbf{Y}_i = \mathbf{G}(\mathbf{X}_i, t_i) + \varepsilon_i &\approx \mathbf{G}(\mathbf{X}_i^*, t_i) + \left[\frac{\partial \mathbf{G}}{\partial \mathbf{X}}\right]_i^* [\mathbf{X}(t_i) - \mathbf{X}^*(t_i)]_i + \varepsilon_i \end{aligned} \tag{3.2}$$

where $[\quad]^*$ indicates that the partial derivative matrix is evaluated on the reference solution integrated from the design initial conditions $\mathrm{X}^*(t_0)$. Besides, the two Jacobians are defined:

$$\mathbf{A}(t) = \left[\frac{\partial \mathbf{F}(t)}{\partial \mathbf{X}(t)}\right]^*; \quad \tilde{\mathbf{H}}_i = \left[\frac{\partial \mathbf{G}}{\partial \mathbf{X}}\right]_i^* \tag{3.3}$$

as well as the state deviation x and the observation deviation y :

$$\begin{array}{l} \mathbf{x}(t) = \mathbf{X}(t) - \mathbf{X}^*(t) \Rightarrow \dot{\mathbf{x}}(t) = \dot{\mathbf{X}}(t) - \dot{\mathbf{X}}^*(t) \\ \mathbf{y}(t) = \mathbf{Y}(t) - \mathbf{Y}^*(t) \end{array} \tag{3.4}$$

Therefore, knowing that:

$$\begin{array}{l} \dot{\mathbf{X}}^* = \mathbf{F}(\mathbf{X}^*, t) \\ \mathbf{Y}_i^* = \mathbf{G}(\mathbf{X}_i^*, t_i) \end{array} \tag{3.5}$$

Eq. 3.1 can be written as:

$$\begin{aligned} \dot{\mathbf{x}}(t) &= \mathbf{A}(t)\mathbf{x}(t) \\ \mathbf{y}_i &= \tilde{\mathbf{H}}_i \mathbf{x}_i + \varepsilon_i \text{ for} \quad i = 1, \ldots, \ell \end{aligned} \tag{3.6}$$

However, one generally does not solve the dynamics with the first equation in 3.6. The problem is most easily formulated in terms of the state transition matrix Φ. The state transition matrix maps the deviations in the state vector from one time to another, for example:

$$\mathbf{x}(t) = \Phi\left(t, t_0\right) \mathbf{x}_0 \tag{3.7}$$

It can be shown that the governing equation for the state transition matrix is:

$$\dot{\Phi}\left(t, t_0\right) = \mathbf{A}(t)\Phi\left(t, t_0\right) \tag{3.8}$$

subjected to the initial conditions $\Phi\left(t_0, t_0\right) = \mathbf{I}$. Now, thanks to Eq. (3.8), it is possible to rewrite also the observation (or output) equation in Eq. (3.6), that in the expanded form will become:

$$\begin{aligned} \mathbf{y}_1 &= \tilde{\mathbf{H}}_1 \Phi\left(t_1, t_0\right) \mathbf{x}_0 + \varepsilon_1 \\ \mathbf{y}_2 &= \overline{\mathbf{H}}_2 \Phi\left(t_2, t_0\right) \mathbf{x}_0 + \varepsilon_2 \\ &\vdots \\ \mathbf{y}_\ell &= \tilde{\mathbf{H}}_\ell \Phi\left(t_\ell, t_0\right) \mathbf{x}_0 + \varepsilon_\ell \end{aligned} \tag{3.9}$$

Like that, all the unknown deviation states are mapped back to only the unknown initial deviation state $\mathbf{x}_0$. Defining:

$$\mathbf{y} = \begin{bmatrix} \mathbf{y}_1 \\ \vdots \\ \mathbf{y}_\ell \end{bmatrix}; \quad \mathbf{H} = \begin{bmatrix} \tilde{\mathbf{H}}_1 \boldsymbol{\Phi}\left(t_1, t_0\right) \\ \vdots \\ \tilde{\mathbf{H}}_\ell \Phi\left(t_\ell, t_0\right) \end{bmatrix}; \quad \varepsilon = \begin{bmatrix} \varepsilon_1 \\ \vdots \\ \varepsilon_\ell \end{bmatrix} \tag{3.10}$$

where $\mathbf{H}$ is the $m \times n$ mapping matrix, Eq. (3.9) can be rewritten in a more compact form:

$$\mathbf{y} = \mathbf{H}\mathbf{x}_0 + \varepsilon \tag{3.11}$$

The least squares method

The linearized system formed by equations (3.7) and (3.8) can't be solved alone for the initial state x_0, since the number m of equations is lower than the $m + n$ unknowns. The least squares method allows for its estimation. A cost or objective function $J(\mathbf{x})$ is defined as the quadratic form of the observation residuals ϵ [51]:

$$J\left(\mathbf{x}_0\right) = \frac{1}{2}\varepsilon^T \boldsymbol{\varepsilon} = \frac{1}{2}\sum_{i=1}^{\ell} \varepsilon_i^T \varepsilon_i = \frac{1}{2}\left(\mathbf{y} - \mathbf{H}\mathbf{x}_0\right)^T \left(\mathbf{y} - \mathbf{H}\mathbf{x}_0\right) \tag{3.12}$$

The minimization of the cost function guarantees the best estimation of x_0 since the quadratic form will always show a global minimum, provided that the matrix $\mathbf{H}$ is full rank. Computing the partial derivatives of J with respect to $\mathbf{x_0}$ and and looking for the critical point leads to the normal equation:

$$\left(\mathbf{H}^T\mathbf{H}\right)\hat{\mathbf{x}}_0 = \mathbf{H}^T\mathbf{y} \tag{3.13}$$

That can be inverted to compute the solution $\hat{\mathbf{x}}_\mathbf{0}$, given that $\mathbf{H}$ is positive definite and full rank n:

$$\hat{\mathbf{x}}_0 = \left(\mathbf{H}^T\mathbf{H}\right)^{-1}\mathbf{H}^T\mathbf{y} \tag{3.14}$$

The cost function can be also defined as:

$$J\left(\mathbf{x}_0\right) = \frac{1}{2}\varepsilon^T\mathbf{W}\varepsilon = \frac{1}{2}\sum_{i=1}^{\ell} \varepsilon_i^T\mathbf{W}_i \cdot \varepsilon_i \tag{3.15}$$

where $\mathbf{W}$ is a weighting diagonal matrix containing the $\mathbf{W_i}$ weights associated to each observation vectors.

$$\mathbf{W} = \begin{bmatrix} \mathbf{W}_1 & 0 & \cdots & 0 \\ 0 & \mathbf{W}_2 & \cdots & 0 \\ \vdots & & \ddots & \\ 0 & 0 & \cdots & \mathbf{W}_\ell \end{bmatrix} \tag{3.16}$$

This is used to include in the optimization trust levels to different observations, such that the observations obtained with greater a priori accuracy will be characterized by a higher value of $\mathbf{W_i}$. Rearranging the terms yields a newly defined normal equation:

$$\hat{\mathbf{x}}_0 = \mathbf{P}_0 \mathbf{H}^T \mathbf{W} \mathbf{y} \tag{3.17}$$

where:

$$\mathbf{P}_0 = \left(\mathbf{H}^T \mathbf{W} \mathbf{H}\right)^{-1} \tag{3.18}$$

The invertibility of the expression required all the parameters in $\mathbf{x}_0$ to be observable. Moreover if an a priori value $\overline{\mathbf{x}}_0$ of the initial state is available, the cost function can be written as:

$$J\left(\mathbf{x}_0\right) = \frac{1}{2} \sum_{i=1}^{\ell} \varepsilon_i^T \mathbf{W}_i \varepsilon_i + \frac{1}{2} \left(\overline{\mathbf{x}}_0 - \mathbf{x}_0\right)^T \overline{\mathbf{W}}_0 \left(\overline{\mathbf{x}}_0 - \mathbf{x}_0\right) \tag{3.19}$$

where $\overline{\mathbf{W}}_0$ is the weighting matrix associated with the a priori value. It can be shown that the solution of the LSM with a priori information is:

$$\hat{\mathbf{x}}_0 = \left(\mathbf{H}^T \mathbf{W} \mathbf{H} + \overline{\mathbf{W}}_0\right)^{-1} \left(\mathbf{H}^T \mathbf{W} \mathbf{y} + \overline{\mathbf{W}}_0 \overline{\mathbf{x}}_0\right) \tag{3.20}$$

Given the mathematical framework, the LSM implementation requires the iterative evaluation of these functions, following the proposed algorithm:

1. Initialize the problem (select an initial guess);

2. Integrate the trajectory and the state transition matrix to obtain the mapping matrix

3. Solve the normal equation and check for the convergence of the process.

If the process converged, i.e. the obtained value for the solution meets some prescribed tolerance, the best estimate is found, otherwise the algorithm must be re-evaluated updating the initial state to recompute the trajectory.
The LSM is not only one kind of batch estimation methods and has some limitations, like the impossibility of using correlated observations, that would lead to a singularity in the normal equation; and the impracticability of utilizing statistical data related to the observation errors. Some methods like the minimum variance estimation and the Bayesian estimation try to overcome these limitations, however these formulations will not be analyzed in this dissertation as they fall outside of the scope of this work, given that the non-linear LSM developed in this research was effectively used to fulfill the thesis objectives.

3.2 Gravity field determination

The problem of estimating the gravitational field is addressed in this research using the batch estimation approach solved by the means of the LSM. In particular, the problem is formulated as an augmentation of the Orbit determination problem, following the steps and ideas developed by Guardalà [43] and Kaula [47].

As commented in the previous section, an optimization problem is developed to estimate the spacecraft orbit about a central body. In a similar fashion, the gravity field determination problem is here formulated as minimization one in which both the initial conditions of the spacecraft and the parameters that characterize the gravity field are part of the optimization vector for the trajectory fitting. In this case the dynamics will be analyzed in the non-linearised form. This is done because theoretically, the non-linear equations makes the convergence easier even with a poor initial guess, that is exactly the case of unknown distant small bodies.

More in the detail, the cost function is now defined as:

$$J\left(\mathbf{X}_0^*\right) = \frac{1}{2}\sum_{i=1}^{\ell}\left(\mathbf{O}_i - \mathbf{C}_i\left(\mathbf{X}_0^*\right)\right)^{\top}\left(\mathbf{O}_i - \mathbf{C}_i\left(\mathbf{X}_0^*\right)\right) \tag{3.21}$$

where observations $\mathbf{C}_i$ and $\mathbf{C}_i$ are both p-dimensional vectors of parameters evaluated at ℓ discrete time instances. The observations are here computed through numerical integration and simulated using the models discussed and with methods later explained, starting from a reference state vector $\mathbf{X}_0^*$.

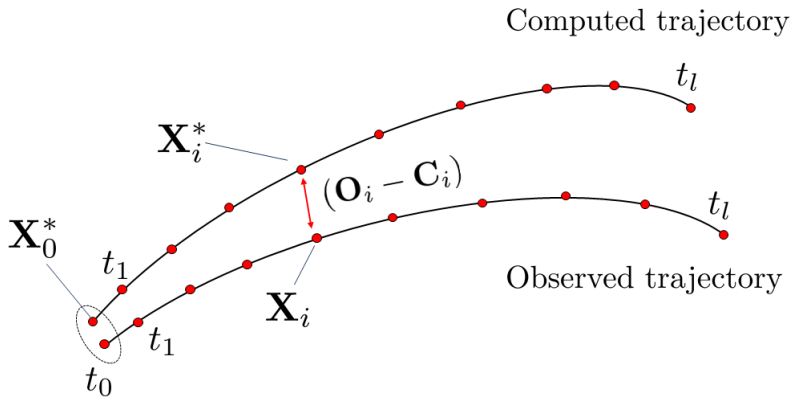

Figure 3.2. Observations and measurements

In a real case scenario, instruments like the ones illustrated in chapter 3, would provide the necessary information to feed to the solver.

For convenience, both the observations and the computed observations are collected in the observations $\mathbf{O}$ and computed observations $\mathbf{C}$, both $\ell \times p$ matrices. For example, the observations matrix is:

$$\mathbf{O} = \begin{bmatrix} \mathbf{O}_1^\top \\ \vdots \\ \mathbf{O}_i^\top \\ \vdots \\ \mathbf{O}_\ell^\top \end{bmatrix} = \begin{bmatrix} \begin{bmatrix} O_1 & O_2 & \dots & O_p \end{bmatrix}_{t=t_0} \\ \vdots \\ \begin{bmatrix} O_1 & O_2 & \dots & O_p \end{bmatrix}_{t=t_i} \\ \vdots \\ \begin{bmatrix} O_1 & O_2 & \dots & O_p \end{bmatrix}_{t=t_\ell} \end{bmatrix} \tag{3.22}$$

In an analogous way, the computed observations matrix is:

$$\mathbf{C} = \begin{bmatrix} \mathbf{C}_1^\top \\ \vdots \\ \mathbf{C}_i^\top \\ \vdots \\ \mathbf{C}_\ell^\top \end{bmatrix} = \begin{bmatrix} \begin{bmatrix} C_1 & C_2 & \dots & C_p \end{bmatrix}_{t=t_0} \\ \vdots \\ \begin{bmatrix} C_1 & C_2 & \dots & C_p \end{bmatrix}_{t=t_i} \\ \vdots \\ \begin{bmatrix} C_1 & C_2 & \dots & C_p \end{bmatrix}_{t=t_\ell} \end{bmatrix} \tag{3.23}$$

$(\mathbf{O}_i - \mathbf{C}_i)$ is the observation residual, that is the difference between the observed and computed trajectories. The n-dimensional state vector at time t_i is now defined as:

$$\mathbf{X}(t_i) = \mathbf{X}_i = \left[\begin{array}{c} X_1 \\ \vdots \\ X_j \\ \vdots \\ X_n \end{array} \right]_{t=t_i} \tag{3.24}$$

So to speak, the objective of the optimisation is to obtain the most accurate value of the unknown reference state vector evaluated at the initial time t_0:

$$\mathbf{X}^*(t_0) = \mathbf{X}_0^*$$

which is the variable of the cost function defined above. It is important to remind that $n \ll \ell \times p$, i.e. there are more equations than variables.

When analyzing precise orbit determination, the state vector contains, the position and velocity of the spacecraft at a given time t_i, those that define the dynamical state of the system:

$$\mathbf{X}_i = \left[\begin{array}{c} \mathbf{R}_i \\ \mathbf{V}_i \end{array} \right]$$

The gravity field determination is achieved considering an extended state vector which includes, not only the actual state of the spacecraft, but also other variables of the OD problem that need to be determined. Those latter, strictly speaking, do not affect the state itself, but rather the integration of the dynamics equations. Hereafter, we will refer to the extended state vector as simply state vector, however this important difference shall be kept in mind.

In gravity field determination, the state vector is augmented including the variables that need to be determined and have influence in the dynamic system integration. In particular, the Earth's gravitational parameter μ and the gravitational coefficients C_{nm} and S_{nm} up to the prescribed subset are added to the initial state vector $\mathbf{X}_0$, as follows:

$$\mathbf{X_0} = \left[\begin{array}{c} \mathbf{R}_0 \\ \mathbf{V}_0 \\ \mu \\ \mathbf{c} \\ \mathbf{s} \end{array} \right] \tag{3.25}$$

where the n_c-dimensional vector $\mathbf{c}$ contains the set of C_{nm} and similarly the S_{nm} are collected in the n_s-dimensional vector $\mathbf{c}$. For brevity, if we consider the case in which a subset of order 2 is used, the vectors $\mathbf{c}$ and $\mathbf{s}$ are, respectively, 3 -dimensional and 2-dimensional, and are defined as follows:

$$\mathbf{c} = \begin{bmatrix} C_{20} \\ C_{21} \\ C_{22} \end{bmatrix}; \quad \mathbf{s} = \begin{bmatrix} S_{21} \\ S_{22} \end{bmatrix} \tag{3.26}$$

The problem of non-linear data fitting was solved in this scope using the Levenberg-Marquadt method (LM). As described in Gavin [52] is one of the most efficients algorithms, as it is an hybridation of the Gauss-Newton method and the gradient descent. Let us briefly discuss it's mathematical formulation.

Being the gradient of the cost function:

$$\begin{aligned} \frac{\partial J}{\partial \mathbf{X}_0^*} &= \sum_{i=1}^{\ell} \left(\mathbf{O}_i - \mathbf{C}_i\left(\mathbf{X}_0^*\right)\right)^\top \frac{\partial}{\partial \mathbf{X}_0^*} \left(\mathbf{O}_i - \mathbf{C}_i\left(\mathbf{X}_0^*\right)\right. \\ &= -\sum_{i=1}^{\ell} \left(\mathbf{O}_i - \mathbf{C}_i\left(\mathbf{X}_0^*\right)\right)^\top \frac{\partial \mathbf{C}_i\left(\mathbf{X}_0^*\right)}{\partial \mathbf{X}_0^*} \\ &= -\sum_{i=1}^{\ell} \left(\mathbf{O}_i - \mathbf{C}_i\left(\mathbf{X}_0^*\right)\right)^\top \mathbf{G}_i \end{aligned} \tag{3.27}$$

where $\mathbf{G}_i$ is the $m \times n$ Jacobian matrix evaluated at time t_i. The Jacobian can be computed analitically when possible, or computed numerically. In this case it's numerically evaluated through central finite differences. The method tries iteratively to find a perturbation $\mathbf{h}_{lm}$ to the parameters $\mathbf{X}_0^*$ that reduces the cost function J, accordingly to the following equation:

$$\sum_{i=1}^{\ell} \left[\mathbf{G}_i^\top \mathbf{G}_i + \lambda_{lm} \operatorname{diag}\left(\mathbf{G}_i^\top \mathbf{G}_i\right)\right] \mathbf{h}_{lm} = \sum_{i=1}^{\ell} \mathbf{G}_i^\top \left(\mathbf{O}_i - \mathbf{C}_i\right) \tag{3.28}$$

where λ_{lm} is the so called damping parameter. Its value is between 0 and 1 and defines which method will give the greater contribution to the solution. The damping parameter is generally initialised to be large (e.g. between 0.1 and 0.01), so that the method performs small steps in the opposite-to-the-gradient direction. If a smaller value of the cost function is achieved, the damping parameter is reduced, otherwise, it is augmented. For small values of λ_{lm} the method is similar to the Gauss-Newton method.

Chapter 4

Swarm propagation

This chapter aims to describe the approaches used in this work to propagate the trajectories of the swarm of satellites. Since the objective is to determine whether it is suitable and convenient to exploit relative position and/or velocity measurements of numerous spacecrafts to improve the solution of the gravity field determination problem, it is of extreme importance to determine how the best quality data can be generated for our simulations.
The most immediate way to approach the problem is to have each spacecraft trajectory independently propagated, starting from the initial conditions of any of them. Then, subtracting the position vectors of each satellite to the position of the mother-ship, you can easily collect data for the relative position at each time instant.

In particular, consider two satellites, SC1 (the primary, or $mother - ship$) and SC2 (the secondary, or $child - ship$ spacecraft) in close formation flying (Fig. 4.1). The relative position vector, also called range vector, is:

$$\mathbf{\Delta R} = \mathbf{R_2} - \mathbf{R} \tag{4.1}$$

where $\mathbf{R}$ is the ACI position vector of SC1 and R_2 is the ACI position vector of SC2. This simple expression entails a fundamental problem related to numerical loss of precision, or catastrophic cancellation [53]. When dealing with floating point arithmetic, the subtraction of two nearly equal numbers generates a reduction in the number of significant digits of the result.
Due to this, if SC1 and SC2 are really close to eachother, the loss of precision that may arise in the evaluation of $\mathbf{\Delta R}$ could reduce the accuracy of the estimation results.

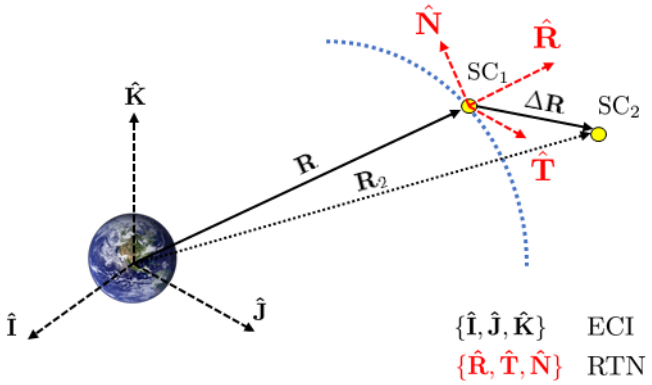

Figure 4.1. Formation flying depiction

Although a number of analytical and semi-analytical methods to propagate the relative motion dynamics, as the ones reported in Casotto [54], this study will focus on analyzing the Encke's method. In particular, the method has been implemented and simulated, and the results compared to the ones obtained in a normal, separate propagation approach.

The performances of Encke's method have already been evaluated in this context referring to keplerian orbits [43], and have proved to generate more accurate relative position data. We will now focus on evaluating the same for perturbed orbits.

4.0.1 The Encke's method

The formulation proposed by Encke allows the propagation of the dynamics of two or more close proximity spacecrafts in the inertial frame, while avoiding the numerical errors previously cited. The method relies in a linearized expression that results in a dynamical system composed by the independent dynamics of the main spacecraft (i.e. mother-ship), and the coupled dynamics of the child-ship, expressed in relative coordinates with respect to the mother [54]. Encke's method was already studied in the previous work by Guardalà [43], where it was implemented for Keplerian relative coordinates propagation only. Here on the other hand, it will be implemented in for the perturbed motion.

Being the perturbed dynamics:

$$\ddot{\mathbf{R}} = -\frac{\mu_{body}}{R^2}\mathbf{R} + \mathbf{P} \tag{4.2}$$

and defining the Newtonian term as:

$$\mathbf{N} = -\frac{\mu_{body}}{R^2}\hat{\mathbf{R}} \tag{4.3}$$

Eq. (4.2) becomes:

$$\ddot{\mathbf{R}} = \mathbf{N} + \mathbf{P} \tag{4.4}$$

The dynamics equations governing the evolution of the relative position vector, namely the relative motion equations, are obtained by simply differentiating the dynamics of the two spacecraft as follows:

$$\Delta\ddot{\mathbf{R}} = \ddot{\mathbf{R}}_2 - \ddot{\mathbf{R}} = \Delta\mathbf{N} - \Delta\mathbf{P} \tag{4.5}$$

where the term $\Delta\mathbf{N}$ represents the differential Newtonian acceleration and $\Delta\mathbf{P}$ the differential perturbation acceleration.
Encke's formulation provides high accuracy computations, by rewriting the relative Newtonian acceleration using an analytical linearization:

$$\Delta\mathbf{N} = -\frac{\mu}{R^3}\{f(q)\mathbf{R} + [1 + f(q)]\Delta\mathbf{R}\} \tag{4.6}$$

where

$$f(q) = q\frac{3(1+q) + q^2}{1 + (1+q)^{3/2}} \tag{4.7}$$

While an elegant expression is available to compute $\mathbf{\Delta N}$, no general expression is there for the perturbing $\mathbf{\Delta P}$, as it depends on the type of perturbations included in the model. As no information is reported in the literature for its evaluation in a complex, high order, gravitational field, the computation is achieved augmenting the already implemented Cunningham algorithm to compute the second order derivatives of the potential field, i.e. the gravity gradient. In particular as a first order approximation is true that:

$$\mathbf{\Delta P} = \frac{\partial \boldsymbol{P}}{\partial \boldsymbol{R}} \cdot \Delta\mathbf{R} \tag{4.8}$$

So that the evaluation of $\mathbf{\Delta P}$ requires the knowledge of the gravity gradient matrix. Being:

$$\frac{\partial \boldsymbol{P}}{\partial \boldsymbol{R}} = \sum_{n,m} \frac{\partial \boldsymbol{P}_{nm}}{\partial \boldsymbol{R}} \tag{4.9}$$

where $\boldsymbol{P}_{nm}$ represents the perturbing acceleration due to the sperical harmonic of order n and degree m.

Using expressions for the terms of degree n and order m derived by Cunningham [48], and being $\ddot{x}$ $\ddot{y}$ and $\ddot{z}$ the cartesian components of the acceleration $\ddot{\mathbf{R}}$:

$$
\begin{aligned}
\frac{\partial \ddot{x}_{nm}}{\partial x} &\overset{(m=0)}{=} \frac{GM_{body}}{R_{body}^3} \cdot \frac{1}{2} \cdot \left\{ (+C_{n0}V_{n+2,2}) - \frac{(n+2)!}{n!} \cdot (+C_{n0}V_{n+2,0}) \right\} \\
&\overset{(m=1)}{=} \frac{GM_{body}}{R_{body}^3} \cdot \frac{1}{4} \cdot \{ (+C_{n1}V_{n+2,3} + S_{n1}W_{n+2,3}) \\
&\quad + \frac{(n+1)!}{(n-1)!} \cdot (-3C_{n1}V_{n+2,1} - S_{n1}W_{n+2,1}) \Big\} \\
&\overset{(m\geq 1)}{=} \frac{GM_{body}}{R_{body}^3} \cdot \frac{1}{4} \cdot \{ (+C_{nm}V_{n+2,m+2} + S_{nm}W_{n+2,m+2}) \\
&\quad + 2\frac{(n-m+2)!}{(n-m)!} \cdot (-C_{nm}V_{n+2,m} - S_{nm}W_{n+2,m}) \\
&\quad + \frac{(n-m+4)!}{(n-m)!} \cdot (+C_{nm}V_{n+2,m-2} + S_{nm}W_{n+2,m-2}) \Big\}
\end{aligned}
$$

$$
\begin{aligned}
\frac{\partial \ddot{x}_{nm}}{\partial y} &\overset{(m=0)}{=} \frac{GM_{body}}{R_{body}^3} \cdot \frac{1}{2} \cdot \{ (+C_{n0}W_{n+2,2}) \} \\
&\overset{(m=1)}{=} \frac{GM_{body}}{R_{body}^3} \cdot \frac{1}{4} \cdot \{ (+C_{n1}W_{n+2,3} - S_{n1}V_{n+2,3}) \\
&\quad + \frac{(n+1)!}{(n-1)!} \cdot (-C_{n1}W_{n+2,1} - S_{n1}V_{n+2,1}) \Big\} \\
&\overset{(m\geq 1)}{=} \frac{GM_{body}}{R_{body}^3} \cdot \frac{1}{4} \cdot \{ (+C_{nm}W_{n+2,m+2} - S_{nm}V_{n+2,m+2}) \\
&\quad + \frac{(n-m+4)!}{(n-m)!} \cdot (-C_{nm}W_{n+2,m-2} + S_{nm}V_{n+2,m-2}) \Big\}
\end{aligned}
\tag{4.10}
$$

$$
\begin{aligned}
\frac{\partial \ddot{x}_{nm}}{\partial z} &\overset{(m=0)}{=} \frac{GM_{body}}{R_{body}^3} \cdot \{ (n+1) \cdot (+C_{n0}V_{n+2,1}) \} \\
&\overset{(m\geq 0)}{=} \frac{GM_{body}}{R_{body}^3} \left\{ \frac{n-m+1}{2} \cdot (+C_{nm}V_{n+2,m+1} + S_{nm}W_{n+2,m+1}) \right. \\
&\quad \left. + \frac{(n-m+3)!}{2(n-m)!} \cdot (-C_{nm}V_{n+2,m-1} - S_{nm}W_{n+2,m-1}) \right\}
\end{aligned}
$$

$$
\begin{aligned}
\frac{\partial \ddot{y}_{nm}}{\partial z} &\overset{(m=0)}{=} \frac{GM_{body}}{R_{body}^3} \cdot \{ (n+1) \cdot (+C_{n0}W_{n+2,1}) \} \\
&\overset{(m>0)}{=} \frac{GM_{body}}{R_{body}^3} \left\{ \frac{n-m+1}{2} \cdot (+C_{nm}W_{n+2,m+1} - S_{nm}V_{n+2,m+1}) \right. \\
&\quad \left. + \frac{(n-m+3)!}{2(n-m)!} \cdot (+C_{nm}W_{n+2,m-1} - S_{nm}V_{n+2,m-1}) \right\}
\end{aligned}
$$

$$
\frac{\partial \ddot{z}_{nm}}{\partial z} = \frac{GM_{body}}{R_{body}^3} \left\{ \frac{(n-m+2)!}{(n-m)!} \cdot (+C_{nm}V_{n+2,m} + S_{nm}W_{n+2,m}) \right\}
$$

Here V_{nm} and W_{nm}, which follow from the recurrence relations (2.13) and (2.14), are the same quantities that are used in the computation of the acceleration. If the partial derivatives of the acceleration due to geopotential coefficients up to C_{nn} and S_{nn} have to be calculated then $V_{v\mu}$ and $W_{v\mu}$ are required up to degree and order $n+2$.

For a non-rotating body the expressions derived so far would directly represent the desired partial derivatives. Due the common rotation of celestial bodies, some additional transformations are, however, required, since the components of $\mathbf{R}$ and $\ddot{\mathbf{R}}$ in the previous refer to the ACAF reference frame. Using indices "ACI" and "ACAF", the desired partial derivatives in the space-fixed reference system are given by:

$$\left(\frac{\partial \ddot{\mathbf{R}}}{\partial \mathbf{R}}\right)_{\text{ACI}} = \mathbf{U}^{-1}(t) \cdot \left(\frac{\partial \ddot{\mathbf{R}}}{\partial \mathbf{R}}\right)_{\text{ACAF}} \cdot \mathbf{U}(t) \tag{4.11}$$

where $\mathbf{U}$ describes the time-dependent transformation to Earth-fixed coordinates according to:

$$r_{\text{ACAF}} = \mathbf{U}(t) \cdot \mathbf{R}_{\text{ACI}} \quad \text{and} \quad \ddot{\mathbf{R}}_{\text{ACI}} = \mathbf{U}^{-1}(t) \cdot \ddot{\mathbf{R}}_{\text{ACAF}} \tag{4.12}$$

4.0.2 Comparison

The separate propagations method and the Encke's formulation are here compared to understand which one produce the best results.
It's worth to underline that, since Encke's formulation is based on a linearized approach, the quality of its solutions will depend on the relative distance between the two satellites. More in detail, it is expected that the solution degrades when the satellites are too far from eachother, where the linearization of the dynamics and of the gravity gradient give inaccurate results.

The propagation accuracy has been computed utilizing trajectories computed with the separate propagation methods evaluated with quadruple precision aritmethics and stringent integration tolerances. This has been done to obtain a baseline solution that contains a higher number accurately computed of significant digits, to be compared with double precision propagations. This was achieved using the Julia programming language, that allows for the resolution of mathematical problem with multiple precision variables. The residual between the reference relative position solution and the specific formulation is computed at a given time as it follows:

$$err = ||\boldsymbol{\Delta}\mathbf{r}_{ref} - \boldsymbol{\Delta}\mathbf{r}|| \tag{4.13}$$

where the subscript ref refers to the quadruple precision computed trajectory. Since the scope is analyze this in a perturbed gravitational environment, it's also worth to define the same metrics for the relative accelerations, that in the Encke's method is computed in a linearized way through the aforementioned term $\mathbf{\Delta P}$:

$$e\ddot{r}r = ||\mathbf{\Delta\ddot{r}}_{ref} - \mathbf{\Delta\ddot{r}}|| \tag{4.14}$$

Trajectories are simulated in Earth gravitational environment according to the following osculating keplerian elements of the mother-ship:

Table 4.1. Mother-ship keplerian elements

SC	a[km]	e[$-$]	i[deg]	ω[deg]	Ω[deg]	ϑ[deg]
Mothership	7000	0.1	30	30	30	0

The secondary is placed on the same orbit. The objective is to study how $e\ddot{r}r$ behave for increasing distance between the two satellites, i.e. for an increasing $\delta\theta$. Results shown in Figure 4.3. underline that, although the relative acceleration deviation of the two methods is almost negligible when $\delta\theta$ is lower than 0.001, its approximation rapidly degrades when the distance increases, suggesting that the linearization of the gravity gradient is results in a loss of information that reflects in the accuracy of the relative position output, that also gets worse for increasing distance.

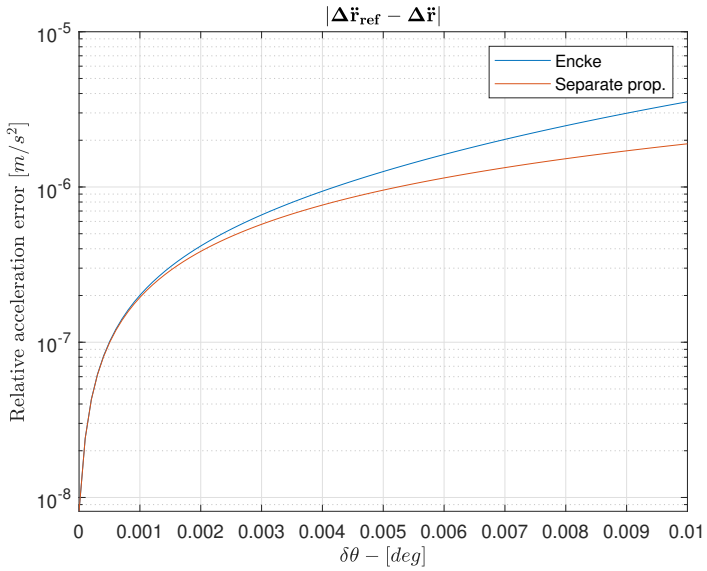

Figure 4.2. Accelerations comparison

Moreover, simulations were conducted for large time-spans, using both propagation methods. The objective was to compare the obtained relative trajectories with a *true* trajectory, computed using higher precision and integration tolerances ($\mathbf{\Delta r_{ref}}$).
Using a $\delta\theta = 10^{-5}$deg, that translate to a relative distance between the satellites of roughly 1.4m, results show that Encke's method performs slightly better then the independent separation method for the first 1/2 orbit in this simulation. After that, its solution degrades to worse values with respect to the reference, suggesting that for long integration times the linearization becomes less accurate, leading to the need for a reinitialization of the problem.

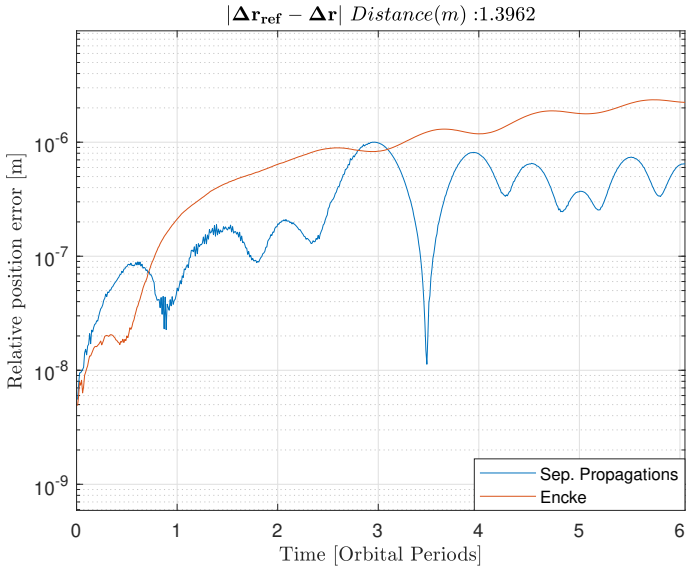

Figure 4.3. Relative position error comparison

In the view of these facts, although the Encke's method gives good results when satellites are flying very close to eachother, all the simulations done to produce the meaningful results reported in this dissertation are computed using the separate propagation method, as no close proximity flight configuration was considered for the swarm deployment, however further deepening on this topic should be addressed in future researches.

Chapter 5

Gravity Field Determination with relative measurements

The first main research objective will be addressed in this chapter, that is to show that the usage of satellites relative position data, with respect to the primary one, can enhance the quality of the solution of the gravity field estimation problem.
It will be firstly described the simulation framework constructed to investigate the questions of this research, then the first results of gravity field determination exploiting the relative measurements between two spacecrafts will be reported and discussed. More in detail, it will be discussed the algorithm finally used to estimate the gravity field of asteroids with multiple spacecrafts, as well as its hypothesis and the metrics utilised to evaluate the *quality* of the solutions.
An explanation of the swarm configurations will follow. After that, a first set of simulations is reported, to study the performance of the algorithm using the different kinds of measurements, when considering only couples of satellites extracted from the swarm configurations implemented.

Eros 433

Let firstly introduce now the asteroid whose model was used as a reference case for the simulations carried during this research. The main reasons are:

- Its highly irregular shape;
- Enough mass to allow for orbiting around;
- Known and available gravity field model, obtained during the NEAR mission.

Eros 433 was discovered in August 1898, and its characterized by a rather uniform structure [30] and low density, indicating a moderate porosity. Its gravitational pull is 1600 times weaker than the Earth's and it's shape is very elongated (5.1). In table 5.1 the main aspects of Eros 433 are reported.

Figure 5.1. Eros 433 pictures [6]

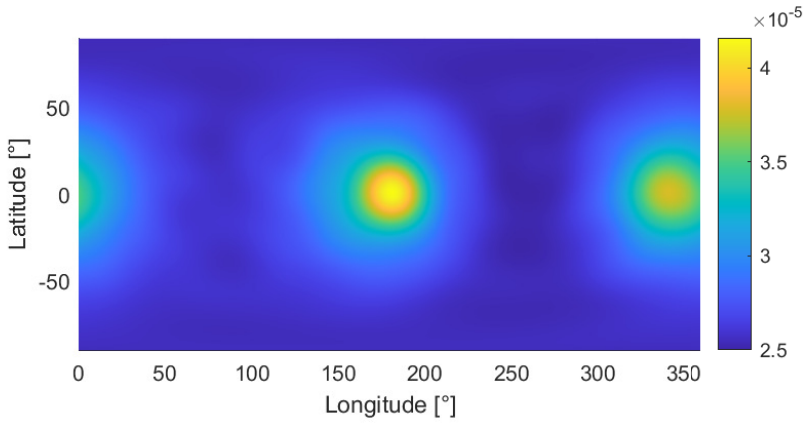

Figure 5.2. Eros 433 potential function computed on a sphere of radius 16 km - NEAR15A model

Table 5.1. Eros 433 characteristics

Parameter	Value
Size	33 km × 13 km × 13 km
Mean Density	2.7×10^3 kg m^{-3}
Mass	6.7×10^{15} kg
Surface Gravity Acceleration	$\sim 3.5 \times 10^{-3}$ m s^{-2}
Rotational Period	1.9×10^4 s
Orbital Period	1.76years
Orbital Eccentricity	0.223
Semi-major Axis	1.458AU
Orbital Inclination	10.8°

5.1 Algorithm

Referring to the optimization problem, the variables to identify are collected into the state vector $\mathbf{X}_0$. Since the variables to optimize cover a wide range of orders of magnitude, a normalization of the state space was performed, in order to help the solver in finding the minimum. It is in fact known that the non-uniformity of the state space usually prevent gradient-descent based solvers to find correctly the solution, or to find it in a feasible number of iterations. A badly scaled problem is characterised by:

- Stopping criteria issues: the difficulty of formulating a reasonable stopping criterion, since the same step could be large in the direction of a small variable and tiny for a large variable;
- Ill-conditioned problem: the solver will try to apply an homogenous perturbation to all variables, leading to either large or ineffective variations in the cost function evaluation. When this happens, it means that the Jacobian matrix is close to singularity.

For this reason, the Stokes coefficients will be normalized according to the normalization reported in eq. 2.18, while the others, namely positions, velocities and μ are normalized after the definition of the dimensionless variables:

$$\begin{cases} L_c = R_{body} \\ T_c = \sqrt{\frac{R_{body}^3}{\mu}} \end{cases} \tag{5.1}$$

where L_c and T_c are the characteristic length and time.
Accordingly, the normalised positions $\overline{\mathbf{R}}$, velocities $\overline{\mathbf{V}}$ and gravitational parameter $\overline{\mu}$ are defined as:

$$\begin{aligned} \overline{\mathbf{R}} &= \frac{1}{L_c}\mathbf{R} \\ \overline{\mathbf{V}} &= \frac{T_c}{L_c}\mathbf{V} \\ \overline{\mu} &= \mu\frac{T_c^2}{L_c^3} = 1 \end{aligned} \tag{5.2}$$

The newly defined normalised variables are then collected into the state vector $\mathbf{X}_0$:

$$\mathbf{X}_0 = \begin{bmatrix} \begin{bmatrix} \overline{\mathbf{R}}_0 \\ \overline{\mathbf{V}}_0 \end{bmatrix}_{sc_1} \\ \begin{bmatrix} \overline{\mathbf{R}}_0 \\ \overline{\mathbf{V}}_0 \end{bmatrix}_{sc_2} \\ \vdots \\ \begin{bmatrix} \overline{\mathbf{R}}_0 \\ \overline{\mathbf{V}}_0 \end{bmatrix}_{sc_N} \\ \overline{\mu} \\ \overline{\mathbf{c}} \\ \overline{\mathbf{s}} \end{bmatrix} \tag{5.3}$$

where N is the number of spacecraft of the considered swarm. Instead of only one satellite, the initial conditions of each satellite is now to be estimated. We will consider the satellite number 1 the mother-ship, while the others will be the child-ships.
In the same way, the observations and the simulations data is collected in the $\mathbf{O^N}$ and $\mathbf{C^N}$ as:

$$\mathbf{O}^N = \begin{bmatrix} \mathbf{O}^{sc_1} \\ \mathbf{O}^{sc_2} \\ \vdots \\ \mathbf{O}^{sc_N} \end{bmatrix}; \quad \mathbf{C}^N = \begin{bmatrix} \mathbf{C}^{sc_1} \\ \mathbf{C}^{sc_2} \\ \vdots \\ \mathbf{C}^{sc_N} \end{bmatrix} \tag{5.4}$$

Since the objective is to analyze different kind of relative measurements, the generic $\mathbf{O}^{sc_n}$ and $\mathbf{C}^{sc_n}$ will contain different kind of data depending on the case at study, namely relative positions and velocities in cartesian coordinates ($\mathbf{\Delta R_n}$ and $\mathbf{\Delta V_n}$), or range and range-rate (r_n and v_n). Noise is also included in the observations. Measurement uncertainty is simulated adding a relative random offset δ to each observation point:

$$\mathbf{O^{noise}} = \mathbf{O} + \delta \cdot \mathbf{O}, \quad \delta \in [-\overline{\delta}, +\overline{\delta}] \tag{5.5}$$

where $\overline{\delta}$ is the maximum relative noise level.

Having defined the relevant variables, the scheme of the algorithm is then summarized (5.3):

- The state vector (5.3) is perturbed according to (3.28) of the LM method;
- The swarm trajectories are propagated utilizing the initial conditions and gravitational parameters contained in the state vector;
- The absolute coordinates of the secondaries are converted into relative coordinates w.r.t. the primary and collected into the C^{Nk}
- Compute J cost function;
- Check the convergence criteria;

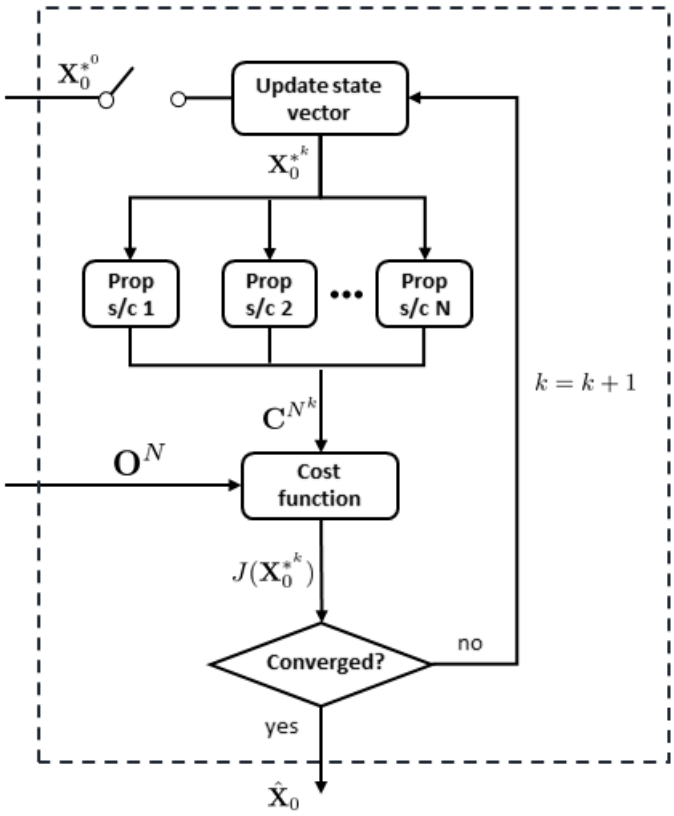

Figure 5.3. Simulation algorithm

If the check returns negative, the next iteration starts from the first point, if negative the optima is found. The conditions for the convergence at the k-th iteration are set as:

- $\left|\frac{J\left(\mathbf{X}_0^{*^k}\right)-J\left(\mathbf{X}_0^{*^{k-1}}\right)}{J\left(\mathbf{X}_0^{*}\right)}\right|$ is less than a prescribed function tolerance;
- $\frac{\left\|\mathbf{X}_0^{*^k}-\mathbf{X}_0^{*^{k-1}}\right\|}{\left\|\mathbf{X}_0^{*^k}\right\|}$ is less than a prescribed step tolerance.

To initialize the algorithm, the set of observations is computed numerically starting from the true initial conditions and gravity coefficients; while the initial guess $\mathbf{X}_0^{*^0}$ for the optimization problem is selected applying a randomly extracted offset:

$$\mathbf{X}_0^{*^0} = \left(\mathbf{I} + \frac{err_{\%}}{100}\,\mathrm{diag}\left(\delta_1, \ldots, \delta_n\right)\right)\mathbf{X}_0, \quad \delta_i \in [-1, 1] \tag{5.6}$$

where $\mathbf{I}$ is the $n \times n$ identity matrix, δ_i are the uniformly distributed random relative offsets, and $err_{\%}$ is the maximum percentage relative error of the initial guess.
The intent of this modelization of the initial guess relies in recreating inaccurate a priori information to be improved through the optimization. For instance, in a real-life scenario, the a priori gravity coefficients could be computed by integration of a constant density shape model already available.

5.1.1 Hypothesis and validity

The main assumptions made when realising this model are now reported.

- Direct observations: the aformentioned observations required for the optimization problem are considered to be readily availible. This is acceptable since it is theoretically possible, also according to the technological methods reported in 1.1, to obtain the kinds of measurements considered in this study.
- Truncated expansion: the gravity field model is truncated up to a prescribed order and degree. Observations and computed observations are generated according to it. This is necessary considering the impossibility of computing a gravitational model of infinite degree and order, and the limited number of harmonics availible in the availible estimated models used.
- Steady problem: the central body gravity field and spinning axis are considered to be constant.
- Uniform sampling: observations are taken at fixed and equally spaced time steps.
- No other perturbations: when describing the model dynamics, only gravitational accelerations are taken into account, this means that other type of perturbations like Solar radiation pressure (the most important one in asteroidal environment) are neglected. This assumption was made to have a general model to study and understand how the solver performs in the context of multi-spacecraft gravity field estimation, however the SRP perturbation effect can indeed be comparable to the gravitational one in the case of small asteroids in the Kuiper belt. This effect will be addressed in the next chapter.

5.1.2 Figure of merit

The problem of quantitatively address the quality of the estimated gravity field is a non-trivial one. In particular, one could think of considering the observation residual, i.e. the cost function J evaluated at the solution point $\hat{\mathbf{X}}_\mathbf{0}$, as a figure of merit (FM) - that is a performance index - for this problem:

$$J\left(\hat{\mathbf{X}}_0\right) = \frac{1}{2}\sum_{i}^{\ell}\left\|\mathbf{O}_i - \mathbf{C}_i\left(\hat{\mathbf{X}}_0\right)\right\| \tag{5.7}$$

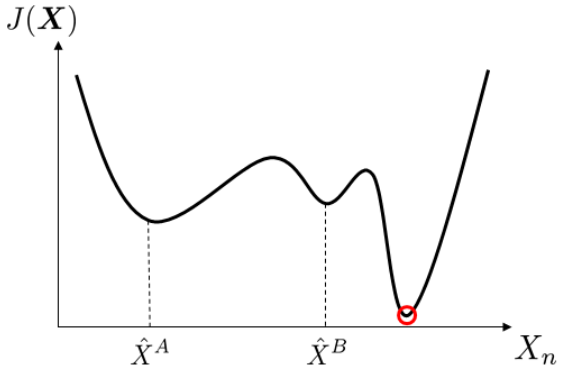

Figure 5.4. Residual general depiction

Being the residual the outcome of the least squares method, its value is surely related to the convergence state, but there's no straightforward relation between it and the gravitational coefficients to be estimated. Due to the high non-linearity of the cost function, it is possible that a *worse* solution, in terms of the estimated parameter, result in a lower residual. Also the value of the residual is not general, as it depends also on the number of observations, making it an inadequate metric to measure the quality of the solution.

For this reason another metric was implemented to address this issue.
Imagine a 2-D Euclidean space and two points identified by (x_1, x_2) and $(\hat{x}_1, \hat{x}_2)$ Cartesian coordinates. The distance between the two points is:

$$d = \sqrt{(x_1 - \hat{x}_1)^2 + (x_2 - \hat{x}_2)^2} \tag{5.8}$$

Generalising to n dimensions, it becomes:

$$d = \sqrt{\sum_{i=1}^{n}(x_i - \hat{x}_i)^2} \tag{5.9}$$

This concept can be generalized considering the so called Hilbert space [55]. The Hilbert space is a complete vector space H that, in direct analogy with the Euclidean space, has a natural inner product $\langle \cdot, \cdot \rangle$ providing a distance function or metric, i.e an operator (a function) that defines a distance between each pair of elements of a set as follows [56]:

$$\| \cdot \| = \sqrt{\langle \cdot, \cdot \rangle} \tag{5.10}$$

Therefore, Hilbert space is an infinite-dimensional function space that allows to represent functions, as opposed to Euclidean space which allows to represent geometric vectors.

As the distance between two functions measure how alike (or different) these are, it is possible to compare two gravity related functions, one estimated (i.e. computed as an output of the gravity field determination process) and the real one (assumed known), to quantify the quality of the estimation:

$$\|f - \hat{f}\| = \sqrt{\langle f - \hat{f}, f - \hat{f} \rangle} \tag{5.11}$$

where f is the real gravity related function and $\hat{f}$ the estimated gravity related function. These are identified in the Hilbert space by the harmonics scalar coefficients, thus a new figure of merit, named Hilbert distance, is arbitrary defined as follow:

$$d_H = \sqrt{\sum_n \sum_m \left[\left(\hat{\bar{C}}_{nm} - \bar{C}_{nm} \right)^2 + \left(\hat{\bar{S}}_{nm} - \bar{S}_{nm} \right)^2 \right]} \tag{5.12}$$

Taking into account also the central body gravitational constant, the previous equation becomes:

$$d_H = \sqrt{\sum_n \sum_m \left[\left(\hat{\mu}\hat{\bar{C}}_{nm} - \mu\bar{C}_{nm} \right)^2 + \left(\hat{\mu}\hat{\bar{S}}_{nm} - \mu\bar{S}_{nm} \right)^2 \right]} \tag{5.13}$$

A smaller FM will then define a more accurate solution. This metric is fast to compute, with respect to other metrics one could think of like point-wise integration of potential function, and its value directly linked to the estimated coefficients, enabling

to quantitatively grasp the quality of the solution. It is important to remark that the computation of the Hilbert distance requires the actual gravitational coefficients to be known, that is, the real gravity field we want to estimate. This is clearly not possible in a real-life scenario, and in that case only the observation residuals could be used, or some more advanced metrics. It will be used for the objectives of this research, since useful for method and algorithm validation, and quantitative assessment of the quality of the solution.

5.2 Swarms configurations

Let us now describe the swarm configurations considered to produce the results contained in the following sections. In particular, the swarms will be characterized by the mother-ship satellite osculating orbital elements, that will deploy, in one or more points of its trajectory, a certain number of secondary satellites, according to the configuration of choice. These will later be analyzed, in order to determine which performs better and possibly to understand the reasons of their differences. The objective was to come up with simple yet effective deployment schemes, that would allow for a systematic study of their performances. Hence the focus was put on circular orbits in order to keep the altitude from the surface fixed at each simulation, since it's one of the most important parameters that affect the solution of the gravity field determination problem. It's important to point that no assumption have been made on *how* the deployment should occur, and eventually a feasibility analysis should be carried out to derive the technological requirements that would make it possible. This, however, is a topic for future developments, as it falls out of the scope of this dissertation. As a remark, the terms *polar* and *equatorial* orbits utilised in the following refer to orbits whose orbital plane is parallel to the spinning axis for the former, perpendicular to it for the latter.

- Equatorial scanner

  The mothership is placed on equatorial orbit, and at fixed time-steps it'll release a child-ship, injecting each of them on orbits with a certain inclination i, and equally spaced RAANs, along the 360° span. From this concept an infinity of different configurations can be generated, depending on the selected inclination.

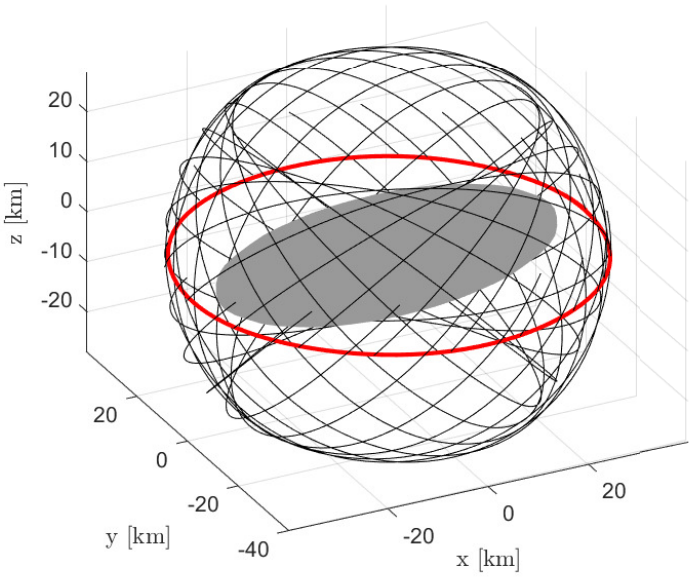

Figure 5.5. Equatorial scanner - in red the mother-ship trajectory

- Polar Scanner

  The mothership is placed on a polar orbit and when in azimutal position, it releases radially the childships, that will still be on polar orbits but with equally spaced RAANs, along the 360° span.

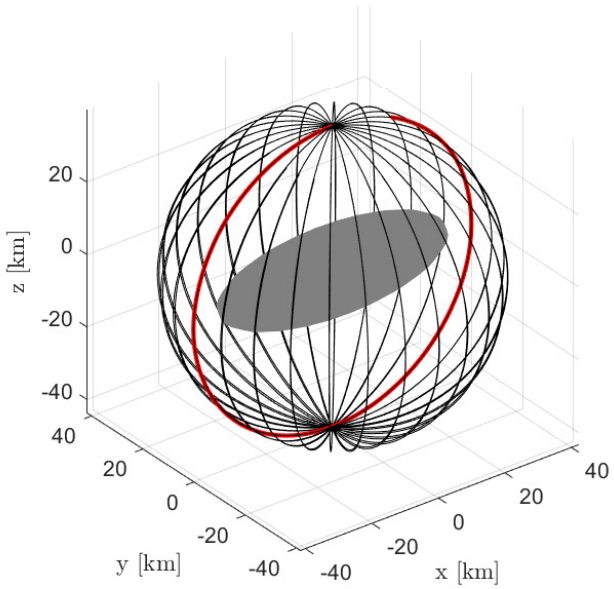

Figure 5.6. Polar scanner - in red the mother-ship trajectory

- Inclination fan

  The child-ships are placed on orbits with different inclinations, spanning from -90 to 90, by the mother-ship that will have the same osculating elements, but with a certain inclination i. From this concept an infinity of different configurations can be generated, depending on the selected inclination.

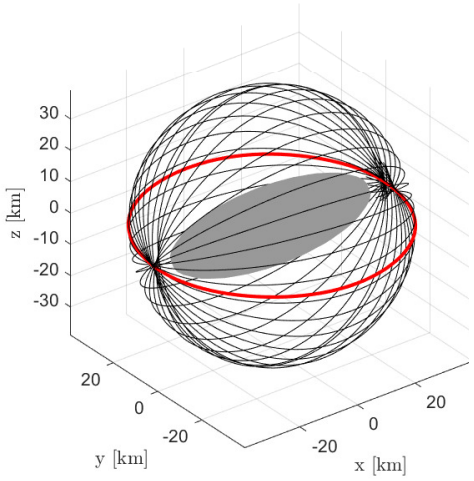

Figure 5.7. Inclination fan $i = 0°$

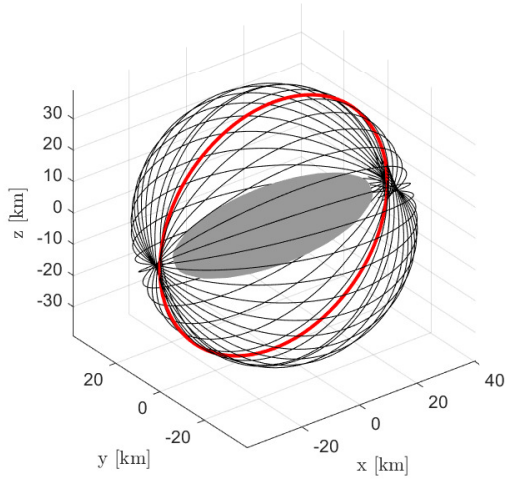

Figure 5.8. Inclination fan $i = 90°$

5.3 Relative position in Cartesian coordinates

Let us now start presenting the first results. In this section and the following ones, the problem of estimating the gravity field of an asteroid with couples of satellites, where the secondary position data is expressed in relative coordinates, is analysed. Considering one of the swarm configuration reported in the previous section, as many optimization problems are solved as the number of secondaries in the swarm. That is, if the swarm is composed of n satellites, $n - 1$ solutions are found, each one extracted using the measurements of the mother-ship and one of the child-ships. This analysis will be useful and extended in the next chapter, when complete swarms are propagated and optimised. The goal is to understand how the solution how the solution behaves when adding a secondary spacecraft relative coordinates depending on its orbit with respect to the primary, and secondly to analyse how the solution behaves when different orbital configurations are used.
In particular, the optimization problem is here solved using the absolute position and velocity Cartesian coordinates of the primary, and the relative ones of the secondary, with respect to the primary. All the simulations are done with circular orbits of semi-major axis $a = 40km$, whereas the noise level $\delta = 1 \cdot 10^{-10}$. As a further remark, since the method proves to effectively estimate the initial conditions of the spacecrafts, with relative errors of -at least- 2 orders of magnitude lower than the other optimimsation variables, they will not be included in the following discussions as they will mainly focus on the quality of the estimated potential field and its parameters error.

5.3.1 Inclination fan

The results obtained using this configuration are notably insightful. The first important remark is that in all simulations a better solution was achieved using the relative position data of the child-ship in addition to the absolute position measurements of the primary. In Fig. 5.9 the Figures of Merit relative to each optimisation are reported, against the relative inclination -with respect to the primary- of each secondary analysed. A swarm of 40 satellites was considered. The primary is placed on equatorial orbit. The analysis of the FM shows a clear profile, values ranging in the order of 10^{-11}, where the highest -worse- values are concentrated around $\Delta i = 0$, indicating that when the secondary is orbiting *close* to the primary, a small improvement in the solution is achieved. An explanation to this behaviour could rely in the redundancy of the information contained in the measurements. In fact, since the gravitational force sensed by a satellite is only function of its ACAF position, the two closely orbiting spacecrafts will *sense* a similar force, providing the solver with redundant data: the information about the gravity field contained in the secondary measurements is then similar to the ones of the mother-ship, resulting in a small improvement of the overall solution. On the other hand, when the relative inclination between the two spacecrafts increases, the solution highly improves, suggesting that the information content of the provided data is indeed capable of helping the solver find a better solution. Still looking at Fig. 5.9 the relative errors of the estimated parameters show an improvement of several orders of magnitude for all the variables with respect to the guess values, except C_{21} and S_{21} whose solution is comparably worse. In all simulations the convergence was reached in less than 15 iterations.
Still looking at Fig. 5.9 the relative errors of the estimated parameters show an improvement of several orders of magnitude for all the variables with respect to the guess values, except C_{21} and S_{21} whose solution is comparably worse. In all simulations the convergence was reached in less than 15 iterations.

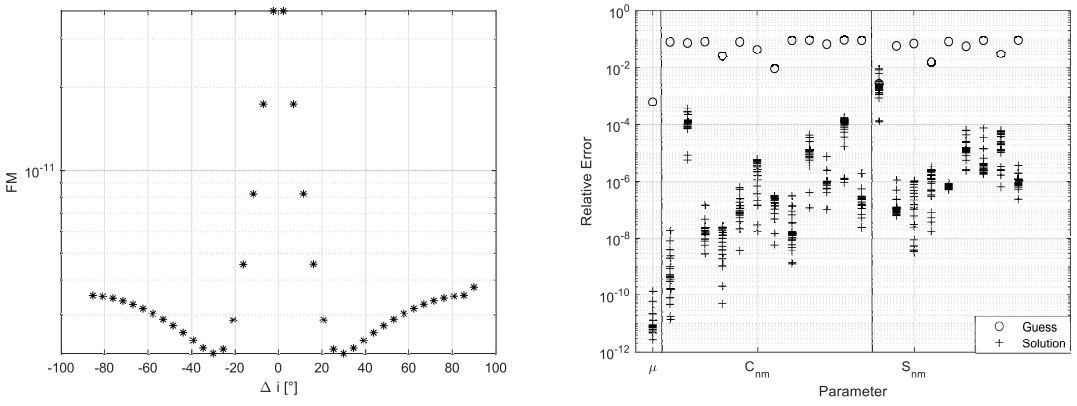

Figure 5.9. Inclination fan simulation results with relative position Cartesian coordinates - $i_{primary} = 0°$

The same kind of simulation was performed but placing the mother-ship into polar orbit and in this case a similar pattern appears (Fig. 5.10). Like in the previous case,

the figure on the left shows the solutions (FM values) for each optimisation done with each pair of satellites (plotted according to the relative inclination of the secondary); on the right, the relative error of each optimisation parameter is reported against the relative error of the guess value. While however better overall solutions are obtained with respect to the previous case, with values in the order of 10^{-12}. For the same reasons explained before, this result suggests that placing the primary spacecraft in polar - or high inclination - orbit may be preferable. Assuming that the relative position data provided by the secondaries is supplementary to the primary one, it is clear that the polar trajectory allows the primary to *sense* a higher variety of gravitational harmonics. Its ground-track is indeed sparser rather than concentrated around the equator, thus providing *more informative* data to the solver, as already reported in Guardalà [43].

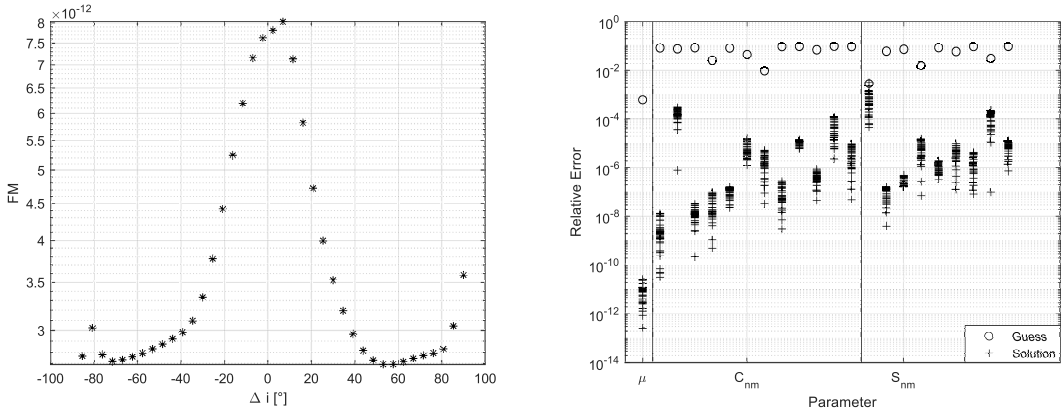

Figure 5.10. Inclination fan simulation results with relative position Cartesian coordinates - $i_{primary} = 90°$

5.3.2 Polar scanner

The polar scanner idea arose from the previous consideration, so that if it's true that a polar motion can provide better data, putting all the spacecrafts on a polar orbit will guarantee the ground-track covering of all the whole asteroid surface, after the right amount of time. Repeating the previous kind of analysis for this configuration, remarkable results are obtained. Values of the FM are in the order of 10^{-13}, which is better than all the other approaches. The relative errors of the estimated parameters is again very small, and an average improvement of 2 orders of magnitude is obtained for C_{21} and S_{21}. Also in this case, the FM shows a sort of profile, although more erratic than the previous ones. This is understandable since here the Keplerian element that is changing for the child-ships is the RAAN (see Sec. 5.2) and all of them have polar inclination. It is a matter of chance that sooner or later a satellite will overfly the same spot already passed by another one, depending also on the asteroid spin velocity. The worst solutions concentrate in the zone where the $\Delta RAAN$ is close to 0° or 360°, that is again when the child-ship orbits very close to the primary, so the same observations made in in the previous subsection (5.3.1).

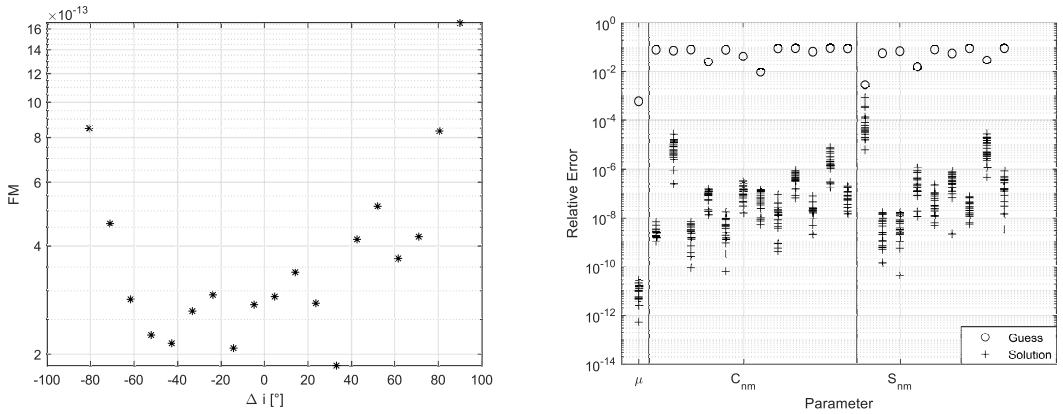

Figure 5.11. Polar scanner simulation results with relative position Cartesian coordinates

5.3.3 Equatorial scanner

In this configuration, the inclination of the secondaries was taken as 30. The choice was driven by the fact that good solutions were found in around this inclination, when analysing the equatorial case of the inclination fan. Figure 5.12 shows again a solution profile, changing with the $\Delta RAAN$ of the child-ship, again indicating that indeed, to overfly some regions results in more informative data for the solver. The FM obtained in these simulations are in the order of 10^{-12}, an improvement with respect to the equatorial inclination fan, but the estimation of S_{21} is still rather poor compared to the initial guess.

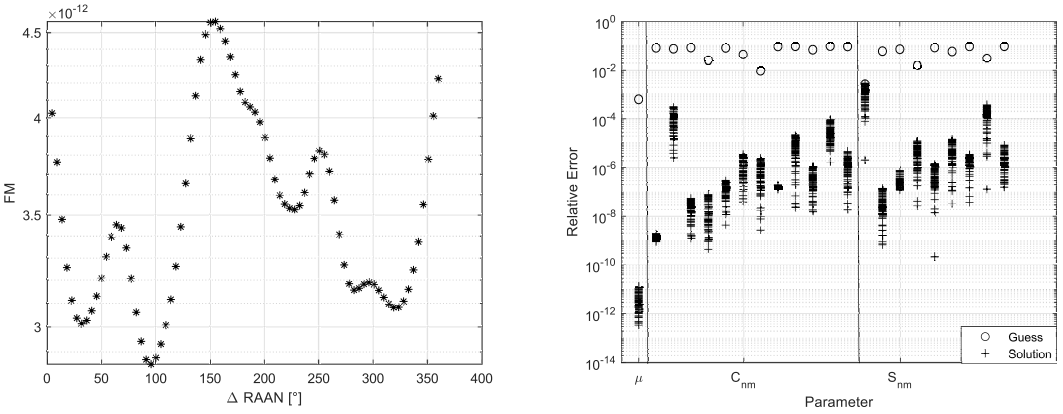

Figure 5.12. Equatorial scanner simulation results with relative position Cartesian coordinates - $i_{secondary} = 45°$

5.4 Range and range-rate measurements

After proving that adding the relative position measurements in Cartesian Coordinates w.r.t. the a primary satellite always seem to guarantee a better solution for the gravity field determination problem, let us now analyse if and how the solution changes when using range and the secondary range-rate measurements instead, being it one of the

main focus of this research. The same scenarios as 5.3 were reproduced in these simulations

5.4.1 Inclination fan

The first good finding is the convergence of the method, in all the simulations, to a better solution than the single-spacecraft case and in a small amount of iterations (less than 15). In Fig. 5.13 the comparison of the solutions between the two multi-spacecraft cases is reported on the left, while on the right the relative error of the estimated parameters in the range and range rate case is reported. While obtaining a rather similar FM solutions profile to the relative coordinates case, the overall values are worse, except for the simulations where Δi is close to 0, where the solution is almost the same. This phenomenon is explainable again referring to the information content of data. The range in fact is just the modulus of the relative position used in the previous case, leading indeed to a loss of information. Nevertheless, the FM are still better than the single-spacecraft case. Looking at the relative error in the parameters estimation, again using this configuration the solver seems to struggle in retrieving accurate values for C_{21} and S_{21}, while converging to very good solutions in almost all the other parameters.

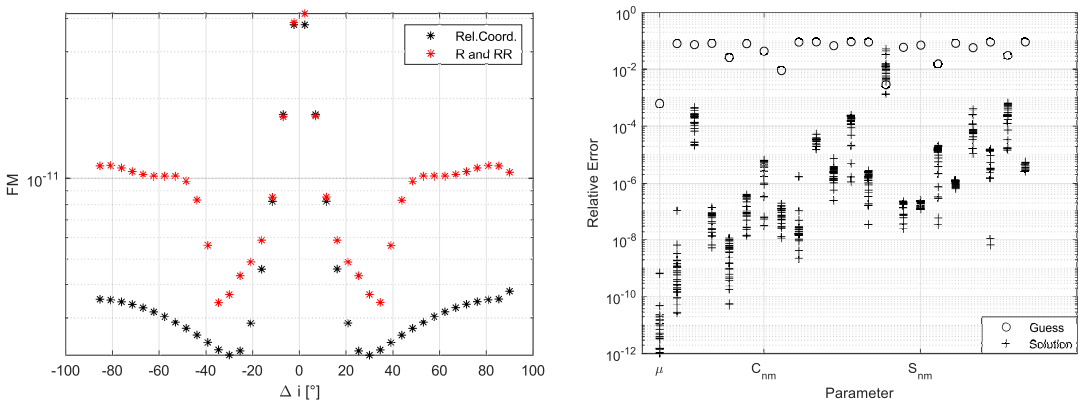

Figure 5.13. Polar scanner simulation results with range and range-rate

5.4.2 Polar scanner

Simulation using the polar scanner configurations show that the loss of information obtained when using range and range-rate data does not always translate in a worse solution. This method can in fact provide sometimes a more accurate estimation, especially when the Cartesian coordinates method performs the worse, i.e. around $\Delta RAAN = 0\,\text{deg}$. Regarding the relative error of the estimated parameters, it is notable again how the polar scanner approach show an improvement in the estimation of C_{21} and S_{21}, since the FMs are on average 2 orders of magnitude than the previous example, while maintaining good estimates for the other parameters.

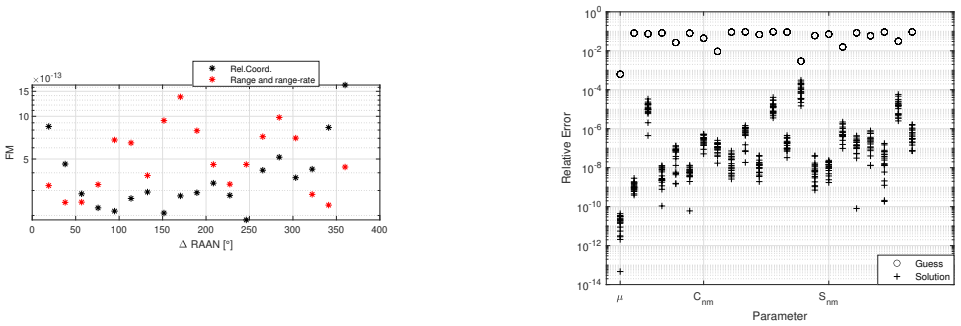

Figure 5.14. Polar Scanner simulation results with range and range-rate

5.4.3 Equatorial scanner

As it can be seen from the results shown in Fig. 5.15, similar considerations can be done as the previous approach when using the equatorial scanner. The usage of this kind of measurements still provides good results, with FMs in the order of 10^{-12}. On average the solution is worse than the relative coordinates case, however it's improved for $\Delta RAAN$ close to 0° and 360°. The bad estimation of the coefficient S_{21} is still present.

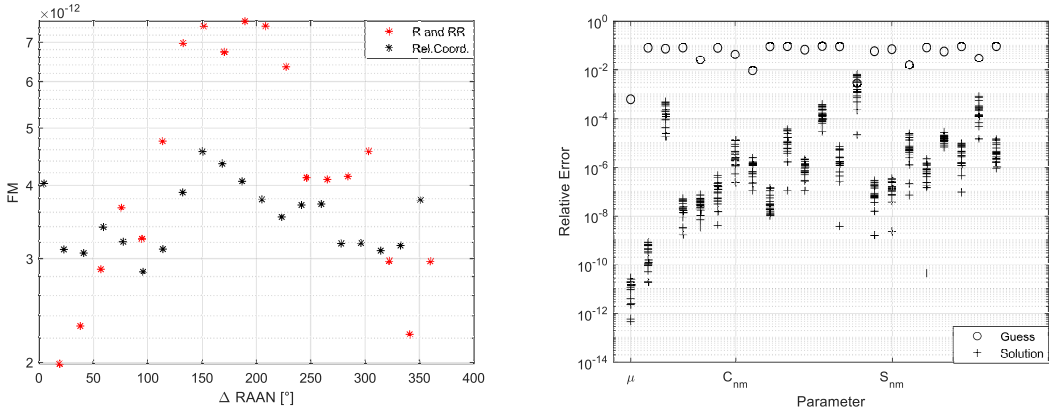

Figure 5.15. Equatorial scanner simulation results with range and range-rate - $i_{secondary} = 45°$

It is worth to point that the same considerations made in this subsection, still apply when analysing the problem using range measurements only. It was found in fact that, especially when considering only couples of spacecrafts, both cases converge to the almost exact same solution. For this reason, results concerning this strategy will be reported in the next chapter where complete swarms are investigated. In that case, relatively bigger variation appear. A reason for this could be that in reality, range-rate data contribute very lightly to the overall solution, and that when more spacecrafts are involved their small contributions add up resulting in a more differentiated outcome.

5.5 An alternative approach I: mascon models

When dealing with the gravity field determination problem, some novel and alternative pathways have been implemented and tested. One of them relies in the evaluation of the problem modeling the gravity field with a mascon model. The set up of the problem remains unchanged as explained in sec. 5.1, while the modification relies in the newly defined parameters to estimate.
For this early analysis, the mascon model was defined as a list of lumped masses each of them with a fixed position, uniformly placed on the surface of the ellipsoid that approximate the asteroid to analyze. Since the position of the mascons is fixed, the parameters to estimate in this approach are the mascon masses, collected in the $k \times 1$ vector $\overline{\mathbf{m}}$, where k is the number of mascons. In this way a new state vector can be defined:

$$\mathbf{X}_0 = \begin{bmatrix} \begin{bmatrix} \overline{\mathbf{R}}_0 \\ \overline{\mathbf{V}}_0 \end{bmatrix}_{sc_1} \\ \begin{bmatrix} \overline{\mathbf{R}}_0 \\ \overline{\mathbf{V}}_0 \end{bmatrix}_{sc_2} \\ \vdots \\ \begin{bmatrix} \overline{\mathbf{R}}_0 \\ \overline{\mathbf{V}}_0 \end{bmatrix}_{sc_N} \\ \overline{\mathbf{m}} \end{bmatrix} \tag{5.14}$$

As explained in Sec.2.2, mascon models need a high number of mascons to generate a good estimated gravity field. For this reason, the optimization problem can become very lengthy, in terms of computational time, since the number of optimization variables is way higher than when solving the problem in terms of spherical harmonics. It's also worth to point out that the measurement data will be computed using a 10-th order spherical harmonics model, due to the unavailability of a ready to use Eros 433 mascon model.

As a proof-of-concept, this method was tested first using only measurement data coming from the mother-ship (i.e. its absolute coordinates Cartesian position).
In Fig. 5.16 the solution for this kind of problem is shown. 6400 mascons were uniformly placed onto the surface of the ellipsoid approximating Eros 433. Remarkably, the method converges and the total mass of the mascon model (i.e. the sum of all the lumped masses) is equal to the mass of the asteroid, with a relative error of 10^{-8}.

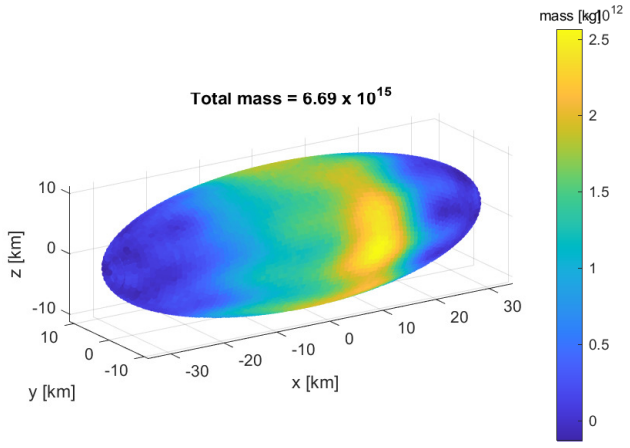

Figure 5.16. Mascon model solution

In Fig. 5.17 the distribution of the mascon masses is reported. It's worth to underline the insurgence of some negative masses. This happened since no constraint was put to the optimization: negative masses are in fact acceptable since we're merely looking for a mathematical representation of the gravity field.

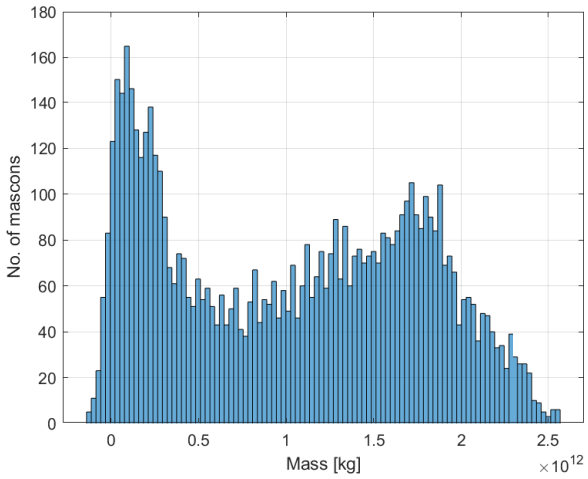

Figure 5.17. Mascon masses distribution

In Fig. 5.19, the evolution of the residual of for the trajectory computed with the estimated model. This is shown since the Figure of Merit previously defined cannot be computed in this case, due to the different modeling of the problem, on the other hand in Fig. 5.18, the resulting potential function (computed on a sphere of 16km) look highly different from the real one (Fig. 5.2). This problem was partially overcome using concentric shells of mascons.

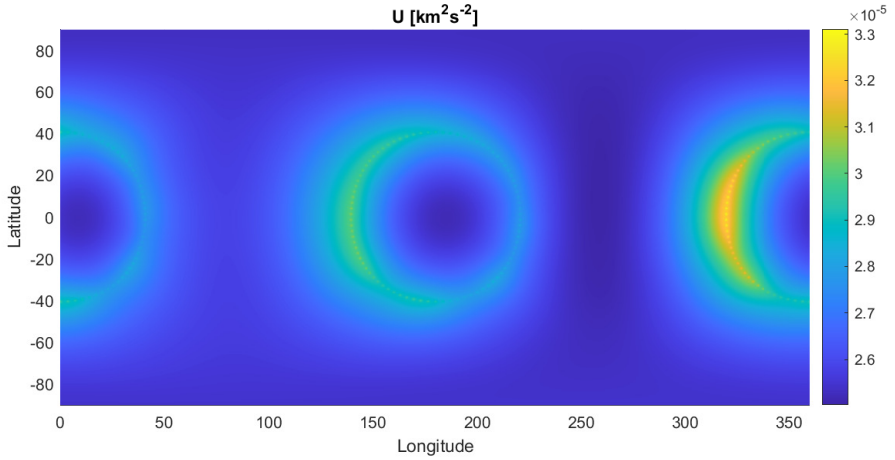

Figure 5.18. Mascon model potential function on a sphere of radius 16 km

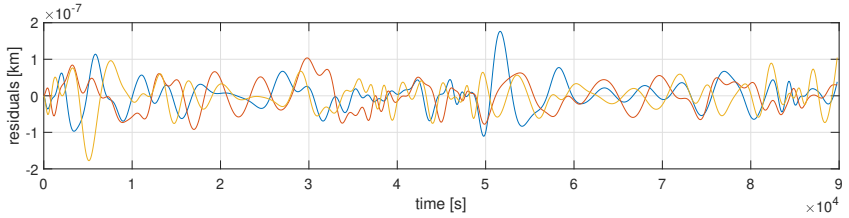

Figure 5.19. Residual evolution

A simulation was conducted with a total number of 8004 mascons, distribuited on 3 concentric shells, where the outer shell is an ellipsoid that approximate the asteroids and the other 2 have semi-major axes of magnitude 1/3 and 2/3 with respect to the first one. Again convergence was achieved, the estimated model is shown in Figure 5.20. When utilizing a multi-shell approach, the solution seem to show a more uniform potential function (Fig. 5.21), suggesting an improvement with respect to the previous approach. Also the most internal mascons are "assigned" more uniform masses by the solver, while the outer ones show bigger variations, including negative mascons (Fig. 5.22).

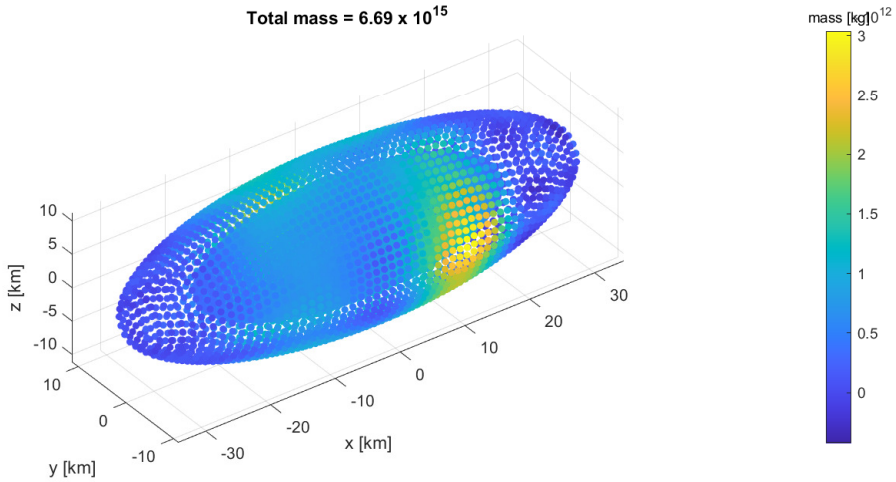

Figure 5.20. Mascon model with 3 concentric shells

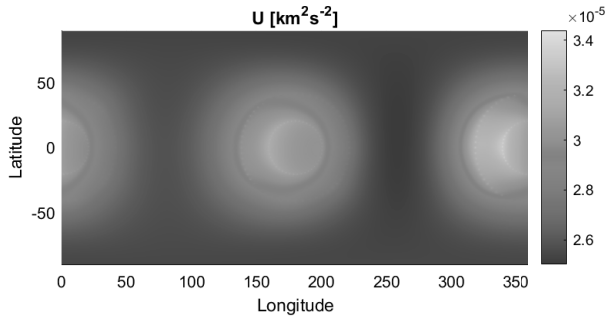

Figure 5.21. Mascon model potential function on a sphere of radius 16 km

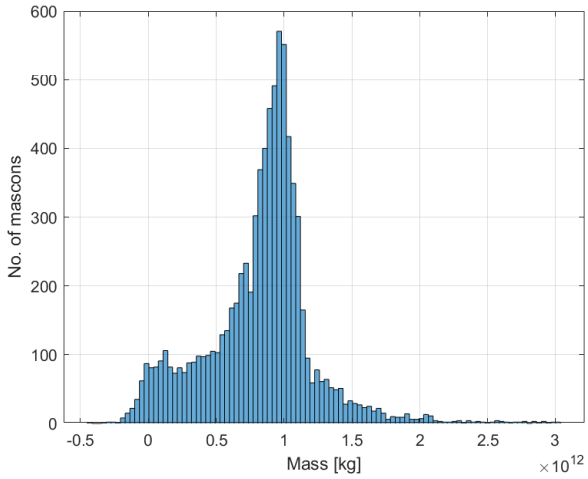

Figure 5.22. Mascon masses distribution

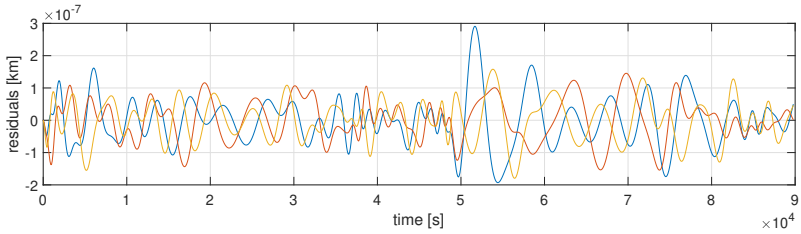

Figure 5.23. Residual of the solution

The results reported in this section underline that it is indeed possible to determine the gravity field of an asteroid using this approach involving mascon models. Being extremely time consuming, and due to the time constraints applicable to this research, this methodology was put aside for the continuation of this work, as the spherical harmonics approach allowed to obtain relevant and insightful in a shorter time-span. Further investigations about this method should though be addressed in future works.

5.6 An alternative approach II: Nayfeh's augmented method

The non-linear orbit determination method proposed by Nayfeh [1], is based upon the idea that if the exact orbit could be determined, the residuals (defined as measured minus computed values) would represent the noise. In case of random noise, then the coefficients of any polynomial that fits through the residuals in the least-squares sense must vanish. Hence, the time axis passes through the residuals in the least-squares sense. Thus, residuals are fit into a polynomial in least-squares sense and the fitting polynomial is used to correct the initial conditions of the assumed orbit. In this way the coefficients of the next polynomial least-squares fit to the new residuals are decreased. The method is an iterative or recursive procedure. It is initialized assuming an orbit (called reference orbit) to start the calculation. To calculate the

reference orbit, we assume values for the initial conditions (initial position and initial velocity vectors) and then integrate the equations of motion. After that, the residual is computed from the measured data and the propagated reference orbit. These residuals $\Delta\underline{\mathbf{r}}_\mathbf{j}$ at time t_j are fitted in the least-squares sense to a linear or a parabolic time-dependent vector. Choosing a linear vector $\Delta\underline{\mathbf{a}}_\mathbf{o} + \Delta\underline{\mathbf{b}}_\mathbf{o}$t:

$$\sum_j \left[\boldsymbol{\Delta}\underline{\mathbf{r}}_\mathbf{j} - (\boldsymbol{\Delta}\underline{\mathbf{a}}_\mathbf{0} + \boldsymbol{\Delta}\underline{\mathbf{b}}_\mathbf{0} t_j)\right]^T \left[\boldsymbol{\Delta}\underline{\mathbf{r}}_\mathbf{j} - (\boldsymbol{\Delta}\underline{\mathbf{a}}_\mathbf{0} + \boldsymbol{\Delta}\underline{\mathbf{b}}_\mathbf{0} t_j)\right] \tag{5.15}$$

is minimum. Minimizing with respect to $\boldsymbol{\Delta}\underline{\mathbf{a}}_\mathbf{0}$ and $\boldsymbol{\Delta}\underline{\mathbf{b}}_\mathbf{0}$ yields

$$\sum_j \left[\boldsymbol{\Delta}\underline{\mathbf{r}}_\mathbf{j} - (\boldsymbol{\Delta}\underline{\mathbf{a}}_\mathbf{0} + \boldsymbol{\Delta}\underline{\mathbf{b}}_\mathbf{0} t_j)\right] = 0 \tag{5.16}$$

and

$$\sum_j t_j \left[\boldsymbol{\Delta}\underline{\mathbf{r}}_\mathbf{j} - \left(\boldsymbol{\Delta}\underline{\mathbf{a}}_\mathbf{0} + \boldsymbol{\Delta}\underline{\mathbf{b}}_\mathbf{0} t_j\right)\right] = 0 \tag{5.17}$$

Solving these equations for $\boldsymbol{\Delta}\underline{\mathbf{a}}_\mathbf{0}$ and $\boldsymbol{\Delta}\underline{\mathbf{b}}_\mathbf{0}$ yields:

$$\begin{bmatrix} \boldsymbol{\Delta}\underline{\mathbf{a}}_\mathbf{0} \\ \boldsymbol{\Delta}\underline{\mathbf{b}}_\mathbf{0} \end{bmatrix} = C^{-1} \begin{bmatrix} \sum_\mathrm{j} \boldsymbol{\Delta}\underline{\mathbf{r}}_\mathbf{j} \\ \sum_\mathrm{j} \mathrm{t_j} \boldsymbol{\Delta}\underline{\mathbf{r}}_\mathbf{j} \end{bmatrix} \tag{5.18}$$

where C^{-1} is the inverse of the matrix C which is given by

$$C = \begin{bmatrix} n & \sum_j t_j \\ \sum_j t_j & \sum_j t_j^2 \end{bmatrix}$$

Once $\boldsymbol{\Delta}\underline{\mathbf{a}}_\mathbf{0}$ and $\boldsymbol{\Delta}\underline{\mathbf{b}}_\mathbf{0}$ have been found, a new epoch state vector is formed. Thus,

$$\underline{\mathbf{a}}_\mathbf{1} = \underline{\mathbf{a}}_\mathbf{0} + \Delta\underline{\mathbf{a}}_\mathbf{0}$$

$$\underline{\mathbf{b}}_\mathbf{1} = \underline{\mathbf{b}}_\mathbf{0} + \Delta\underline{\mathbf{b}}_\mathbf{0}$$

Using the new epoch state vector obtained, we compute a new reference orbit by integrating the full orbital equations of motion. Then, we form the residuals $\boldsymbol{\Delta}\underline{\mathbf{r}}_\mathbf{j}$ and fit them in the least-squares sense to a linear time-dependent vector $\left(\Delta\underline{\mathbf{a}}_\mathbf{1} + \Delta\underline{\mathbf{b}}_\mathbf{1} t\right)$.

Once $\Delta\underline{\mathbf{a_1}}$ and $\Delta\underline{\mathbf{b_1}}$ are found, we determine a new epoch state vector (initial conditions $\underline{\mathbf{a_2}}$ and $\underline{\mathbf{b_2}}$) according to

$$\begin{aligned}\underline{\mathbf{a_2}} &= \underline{\mathbf{a_1}} + \Delta\underline{\mathbf{a_1}} \\ \underline{\mathbf{b_2}} &= \underline{\mathbf{b_1}} + \Delta\underline{\mathbf{b_1}}\end{aligned} \tag{5.19}$$

We repeat the above procedure by calculating a new orbit, computing the residuals, fitting them to a straight line time-dependent vector, and then updating the epoch state vector. The iteration is ended when $\left|\Delta\underline{\mathbf{a_i}}\right|$ and $\left|\Delta\underline{\mathbf{b_i}}\right|$ are less than preassigned small positive convergence numbers.
The mathematical proof of the convergence of this method is reported in [1]. Being it extremely effective for orbit determination, a generalization of this method was also used to estimate perturbative parameters like the ballistic coefficient in the case of drag estimation. Taking inspiration from it, a method to estimate gravitational parameter was derived.

Recalling the notation reported in 2.17, and assuming that a 2-nd order spherical expansion is considered, the method is described in this way:

- We fit the first, say, ten data points to a straight line time-dependent vector $\mathbf{a}_0 + \mathbf{b}_0 t$ in least-squares sense. We choose $\mathbf{a}_0$ and $\mathbf{b}_0$ to be the initial position and velocity of the trajectory and guess values for $C_{20}/\mu, C_{21}/\mu$, and C_{22}/μ. Using these values for the aerodynamic parameters and the initial position and velocity, we calculate a reference trajectory by integrating 2.17, and calculate the initial acceleration $\mathbf{c}_0$.

- We form the residual differences between the measured discrete data points and the values obtained from the computed reference trajectory at the corresponding times. We fit these residuals in a least-squares sense to a parabolic time-dependent vector $\Delta\mathbf{a_0} + \Delta\mathbf{b_0}\mathrm{t} + \frac{1}{2}\Delta\mathbf{c_0}t^2$

- We update the initial position, velocity, and acceleration. Thus,

$$\begin{aligned}\mathbf{a_1} &= \mathbf{a_0} + \frac{1}{2}\Delta\mathbf{a_0} \\ \mathbf{b_1} &= \mathbf{b_0} + \frac{1}{2}\Delta\mathbf{b_0} \\ \mathbf{c_1} &= \mathbf{c_0} + \frac{1}{2}\Delta\mathbf{c_0}\end{aligned}$$

  The new initial position, velocity, and acceleration obtained are substituted in 2.17. New values for $C_{20}/\mu, C_{21}/\mu$, and C_{22}/μ are obtained inverting the system 2.17. Using the new initial position $\mathbf{a}_1$, velocity $\mathbf{b}_1$, and gravitational coefficients, we calculate a new reference orbit and continue iterating until the change in initial position, velocity, and acceleration is smaller than some assigned convergence numbers.

It is worth to underline that the method only allows for the estimation of 3 parameters, being them estimated inverting 2.17. In this sense, it could be possible

to estimate more than three parameters if more than one spacecraft is considered. In fact, inverting a system of $3 \times n$ equations of the estimated initial accelerations, $3 \times n$ gravitational coefficients can be computed as long as the equations are not redundant, i.e. the initial conditions of the n spacecrafts are different between each other.

After extensive iterations and simulations, this method proved ineffective when estimating gravitational parameters. As shown in figure 5.24, while the convergence is achieved for the initial conditions of the satellite, no improvement is made on the relative error of the gravitational coefficients. This is due to the failure of exactly estimating the initial acceleration with this method. Due to the small time-frames that can be considered with this method, only small deviations of the trajectory are produced due to the gravitational perturbation, so that a slightly wrong gravitational model will still produce a trajectory close to the original one, being this more importantly influenced by the values of the initial conditions. Further studies are needed to make this method effective, but due to time constraints and since a working method was already derived to tackle the gravity field determination problem, it was put aside and left for future researches.

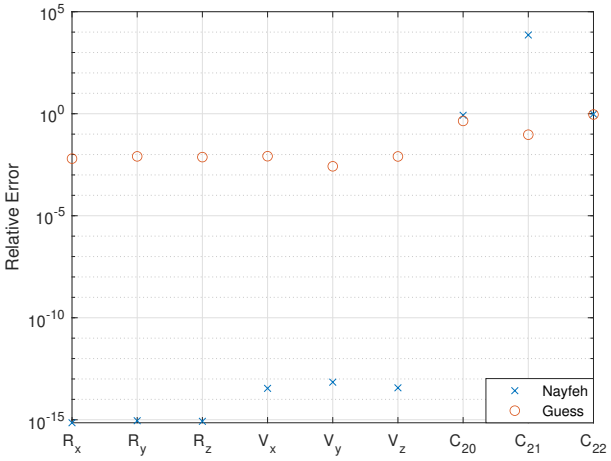

Figure 5.24. Relative error of the estimated parameters

Chapter 6

Estimation of the gravity field with swarms

This chapter will ultimately focus on the simulations and the refinement of the solutions of the gravity field determination problem with swarms. An answer to some of the questions posed at the beginning of this dissertation will be given. After studying the solution behaviour when considering only single spacecrafts belonging to the swarm, it will be now discussed how the solution improves when increasing the size of the swarm, addressing more fundamental aspects regarding the sensitivity of the model to certain parameters, like: noise, size of the semi-major axis, observation time and un-modeled dynamics neglected in the model like the SRP perturbation. An algorithm to identify eventual *bad points* present in the data will be discussed and implemented to understand whether the solution can benefit off it. Lastly a comparison of the performance of the model using either one of the types of measurement strategy discussed will be made to draw conclusions about which one could be more suitable in a real-life scenario.

6.1 Size of the swarm

One of the main interrogatives posed at the beginning of this writing was whether it was possible to improve the solution of the gravity field determination problem using the relative position data of a swarm of satellites, with respect to the mother-ship, instead of only one satellite. In 5.3 the problem was analysed considering a single child-ship, leading nonetheless to an improvement of the solution. The effect of the size of the swarm will now be addressed, trying to understand if there is an optimal number of satellites to obtain the best possible solution.

Results for a polar scanner swarm, with semi-major axis $a = 40km$ is reported in 6.1 for an increasing number of satellites belonging to the swarm (from 2 to 50). Measurements are taken as relative position relative coordinates. The figure of merit is sparsely improving when considering more secondaries, thus more data to feed the solver. Although kind of irregularly, the cloud of points is descending, and flattening out when passed the 30 spacecrafts. In this region the best solutions are found, with a FM more than 20 times smaller than when considering 2 satellites only.

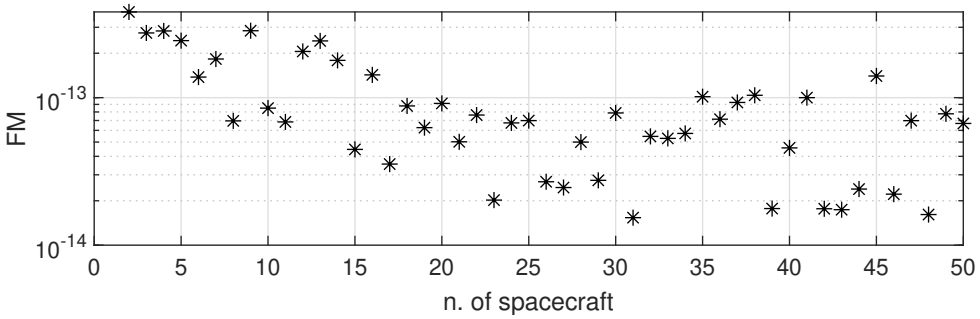

Figure 6.1. Polar scanner results swarms with increasing satellites

Let us now inspect how the solution is affected by the type of measurement. An equatorial inclination fan was propagated with an increasing number of spacecrafts and using all the types of measurement strategy reported in 5.2. As in the previous case, results in 6.2 show a clear decreasing pattern for all the examples considered. In particular it is still clear that relative position Cartesian coordinates still tend to yield the better outcome among the three. As explained in the previous chapter, optimisation with only range measurements yield results very similar, or sometimes equal, to the range and range-rate case, although bigger variations seem to appear when increasing the number of satellites to analyse, suggesting that the range-rate data information contribution to the solution is small but sums up when more measurements are stacked, leading to slightly better solutions.

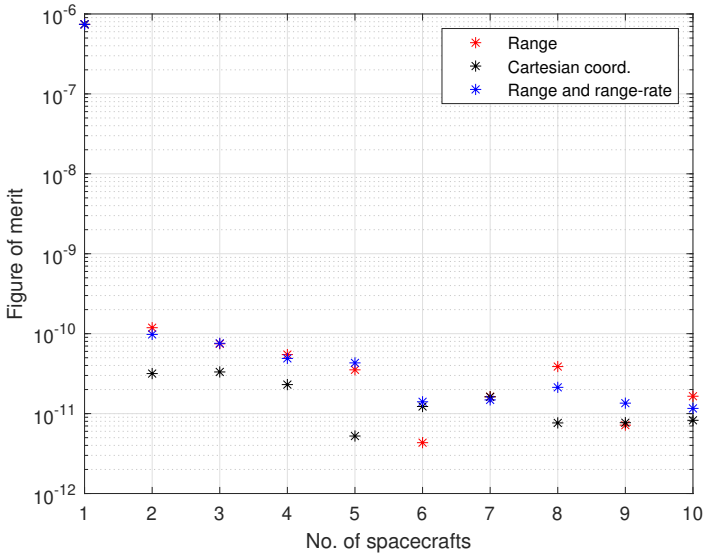

Figure 6.2. Inclination fan swarm measurements comparison

6.2 Outlier rejection

We want now to analyse if and how the solution could improve if an effective method of *filtering* the data for the estimation problem could be found. Taking as a reference the results reported in section 5.4, a wide range of FM can be obtained extracting the

solution from single satellites belonging to the swarm, moreover thinking of defects in one of the single satellite of the swarm, worse solution could be obtained due to higher noise. The problem of identifying outliers in this application is non-trivial, since there's no *a priori* way to determinate which solutions are the better, since no information on the actual field is known. Due to this, the FM cannot be considered for the recognition of the outliers. A method based on the solution of the state vector was implemented to this scope. Consider a swarm of N particles and that n is the dimension of the state vector. The elements of $\hat{X}_0$ can be seen as the spatial coordinates of the N solution. In 6.3 it is shown a depiction of the method if a 3-dimensional domain was considered. The set of particle solutions generates a cloud of points. If it is assumed that a sufficient number of solutions has succeeded in converging, those $\hat{N}$ points create a cluster around the global minimum (namely, the inliers), and the remaining $N - \hat{N}$ out-of-cluster rejected points are referred to as outliers. The clustering technique implemented for the research of the outliers is the Density-Based Spatial Clustering of Applications with Noise (DBSCAN).

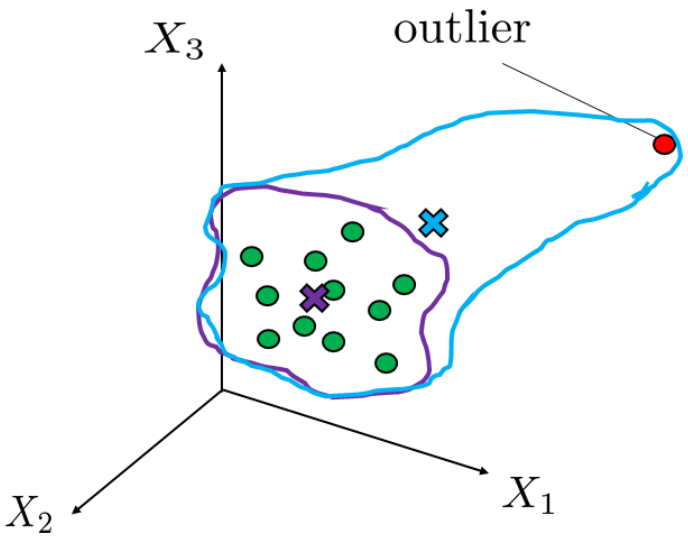

Figure 6.3. Cluster and outliers

6.2.1 Density-Based Spatial Clustering of Applications with Noise

The DBSCAN (Density-Based Spatial Clustering of Applications with Noise) is a data clustering method proposed by Ester et al. [17] in 1996. It is a density-based algorithm which is able to identify points in clusters and to exclude the outliers in areas with a low density of points [57]. The points are classified into four categories [6.4]:

- p is a core point, if there are at least N_{min} points within a n-dimensional sphere of radius ϵ with centre p itself (red points in 6.4;

- q is directly-reachable point, if it is within ϵ from p;
- q is reachable, if there is a path between p and q where p_{i+1} is directly reachable from p_i;
- All the point not reachable from any other point are outliers (point N in 6.4).

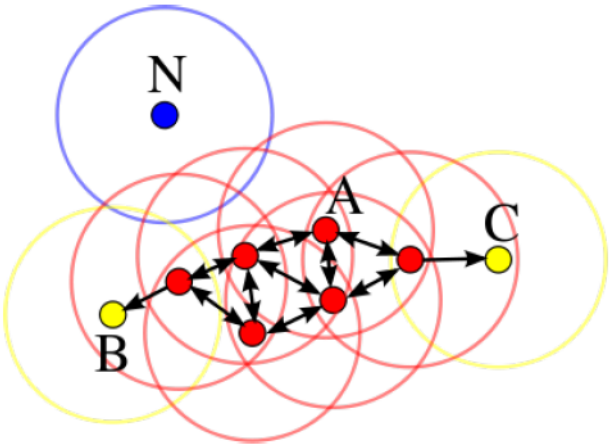

Figure 6.4. DBSCAN

The cluster is the set of points reachable from p. Non-core points can belong to a cluster, but they form its edge. The algorithm identifies the points in the neighbour of each points, finds the connected components of core points and finally assigns each non-core point to a cluster or identifies it as an outlier. The algorithm is implemented in MATLAB2021a and in the following versions, within the Statistics and Machine Learning Toolbox.

The general scheme of the algorithm implemented is reported in Fig. 6.5 and here summarised. Given N orbiting spacecrafts, where the spacecraft 1 is the mother-ship

- $N-1$ different solutions for the gravity field assessment ($\hat{X}_0$), one for each pair primary-secondary, are obtained;
- Selected a suitable ϵ and N_{min}, DBSCAN identifies the outlier solutions;
- The filtered best estimate solution $\hat{\mathbf{X}}_\mathbf{0}$, is computed discarding data from the outliers.

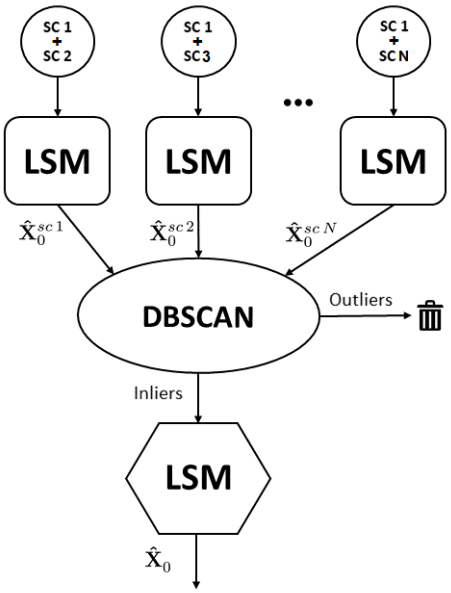

Figure 6.5. Outlier rejection algorithm

6.2.2 Results

Let's consider for example the solutions relative to a swarm of 40 spacecrafts in polar inclination fan, where a steep variation of the FM was obtained for the small relative inclination spacecrafts. The DBSCAN algorithm was applied to this set of solutions. After accurate tuning, the parameters were set as $\epsilon = 2 \cdot 10^{-9}$ and $N_{min} = 5$. As shown in 6.6, it's clear that the algorithm is able to differentiate the solutions, in particular the low-valued FM ones belong to the cluster, while the worse are labeled as outliers.

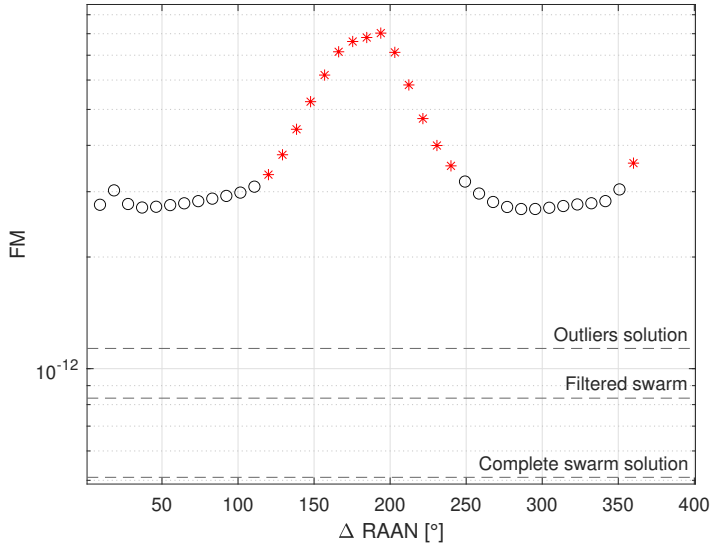

Figure 6.6. Outliers identificaition and solutions

This impressive result suggests that it is true that all the better solutions are *neighbours* in the state space. The next step is assessing whether the rejection of the outliers leads to an improvement of the overall solution. The horizontal lines on plot indicate the FM of the solution obtained using for the optimization the data obtained from: the complete swarm, the swarm without outliers, only the outliers. It is clear that, even though an improvement of the overall FM is obtained in any case, no improvement is achieved filtering out these outliers. The relative errors of the parameters, show that some of them are in fact better estimated with the outliers. It could be said that, although with the outliers data the solution is globally worse, it contains valuable information about some harmonics (i.e. parameters) that are worsly identified by high inclination orbits (6.7).

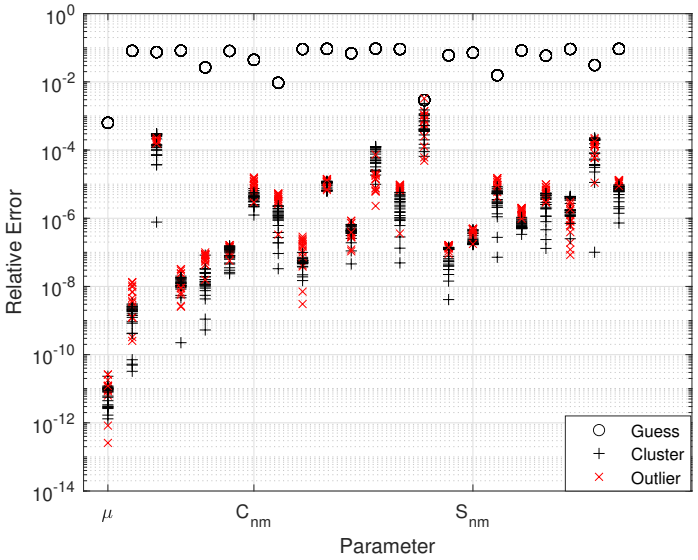

Figure 6.7. Noisy solutions identification and rejection

Discarding the outliers, from this point of view, would then not be a good idea. However the DBSCAN algorithm can still prove valuable when the objective is discard points affected by excessive noise. As explained before, it's not possible to say *apriori* which solution is the better. If for example we include in our model the presence of high noise (5 increase in the noise level) on some randomly extracted spacecrafts from the swarm, the solution profile of the FM looks as in 6.8. It's clear that some points are offset because of the high noise content. The DBSCAN algorithm applied to this situation is again able to distinguish them from the other clustered solutions. The parameters were set as $\epsilon = 1 \cdot 10^{-8}$ and $N_{min} = 5$. Repeating the same simulations about the overall solutions, it is now found that the filtered solution is indeed better than the complete swarm one, containing high noise data from the outliers.

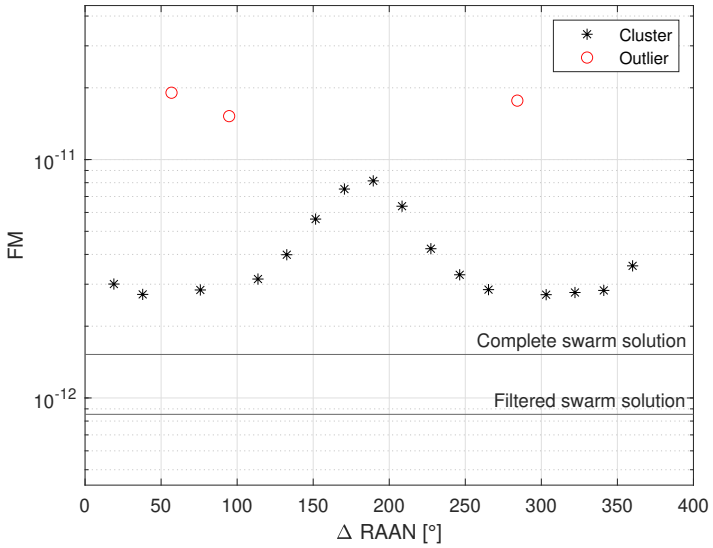

Figure 6.8. Outlier rejection algorithm solutions

It is then proved that the DBSCAN algorithm, or other clustering techniques, can prove valuable for data filtering in this scope, thus inducing interest for further, more detailed, studies.

6.3 Noise level

As already mentioned, noise is referred to inaccuracy in the observations. In other words, instead of considering the position and velocity coordinates of the spacecraft as exactly known, a random error is added in order to simulate measurement uncertainty. More precisely, the noised observations O_i^{noised} are computed adding (or subtracting) a relative maximum random offset to each component of O_i^{noised}. For instance, 0.1% noise level on the Cartesian coordinate R_I at a given time t will be:

$$R_x^{\text{noise}}(\bar{t}) = R_x + \delta \cdot R_x \tag{6.1}$$

Let us analyse how the value of δ affects the solution. The same kind of optimization was run including in the model an increasing amount of noise in the measurements, starting from 0. The results shown in 6.9 for a polar inclination fan swarm, that the sensitivity of the method to noise is very high, thus high-accuracy results are guaranteed just with very precise measurements. However that's not a big of a problem, since we already talked about how recently developed technologies are able to detect range variations in the order of manometers.

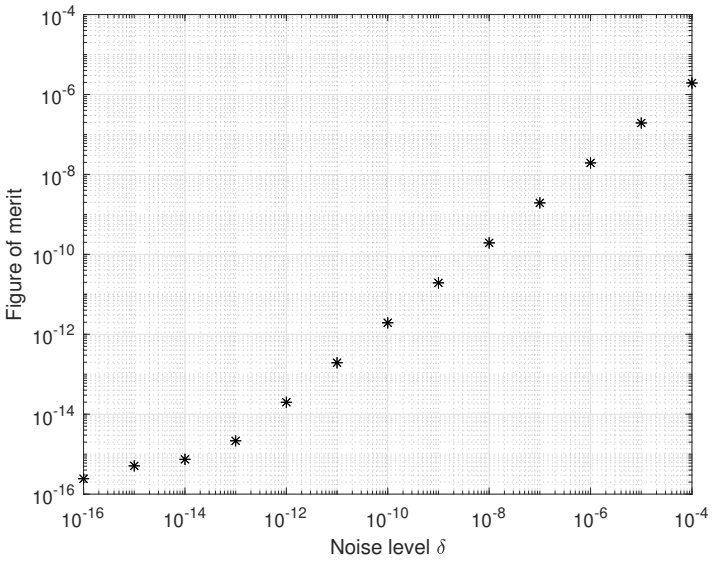

Figure 6.9. Effect of the noise level on the solution

The evolution of the FM with respect to the noise is linear in a log-log plot. In particular, except the points with lower noise, that show no clear relation with it, the evolution of the FM roughly follows:

$$\begin{aligned} \log_{10}(d_H) \approx & k_1 \log_{10}(\delta) - k_2 \\ & k_1 \approx 1 \\ & k_2 \approx 2 \end{aligned} \tag{6.2}$$

Thus, if the observation noise is small enough, the solution is dominated by numerical noise, otherwise, the solution is ruled by the effect of the observation noise, that creates a sort of boundary, such that it does not permit to minimise the cost function below a certain level.

6.4 Size of the orbit

The importance of the distance of the probe from the central body is known when dealing with gravity field estimation. As already reported, the perturbing effect of the spherical harmonics gets smaller for increasing order and degree, and the overall gravitational pull decreases with the square of the distance from the body. For these reasons, the bigger the orbit, the lower is the effect of the non keplerian gravitational perturbations. Viceversa, close orbiting spacecraft can guarantee more informative data, since their trajectory highly deviates from the keplerian path, especially when influenced by highly irregular gravity fields, like in this case. In the following figures, results for polar scanner swarms satellites, optimised in pairs, are reported for different orbit sizes, namely: $a = 40$ km, $a = 30$ km, $a = 25$ km. Simulations were repeated considering range and range-rate measurements to compare any possible

difference. Care was taken in avoiding choosing too small orbits such that one of the trajectories may fall within the Brillouin sphere, where the gravitational model incurs in high errors [58]. Figures clearly show that, as expected, with low altitude orbits an improvement in the accuracy of the solution is achieved.

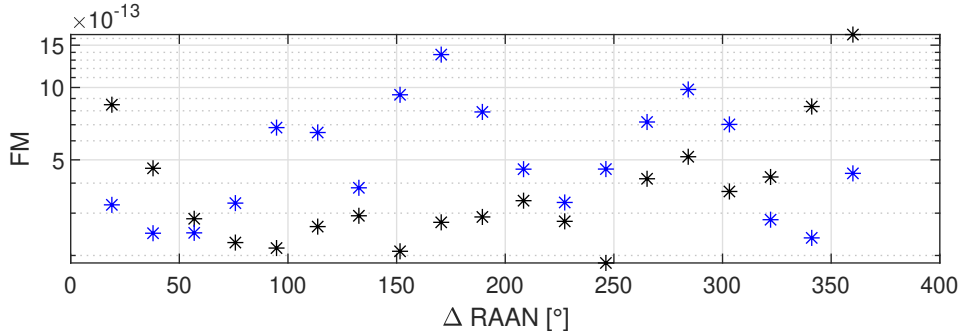

Figure 6.10. Polar scanner results for $a = 40$. Red: relative position coordinates; Blue:range and range-rate

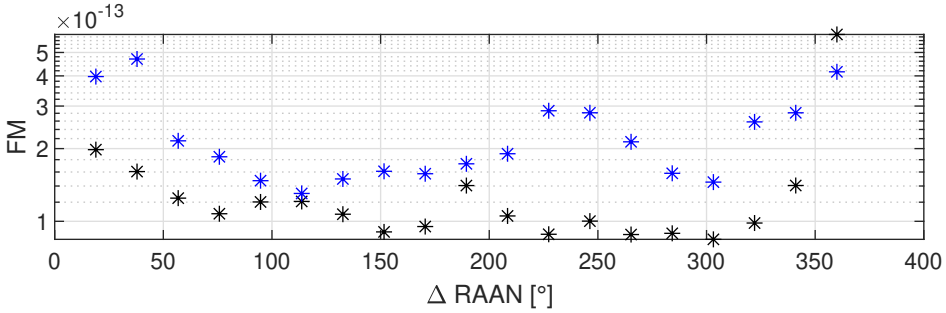

Figure 6.11. Polar scanner results for $a = 30$. Red: relative position coordinates; Blue:range and range-rate

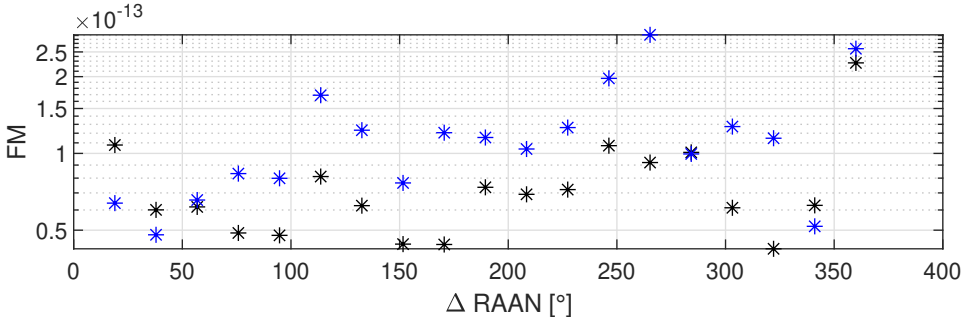

Figure 6.12. Polar scanner results for $a = 25$. Red: relative position coordinates; Blue:range and range-rate

6.5 Observation time

The discussion about the information content of data must be now be addressed regarding the length of the observations accounted for optimisation. It could be

said that it is not the increasing number of satellites data to improve the solution, rather the increasing of the amount of data fed to the optimisation. Keeping the same sampling time, polar inclination fan swarms were propagated for 1, 2 and 5 orbital periods, with increasing swarm size. Chart in 6.13 suggest that projecting the trajectories for longer time-span doesn't seem to have a big influence on the solution, while the effect of the increasing swarm size is more evident. The reason for this behaviour could be attributed to the performances of the integration scheme: the error accounted for increased integration time could be *spoiling* the solution even though an bigger data-set is used for the optimisation.

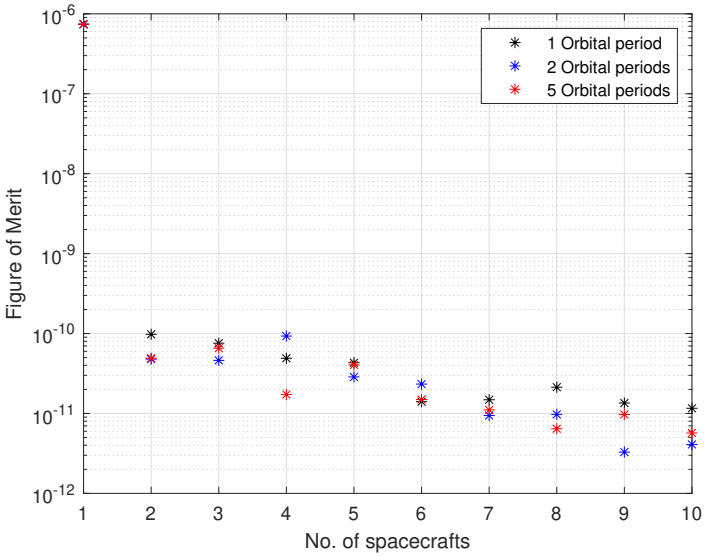

Figure 6.13. Solution for increasing observation time and spacecrafts

6.6 Solar radiation pressure

SRP revolves around the idea that electromagnetic waves are massless, but exhibit mass-like properties. The photons in light emitted from the Sun move at the speed of light and have momentum. Because they have momentum, when they hit other objects, they transfer momentum to the that object, giving it a boost in velocity. However, the momentum these photons carry is extremely small. Thus, the perturbing force isn't really observed in LEO spacecraft. However can be significant especially in the scope of asteroidal applications, since it could affect the measurements of the tiny fluctuations in the gravitational force field. In 6.3 the equation for the SRP force acting on the satellite is reported:

$$\mathbf{F_{SRP}} = -v \cdot \frac{S}{c} \cdot C_R \cdot A_s \hat{\mathbf{S}} \tag{6.3}$$

where v is the shadow boolean function, S is the solar constant, c is the speed of light, C_R the reflectivity coefficient, A_s is the *wet* area of the satellite and $\hat{\mathbf{S}}$ is the Sun

direction unit vector. In Fig. 6.14 a comparison of the accelerations proportioned by the single J terms of the spherical harmonics expansion of Eros 433 gravity field, and the SRP acting on a spacecraft orbiting Eros, as a function of the distance from the body. This rough computation was made to have an understanding of the limitations of the model, i.e. when the effect of the unmodeled SRP becomes comparable with the considered dynamics. The satellites mass was chosen as $m = 0.01$ kg, $v = 1$ and their wet area $A_s = 10^{-5}$ m^2. The results reflect that the SRP acceleration should not be neglected, especially when dealing with altitudes higher than 50 km, since its value becomes comparable with the one proportioned by the gravitational harmonics.

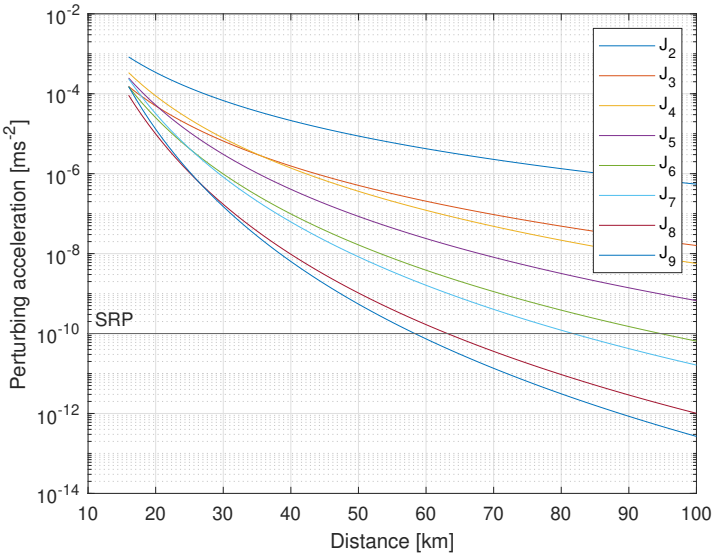

Figure 6.14. SRP and J_n acceleration comparison

To appreciate quantitatively how the solution is affected by the unmodeled dynamics of SRP, a polar scanner swarm with $a = 30km$ was simulated in both cases: black dots in Figure 6.15 show the solutions for the single spacecrafts of the swarm with no SRP; red dots show the solutions where SRP was considered for the measurements, but not included in the model to optimise: it is clear that in this approach, SRP acts as a *noise* on our measurements, leading to overall worse solutions with FM of 2 orders of magnitude higher. This underlines that the model is still able to converge under the presented assumptions, however an augmentation of the model is needed, accounting for the SRP, to achieve better solutions especially for high altitude orbits. This problem should be thoroughly investigated in future researches.

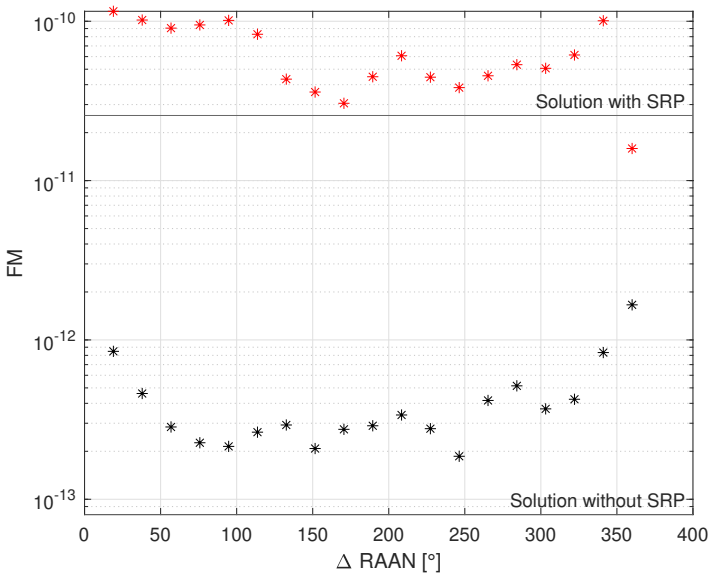

Figure 6.15. Solution comparison with and without SRP effect

6.7 Type of measurements

Lastly, let's analyse the solution behaviour when taking in account the different types of measurements treated in this research. The objective is to determine which one performs the best -in an absolute way- but also which one may be the most suitable according to the effort required in obtaining such measurements, considering a real-life application.

It's been already discussed in previous sections, whenever a comparison between measurement strategy was made, that most of the times the solution obtained with relative position Cartesian coordinates results in the best solution among the others. In the same way, the simulations with range and range-rate measurements seem to perform slightly better with respect to the only range measurements cases, although very similar solutions are often found between these.

A quantitative analysis was sought in order to retrieve a definitive response. To do this, a statistical approach was utilized. In particular, a database of simulations was built, containing the solutions for 120 simulations, generated with different kinds of swarm configurations and number of satellites. Care was taken in selecting fixed noise level and orbit sizes for all iteration.
Each scenario was repeated 3 times, and optimized each time with one of the different measurements approach discussed. After collecting all the solutions, each FM obtained from range and range-rate measurements, and from range measurements only, was subtracted to the ones obtained with relative position Cartesian measurements.
These two sets of data, were used to generate histograms where the bar height reflects the number of simulations in which the values of $FM_{cartesian} - FM_{rangerangerate}$ and $FM_{cartesian} - FM_{range}$ fall within that fixed interval.

Histograms are shown in 6.16 and 6.16, while statistical facts are reported in 6.1. While *sometimes* both the approaches regarding range data perform better, we can safely deduce that -on average- the relative position in Cartesian coordinates approach gives the best solutions. Based on the same data, it can be said that the range only measurement approach result in the worst solutions. Although this being rather expected, since the solution is affected by the information content of the input data for the optimisation (as already discussed), these results must not be taken in an absolute way, and should not determine the selection of a strategy rather than the other.
The type of measurement selected strongly affects the technological requirements of a real-life mission. In particular, the acquisition of relative position Cartesian coordinates of the secondaries would necessarily require heavier and bigger instrumentation on-board such that would make the mission unfeasible for a high number of satellites. On the other hand, range and range-rate data can be obtained very easily, for example measuring the echo of the secondaries hit by a carrier wave. This means that the child-ship could be small and *stupid*, in the sense that they would not be required to handle and transfer data. For this reason, the selection of only range measurements would be justified, accepting an average reduction of $2.11 \cdot 10^{-12}$ in the Figure of Merit in exchange of a lightweight and compact instrumentation.

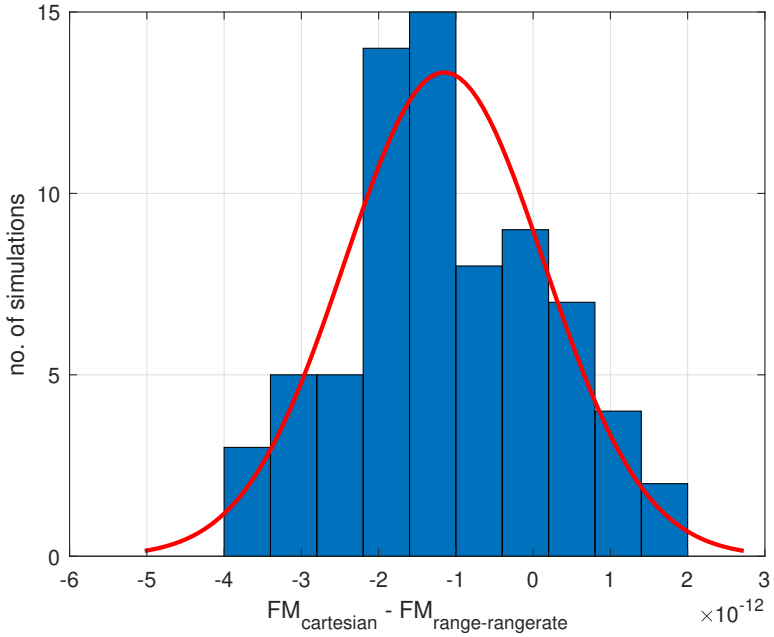

Figure 6.16. FM comparison between relative Cartesian coordinates and range+range-rate measurements

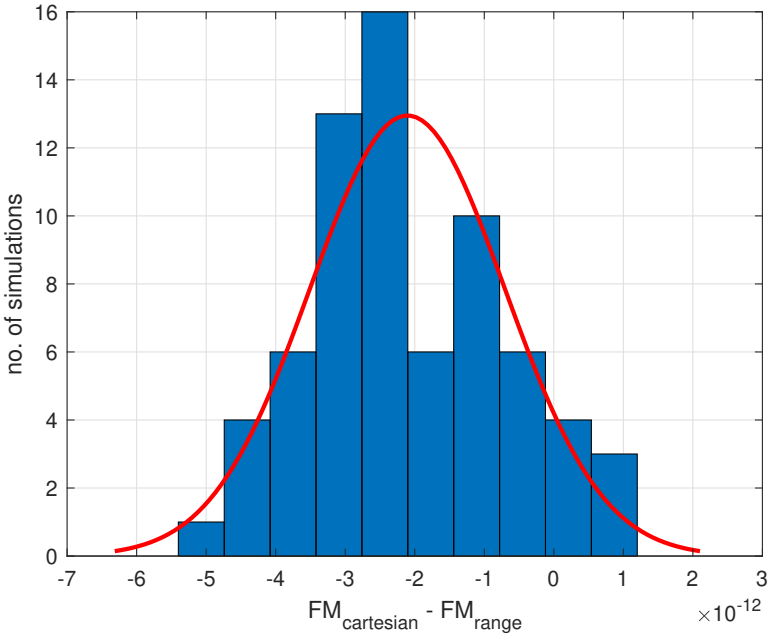

Figure 6.17. FM comparison between relative Cartesian coordinates and range measurements

Table 6.1. Measurements comparison against the FM obtained with Cartesian relative positions

-	Range and range-rate	Range only
μ	$-1.15 \cdot 10^{-12}$	$-2.11 \cdot 10^{-12}$
μ confidence interval	$[-1.45 \cdot 10^{-12}, -8.47 \cdot 10^{-13}]$	$[-2.44 \cdot 10^{-12}, -1.77 \cdot 10^{-12}]$
σ	$1.29 \cdot 10^{-12}$	$1.40 \cdot 10^{-12}$
σ confidence interval	$[1.11 \cdot 10^{-12}, 1.55 \cdot 10^{-13}]$	$[1.20 \cdot 10^{-12}, 1.69 \cdot 10^{-12}]$

Conclusions

Small solar system bodies represent an important field of study, that gained huge interest thanks to the possible technological and scientific outcomes of it. In particular, the estimation of their gravity field is the necessary step to be made in order to visit and/or land on them. Deep understanding of their composition and structure through their gravity field assessment is needed to gain information required to comprehend how and when they originated or more practically to design asteroid deflection techniques and indentify possible targets for asteroid mining missions. This chapter wants to summarize the subjects and the results obtained and reported in this thesis. Moreover future research objectives are addressed, to indicate pathways that are worth to pursue and were not included in this research for reasons of time, or because their scopes were *parallel* to the ones belonging to this thesis.

Started as a continuation of the research proposed by Guardalà [43], where gravity field determination was addressed in detail using a single or a multi-spacecraft approach mostly in Earth environment and using absolute coordinates measurements only, the problem was reformulated, and this thesis analysed the problem of gravity field determination of asteroids through a novel concept, namely the recovery of it using relative coordinates measurements of a swarm of small satellites. The objectives identified at the beginning of this work were fully achieved, and most of the questions posed were answered thanks to the results obtained.

Firstly, after picking and explaining the main tools needed to model the phenomenon, namely the gravity field models, the estimation techniques and the orbit propagation methods, the most relevant and/or *feasible* ones to use were implemented to generate the simulation framework to be analysed. This was used to demonstrate not only that it is possible to estimate the gravity field of a small body using relative position measurements obtained from a swarm of formation flying satellites with respect to a primary one, but also that a refinement of the solution can be obtained with that.
In more detail, a batch estimation approach was used to estimate gravity fields modeled through spherical harmonics expansion, using a LM method as a solver, differently from other studies like [44] and [45] where semi-analytical methods were used to partially solve the gravity field determination problem. Trajectories were integrated using an independent swarm propagation method, since the Encke's method did not fulfill the expectations of obtaining more accurate relative trajectories in this scope. The gravity field was modeled with a spherical harmonics expansion, however modelisation using Mascon models was also investigated in a novel approach. Moreover a newly defined gravity field estimation method, derived from the orbit

determination algorithm of Nayfeh [1], was proposed and simulated.

Several swarming strategies were devised, and the effect of each of them to the overall solution was investigated. The contribution of each single satellite to the solution was evaluated, and an outlier rejection algorithm was proposed in order to obtain a more accurate overall solution, successfully achieving it when dealing with noise-based outliers.

Full swarm optimisations were carried to demonstrate the concept, and the performances of the model evaluated for increasing swarm size, orbit sizes and noise level. Moreover the effect of unmodeled dynamics was addressed, with particular attention on SRP. A comparison of the magnitudes of the perturbing accelerations was used to define the altitude threshold above which the magnitude of the SRP acceleration becomes non-negligible.

To conclude, a statistical assessment of the solutions was carried to evaluate the best performing measurements strategy. Solutions generated using measurements involving relative position Cartesian coordinates, range and range-rate, and range only, were compared. As expected, relative position Cartesian coordinates yielded -on average- the best solutions. However the solutions obtained with the two other strategies only got worse by a small fractions of the Figure of Merit. Range data was ultimately selected as the most feasible approach, since the small deterioration of the solution is counterbalanced by the fact that -technologically speaking- obtaining range data of the secondaries, from the primary spacecraft, involves cheaper, lighter and smaller instrumentation. This enables the use of micro-sized spacecrafts as child-ships that should only act as reflectors of the signal emitted by the beacon mother-ship.

Future work

The conclusions derived in this research open the way to the developing of a technological feasibility analysis of a real mission scenario. However as a proof of concept, a simplified framework has been considered at this stage.

Swarm deployment was not taken in account, and should be addressed in future research since the selection of the swarm configuration will depend on the architecture of a particularly conceived deploying mechanism, and on the measurements instrumentation. Very precise instrumentation for the satellites tracking to achieve accurate estimation, so that trade-offs should be done between the technological complexity and the estimated solution precision.

The possibility of multi-spacecraft gravity field estimation using hyperbolic trajectories should be discussed, as it would enable to target more than one body.

Regarding the model, augmentation of the dynamics should be discussed to investigate more deeply the influence of other perturbations like the SRP or gravitational fluctiation generated by third bodies.
Sensitivity to other parameters like asteroid angular velocity and orbits eccentricity

should be evaluated. The model should also be tested with other asteroids gravity field models, between the ones available or artificially generated ones, to verify its robustness.

Bibliography

[1] A. H. Nayfeh, "Non-linear orbit determination methods," *Satellite Orbits*, pp. 1–12, 1968.

[2] H. J. Kramer, "Egs (experimental geodetic satellite." [Online]. Available: https://directory.eoportal.org/web/eoportal/satellite-missions/content/-/article/egs-ajisai

[3] G. Seeber, "Satellite geodesy," pp. 119–122, 135–482, 2003.

[4] V. D. A., "Fundamentals of astrodynamics and applications," 1997.

[5] R. W. Abhishek Srinivas and G. Zachmann, "Fast and accurate simulation of gravitational field of irregular-shaped bodies using polydisperse sphere packings," *ICAT-EGVE 2017 - International Conference on Artificial Reality and Telexistence and Eurographics Symposium on Virtual Environments. Ed. by Robert W. Lindeman, Gerd Bruder, and Daisuke Iwai. The Eurographics Association*, 2017.

[6] NASA, "Near encounter with asteroid 433 eros," 2020. [Online]. Available: https://nssdc.gsfc.nasa.gov/planetary/mission/near/near_eros_approach.html

[7] F. L. et al, "The development of the joint nasa gsfc and the national imagery and mapping agency (nima) geopotential model egm96," 1998.

[8] A. K. et al, "A global solution for the gravity field, rotation, landmarks, and ephemeris of eros," *Icarus 160*, p. 289–299, 2002.

[9] S. Daily, "Weird, wild gravity of asteroid bennu," *University of Colorado at Boulder*, 2020.

[10] J.-P. Sánchez and C. Colombo, "Impact hazard protection efficiency by a small kinetic impactor," *Journal of Spacecraft and Rockets 50*, p. 380–39, 2013.

[11] A. C. et al., "Asteroid impact deflection assessment mission: Kinetic impactor," *Planetary and Space Science 121*, pp. 27–35, 2016.

[12] D. L. Cahndler., "Gravity tractor could deflect asteroids.." [Online]. Available: https://www.newscientist.com/article/dn14414-gravity-tractor-could-deflect-asteroids/

[13] I. N. H.J. Melosh and Y. I. Zetzer, "Non-nuclear strategies for deflecting comets and asteroids," *Hazards Due to Comets and Asteroids*, p. 1111–1132, 1994.

[14] L. David, "Asteroid-mining plan would bake water out of bagged- up space rocks." [Online]. Available: https://www.space.com/30582-asteroid-mining-water-propulsion.html

[15] H. A. Gustav Arrhenius and R. Fritzgerald, "Asteroid and comet exploration," pp. 20–22, 1973.

[16] D. B. G.J. Consolmagno and R. Macke, "The significance of meteorite density and porosity," *Geochemistry 68.1*, pp. 1–29, 2008.

[17] M. E. et al, "A density-based algorithm for discovering clusters in large spatial databases with noise," p. 226–231, 1996.

[18] Y. C. et al., "Optical landmark detection for spacecraft navigation," 2003.

[19] JAXA, "About experimental geodetic satellite "ajisai" (egs)." [Online]. Available: https://global.jaxa.jp/projects/sat/egs/index.html

[20] H. J. Kramer, "Starlette / stella - geodetic satellites." [Online]. Available: https://earth.esa.int/web/eoportal/satellite-missions/s/starlette

[21] E. Society, "European involvement in juno." [Online]. Available: https://www.europlanet-society.org/juno-europe/

[22] H. J. Kramer, "Icesat (ice, cloud and land elevation satellite)." [Online]. Available: https://directory.eoportal.org/web/eoportal/satellite-missions/i/icesat

[23] R. R. et al, "Dedicated gravity field missions—principles and aims," *Journal of Geodynamics 33*, pp. 3–20, 2002.

[24] G. B. et al., "Champ, grace and goce: mission concepts and simulations," *Bollettino di Geofisica Teorica ed Applicata 40.3-4*, p. 309–319, 1999.

[25] Wikipedia, "Small solar system body." [Online]. Available: Bhttps://en.wikipedia.org/w/index.php?title=Small_Solar_System_body&oldid=936121272

[26] ESA, "Structure and composition of asteroids." [Online]. Available: https://www.esa.int/Science_Exploration/Space_Science/Asteroids_Structure_and_composition_of_asteroids

[27] NASA, "Cosmic detective work: Why we care about space rocks." [Online]. Available: https://www.nasa.gov/feature/jpl/cosmic-detective-work-why-we-care-about-space-rocks/

[28] Britannica, "Asteroid." [Online]. Available: https://www.britannica.com/science/asteroid

[29] B. S., "Autonomous navigation for deep space missions," *SpaceOps 2012 Conference*, pp. 1–13, 2012.

[30] J. M. et al, "Determination of shape, gravity, and rotational state of asteroid 433 eros," *Icarus 155*, pp. 3–17, 2002.

[31] JAXA, "Hayabusa." [Online]. Available: http://www.isas.jaxa.jp/en/missions/spacecraft/past/hayabusa.html

[32] M. P. et al, "Gravity field determination of a comet nucleus: Rosetta at p/wirtanen," *AA 375*, 2001. [Online]. Available: http://dx.doi.org/10.1051/0004-6361:20010829

[33] NASA, "Osiris-rex mission." [Online]. Available: https://www.asteroidmission.org/objectives/

[34] M. J. W. et al, "The osiris-rex radio science experiment at bennu," *Space Science Reviews 214.1*, 2018.

[35] D. S. et al, "Osiris-rex gravity field estimates for bennu using spacecraft and natural particle tracking data," *EPSC-DPS Joint Meeting 2019*, 2019. [Online]. Available: https://ui.adsabs.harvard.edu/abs/2019EPSC...13..106S

[36] N. JPL, "Mission to a metal world: Psyche." [Online]. Available: https://www.jpl.nasa.gov/missions/psyche/

[37] X. W. and J. J. L, "Formation flying: a subject being fast unfolding in space," *Tech. rep.*, 1997.

[38] J. L. et al, "Absolute orbit determination and gravity field recovery for 433 eros using satellite-to-satellite tracking," *AIAA/AAS Astrodynamics Specialist Conference*. [Online]. Available: https://arc.aiaa.org/doi/abs/10.2514/6.2012-4877

[39] S. H. et al., "Small body gravity field estimation using liaison supplemented optical navigation," 2015.

[40] J. Atchison, "Niac swarm flyby gravimetry phase ii report," 2017.

[41] R. S. William Ledbetter and J. Keane, "Smallsat swarm gravimetry: Revealing the interior structure of asteroids and comets," 2018.

[42] N. S. Kohei Fujimoto and J. M. Turner., "Stereoscopic image velocimetry as a measurement type for autonomous asteroid gravimetry," *AIAA/AAS Astrodynamics Specialist Conference*, 2016.

[43] G. Guardalà, "Single and multi-spacecraft solutions for the gravity field determination of irregular bodies."

[44] A. Bassani, "Recovery of the gravity field of a small body through autonomous and relative navigation between two spacecraft," 2020.

[45] S. D. Corinne Lippe, "Spacecraft swarm dynamics and control about asteroids," vol. 67.

[46] C. J. W. James K. Miller and L. J. Wood, "Orbit determination strategy and accuracy for a comet rendezvous mission," *Satellite Orbits*, pp. 53–68, 244–247, 2000.

[47] W. M. Kaula, "Theory of satellite geodesy," *Dover Publications Inc.*, pp. 1–11, 100–107, 1966.

[48] L. E. Cunningham., "On the computation of the spherical harmonic terms needed during the numerical integration of the orbital motion of an artificial satellite," *Celestial Mechanics 2.2*, pp. 207–216, 1970.

[49] P. Geissler, J.-M. Petit, D. D. Durda, R. Greenberg, W. Bottke, M. Nolan, and J. Moore, "Erosion and ejecta reaccretion on 243 ida and its moon," *Icarus 120*, pp. 140–157, 1996. [Online]. Available: https://www.sciencedirect.com/science/article/pii/S0019103596900421

[50] R. Russell and P. Wittick, "Mascon models for small body gravity fields," 2017.

[51] B. E. S. Byron D. Tapley and G. E. Born, "Statistical orbit determination," *Academic Press*, pp. 159,211, 2004.

[52] H. P. Gavin, "The levenberg-marquardt method for nonlinear least squares curve-fitting problems," 2013.

[53] Wikipedia, "Loss of significance." [Online]. Available: https://en.wikipedia.org/w/index.php?title=Loss_of_significance&oldid=952171075

[54] S. Casotto, "An autonomous passive navigation method for nanosatellite exploration of the asteroid belt," *Celestial Mechanics and Dynamical Astronomy 124*, pp. 215–234, 2015.

[55] Wikipedia, "Hilbert space." [Online]. Available: https://en.wikipedia.org/w/index.php?title=Hilbert_space&oldid=951495500

[56] C. S. C. M. Space, "European involvement in juno." [Online]. Available: https://www.britannica.com/science/metric-space

[57] Wikipedia, "Dbscan." [Online]. Available: it.wikipedia.org/w/index.php?title=Dbscan

[58] Y. Takahashi and D. J. Scheeres, "Spherical harmonic potentials within the brillouin sphere," *AIAA/AAS Astrodynamics Specialist Conference*.